

8. SITE 1069¹

Shipboard Scientific Party²

HOLE 1069A

Position: 40°43.612'N, 11°46.633'W

Start hole: 0530 hr, 22 May 1997

End hole: 1445 hr, 31 May 1997

Time on hole: 225.25 hr (9.4 days)

Seafloor (drill pipe measurement from rig floor, mbrf): 5086.0

Total depth (drill pipe measurement from rig floor, mbrf): 6045.3

Distance between rig floor and sea level (m): 11.2

Water depth (drill pipe measurement from sea level, m): 5074.8

Penetration (mbsf): 959.3

Coring totals:

Type: RCB; Number: 25; Cored: 240.5 m; Recovered: 96.3 m; Average recovery: 40.0%

Type: G; Number: 1; Cored: 0 m; Recovered: 0.4 m; Average recovery: N/A

Sedimentary sequence:

Subunit IIB: (718.8–805.8 mbsf); claystone, calcareous claystone, nannofossil chalk, and calcareous sandy siltstone (middle Eocene to late Paleocene)

Subunit IIC: (805.8–865.5 mbsf); claystone, calcareous sandstone, calcareous claystone, and nannofossil chalk (early Paleocene to late Campanian)

Unit IV: (865.5–867.8 mbsf); nannofossil chalk (Early Cretaceous [late Berriasian to ?early Valanginian])

Subunit VA: (867.8–873.7 mbsf); conglomerate containing clasts of grainstone, boundstone, rudstone; minor clay (Late Jurassic [?Tithonian])

Subunit VB: (873.7–959.3 mbsf); barren metasilstone, meta-arkosic wacke, and dolomitic meta-arkose

Principal results: The site is situated in the southern Iberia Abyssal Plain in a water depth of 5075 m and lies on a north-south seismic line over the crest of a relatively flat-topped north-south basement ridge. The east flank of the ridge is underlain by a west-dipping reflector that bounds the west side of the next basement high to the east, and its west flank appears to coincide with a similar reflector. Both reflectors have the appearance of normal faults. A few kilometers southward, the high is smaller and is underlain by a subhorizontal reflector that seems to be the prolongation of the normal fault bounding the next block toward the east, on top of which are located Sites 900, 1067, and 1068. Thus, the seismic data suggest that the basement ridge is a possible fault block tilted toward the continent. This block is the southern extension of Vasco da Gama Seamount that dies out southward. The site lies in a location where a variety of structural and geophysical models for the development of the ocean/continent transition (OCT) can be tested.

Biostratigraphic data from Site 1069 indicate that this site was at shelf depths in the earliest Cretaceous and then subsided, reaching abyssal depths by the late Campanian. This evidence, together with very low-

grade metasediments (probably occurring as clasts in a conglomerate) found in acoustic basement at the bottom of the hole, leads to the tentative conclusion that the site was drilled on a continental fault block. There is no sign of the mafic or ultramafic rocks that were encountered at Sites 897, 899, 900, 1067, or 1068.

The middle Eocene to upper Campanian 147-m-thick sedimentary succession cored at Hole 1069A is dominated by upward-darkening sequences (2 to 55 cm thick) of calcareous siltstone or sandstone, overlain by calcareous claystone or nannofossil chalk, and capped by dark hemipelagic claystone. Two subunits are recognized in this interval based on an increase in the frequency, proportion, and thickness (up to 50 cm) of sandstone lithologies at the base of individual turbiditic sequences from Subunit IIB to Subunit IIC. These sequences are interpreted as being deposited by turbidites near or below the carbonate compensation depth (CCD). A 2.3-m-thick upper Berriasian to ?lower Valanginian yellow nannofossil chalk is defined as Unit IV. The chalk is interpreted to have been deposited above the CCD as a thin pelagic drape overlying resedimented chalk occupying a hollow in the underlying basement ridge. The chalk in turn is separated from an underlying Tithonian black silt by an erosional unconformity. A 9-cm interval of Upper Jurassic (?Tithonian) hemipelagic/pelagic gray clay occurs above eight curated pieces of limestone conglomerate containing granules of pelites and metabasic arenite. The limestone clasts consist of grainstones and algal boundstones. The thin clay and limestone pieces are defined as Subunit VA. The lithology of the limestone clasts is similar to the Upper Jurassic limestones drilled on the Galicia Margin and to clasts occurring within the conglomerates in Unit V at Site 1065. The limestone clasts were probably transported and resedimented from a carbonate shelf situated to the north, probably above the present day Vasco da Gama Seamount and associated basement highs.

The calcareous nannofossil sequence at Site 1069 began in the middle Eocene (CP12b) and then passed downhole through a more or less continuous succession of zones and subzones to a barren interval within the Paleocene in which zones CP5 to CP4 are not represented. Interbedded hemipelagites barren of coccoliths indicate that most of the carbonate in the lower Paleocene was deposited below the CCD as turbidites. The Cretaceous/Tertiary transition lies within a bioturbated turbidite sequence in Core 173-1069A-12R; the boundary has been obliterated. The lithologic succession then continues from the uppermost Maastrichtian to the uppermost Campanian. It is interrupted in Section 173-1069A-16R-2 by an unconformity, below which lies the yellowish chalk described above (Unit IV). The upper portion of the chalk is dominated by nannoconids.

Palynological analyses indicate that Subunit VA was deposited in a marine environment with a strong terrestrial influence in mid-Kimmeridgian to upper Portlandian time.

Paleogene planktonic foraminifers are common and moderately well preserved in the upper part of Subunit IIB (718.8–757.4 mbsf), but, with one exception, are rare to absent and generally poorly preserved below (757.4–873.3 mbsf). Calcareous benthic foraminifers and agglutinated foraminifers are present in most core-catcher samples above Core 173-1069A-14R. Within the latter group, the persistent occurrence of species such as *Ammodiscus* spp., *Bathysiphon* spp., and *Glomospira* spp. suggests that these Paleogene sediments were deposited in a fully marine environment, probably at abyssal depths.

Pieces of very hard rock were first encountered in Core 173-1069A-17R (beneath the Tithonian clay and limestone clasts) and continued to the bottom of the hole (Core 173-1069A-25R). These rocks (Subunit VB) consist of meta-arkosic wacke, metasilstone, and dolomitic meta-arkose.

¹Whitmarsh, R.B., Beslier, M.-O., Wallace, P.J., et al., 1998. *Proc. ODP, Init. Repts.*, 173: College Station, TX (Ocean Drilling Program).

²Shipboard Scientific Party is given in the list preceding the Table of Contents.

Some of the pieces are moderately rounded and lack drilling percussion marks, which suggests that they are clasts whose original surfaces are preserved. The rocks are weakly deformed, with a metamorphic foliation defined by aligned sericite and chlorite. Relict sedimentary textures such as detrital grains and bedding/lamination are also preserved. In the siltstones, many quartz fragments are elongate parallel to the foliation. Pyrite-quartz vugs are common and, in some pyrite-rich samples, thin pyritic veins and elongate pyrite-quartz vugs also parallel the foliation. Core recovery in Subunit VB was extremely low yet the rate of penetration was relatively fast (35–80 min/core). The only material recovered from Subunit VB (85.6 m thick) that could have been the original intraclast matrix was small amounts of dark sandy clayey silt in Cores 173-1069A-21R and 24R. Headspace gas from the Core 21R material contained 101.7 ppm methane and 1.6 ppm ethane.

Metasedimentary rocks in Subunit VB contain abundant detrital quartz and plagioclase and a metamorphic mineral assemblage that includes sericite, chlorite, and, in some cases, dolomite. Unusually large ilmenite and leucoxene pseudomorphs (after ilmenite) appear to be metamorphic porphyroblasts, although a detrital origin in some rocks cannot be ruled out, especially for finer grained ilmenite and leucoxene. Dolomite forms subhedral porphyroblasts in one sample and may be part of the diagenetic assemblage in the second. The stable coexistence of dolomite + chlorite and dolomite + muscovite indicates very low-grade metamorphism, probably subgreenschist. Similar rocks of Paleozoic age have been reported from Galicia Bank, where they also underlie Tithonian sediment.

Overall, the bedding in Subunits IIB and IIC is shallowly inclined. Within Subunit IIB, a marked change occurs at 760 mbsf. Above, the true dip is about 12°, below, only about 4°. At the base of Unit II and in Unit IV the bedding is again more steeply inclined (about 14°). Whereas Unit II is essentially undeformed (only some minor normal faults), Unit IV was pervasively affected by pre-Unit II soft-sediment folding and normal faulting. The deformation of the basement rocks (Subunit VB) was dominated by pressure solution. The dip of the bedding is variable in the few basement pieces that could not have rolled over in the core liner. The foliation is often subhorizontal.

The magnetic intensities of sediments in Subunits IIB and IIC are generally weak. Characteristic peaks in NRM intensity and volume susceptibility associated with an early Eocene brown bed, which has been observed at four other Iberia Abyssal Plain sites, were detected in Core 173-1069A-7R at ~777 mbsf. Cryogenic magnetometer measurements on whole cores and on discrete samples indicate that several polarity reversals are recorded in Cores 173-1069A-3R through 14R (738.1–854.0 mbsf). In the lower part of Subunit IIC, below 854.0 mbsf, the sediments are entirely normally magnetized, which is consistent with the Late Cretaceous long normal superchron and the late Campanian age of the sediments. The metasediment clasts have much higher susceptibility and intensity values than the overlying sedimentary sections. Magnetic inclinations were measured on six samples from clasts that demonstrably have not rotated in the core barrel. Both positive and negative low-angle inclination values were measured. In addition, the inclinations are at low angles to the rock foliation; this is consistent with synmetamorphic reorientation of ilmenite grains along the foliation. This evidence indicates that the recovered material is redeposited metasedimentary cobbles.

Claystones have bulk densities from 1.94 to 2.21 g/cm³ and porosities from 31% to 44%, and calcareous claystones have bulk densities from 2.18 to 2.36 g/cm³ and porosities from 22% to 38%. Whereas sandstones have bulk densities from 2.16 to 2.34 g/cm³ and porosities from 21% to 32% in Subunit IIB, the values of bulk density and porosity are more variable in Subunit IIC (bulk density = ~2.20–2.63 g/cm³ porosity = ~5%–30%). Compressional-wave velocities have a reasonable correlation with porosity and bulk density. Metasediment samples of Subunit VB have high densities from 2.70 to 2.73 g/cm³, and high velocities from 4521 to 5639 m/s and very low porosities (<3%). Consequently, acoustic basement at this site is identified at the top of Subunit VB.

The triple combination tool was run successfully between 102 and 778 mbsf. The logs overlap the cored interval between 719 and 770 mbsf (Cores 173-1069A-1R through 5R), which represents part of Subunit IIB, a calcareous claystone. Preliminary analysis of the logs shows a good correlation with Site 1068 between 100–390 and 610–750 mbsf. Variations of inferred sedimentation rates between sites suggest a greater rate during the Miocene at Site 1069 and a slightly lesser rate during the Eocene, relative to Site 1068. A water overpressure encountered at 650 mbsf during the final pipe trip to the rig floor may be tentatively related to a 20-m-thick interval (670–690 mbsf) where high porosity and low resistivity were recorded.

BACKGROUND AND OBJECTIVES

The basement cores obtained during Leg 149 (Sawyer, Whitmarsh, Klaus, et al., 1994) revealed outcrops of serpentinized peridotite at Site 897, situated on the crest of a segment of the margin-parallel peridotite ridge, and of gabbro that had undergone synrift deformation at Site 900 on another basement high farther east (Figs. 1, 2). At a third site (Site 899), between the other two sites, the acoustic basement cores consisted of serpentinite breccia, possibly of local origin. However, the magnetic anomaly associated with Site 899 suggests that the basement high on which the site is located may be atypical of the OCT in the southern Iberia Abyssal Plain (Whitmarsh and Sawyer, 1996). Thus, there is a gap without basement samples of some 76 km between Sites 897 and 900 (and of at least 60 km between Sites 899 and 900). This distance represents about half the width of the OCT in the southern Iberia Abyssal Plain. Therefore, the principal objective of Site 1069 was to obtain basement cores within this part of the OCT to better constrain models of its development (see below). This site was originally designated IBERIA-07A but was moved 1200 m north along the crest of the basement ridge, where the sediments are ~50 m thinner, to become IBERIA-07B (Fig. 3).

A variety of structural and geophysical models for the development of the OCT in the southern Iberia Abyssal Plain has been proposed (Beslier et al., 1995; Brun and Beslier, 1996; Krawczyk et al., 1996; Pickup et al., 1996; Sawyer, 1994; Whitmarsh and Miles, 1995; Whitmarsh and Sawyer, 1996). These can be divided into three groups, which are briefly discussed below. Each predicts a different geodynamic context, and even rock type, for the crystalline basement within the gap alluded to above. The situation may be even more complex; the models are all essentially two-dimensional in the sense of assuming a constant structure parallel to the continental margin. In reality, as Pickup et al. (1996) suggested, quite significant changes may occur parallel to the margin in the OCT, particularly between the two deep multichannel seismic profiles Lusigal-12 (Beslier, 1996; Krawczyk et al., 1996) and IAM-9 (Pickup et al., 1996) at 40°40'N and about 40°30'N, respectively. The predictions of the individual models concerning the nature of the crystalline basement at Site 1069 are summarized in Table 1.

Sawyer (1994), Whitmarsh and Miles (1995), and Whitmarsh and Sawyer's (1996) Hypothesis 1, by analogy with what appears to happen on some slow-spreading mid-ocean ridges (Cannat, 1993; Karson, 1990), discuss the possibility that the OCT is a product of very slow seafloor spreading. At a mid-ocean ridge formed by very slow seafloor spreading, a relatively limited amount of melt reaches the seafloor, and the uppermost lithosphere consists not only of basalt but also of gabbro and mantle peridotite. Further, this basement may be extensively tectonized and broken into fault blocks. Gabbros and peridotites have been found within the southern Iberia Abyssal Plain OCT and fault blocks appear on seismic profiles. The weaknesses of the hypothesis, however, are the apparent general lack of synrift basalt in the OCT and the inability of seafloor-spreading models to explain the observed magnetic anomalies. This hypothesis predicts the

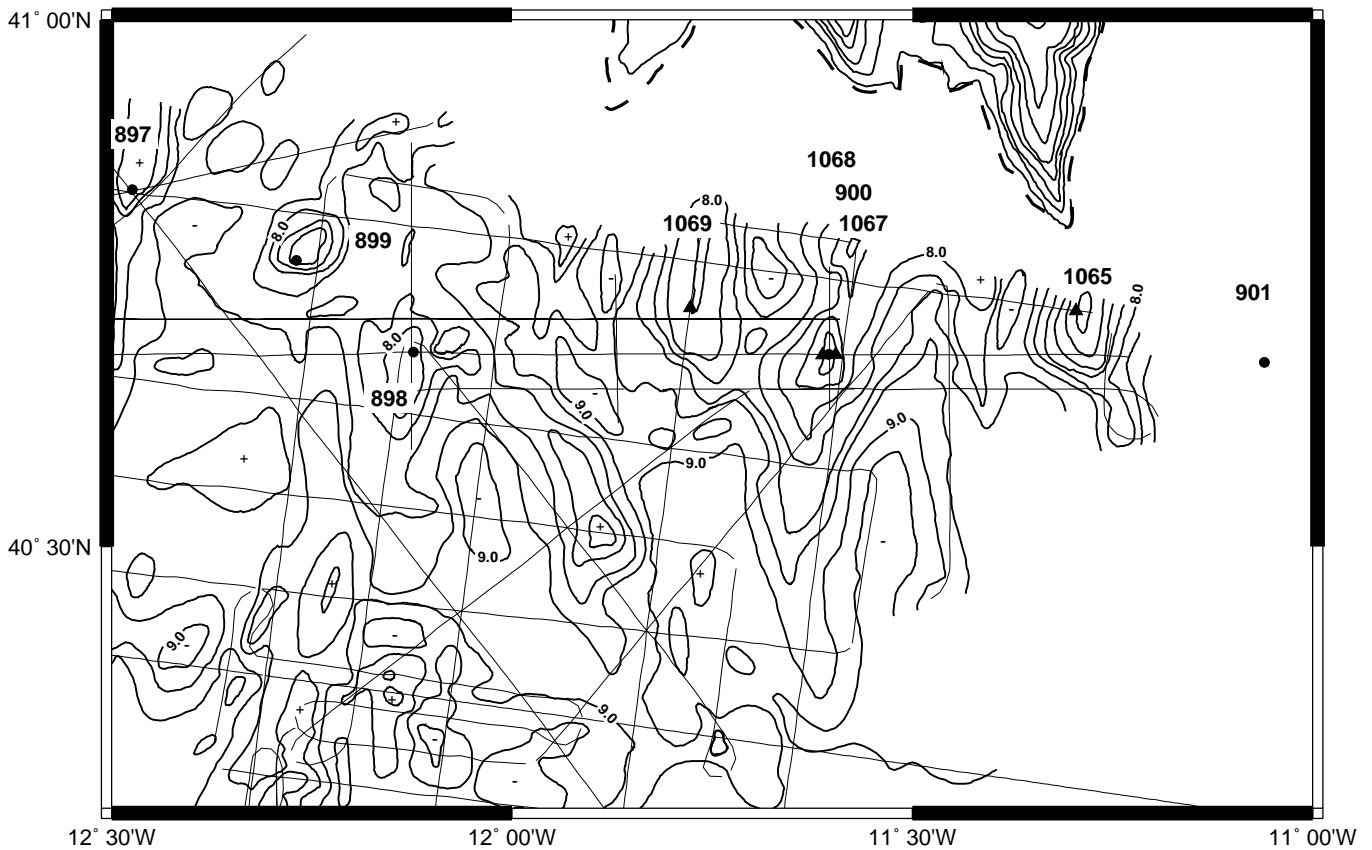


Figure 1. Contour chart of two-way traveltimes (TWT) to basement (contour interval 0.25 s TWT, ~250 m; contouring based on work by C.M. Krawczyk, L.M. Pinheiro, S.M. Russell, and R.B. Whitmarsh) combined with bathymetry of the relief bordering the Iberia Abyssal Plain (contour interval 250 m; courtesy J-C. Sibuet). Dashed line denotes edge of the abyssal plain. Leg 149 and Leg 173 sites are shown by solid circles and solid triangles, respectively. Fine lines are tracks of seismic lines used to contour basement. Selected basement highs and lows are indicated by + and -, respectively.

presence of oceanic basalt, oceanic gabbro or peridotite, and the absence of continental crustal rocks at Site 1069.

Whitmarsh and Miles (1994) and Whitmarsh and Sawyer's (1996) Hypothesis 2 describe a scenario in which the OCT between the peridotite ridge and the thinned continental crust, characterized by gently tilted fault blocks such as at Sites 901 and 1065, consists of blocks of tectonically dismembered continental crust that have been surrounded and impregnated by intrusive, and possibly extrusive, magmatic material. This material is produced by the limited adiabatic partial melting of the asthenosphere, which occurs during the continental rifting. This hypothesis also considers the formation of the OCT in the context of a propagating rift.

A third class of model for the OCT is one in which the OCT consists of tectonically exposed ("unroofed") deep lithospheric levels (lower crust and/or upper mantle). Boillot et al. (1988a) and then other authors (Beslier and Brun, 1991; Brun and Beslier, 1996; Reston et al., 1996) suggested such models for the Galicia margin. Such models were subsequently discussed and applied to the southern Iberia Abyssal Plain by Beslier et al. (1995, 1996), Brun and Beslier (1996), Krawczyk et al. (1996), Pickup et al. (1996), and Whitmarsh and Miles (1995). Some of these models take into account the modes of lithospheric stretching and breakup during the rifting, and predict the exposure of progressively deeper lithospheric levels in the OCT. (1) Beslier et al. (1995) and Brun and Beslier (1996) propose a model of necking of the whole lithosphere that is nearly symmetrical (pure shear), but asymmetrical structures (simple shear) develop internally. Conjugate ductile shear zones develop both in the lower crust and the

upper mantle and lead to the tectonic exhumation of deep lithospheric levels (lower continental or synrift underplated crust and upper mantle) in the OCT, which is a tectonic window opened in the crustal breakup zone (see "Introduction" chapter, this volume). This model does not exclude the possibility that isolated continental blocks lie in the OCT, as "klippes" in the tectonic window. (2) Krawczyk and Reston (Krawczyk et al., 1996) discuss the nature of the OCT in the context of a model of OCT development that is strongly influenced by lithospheric simple shear (Wernicke, 1981). When discussing Leg 149 results, they remark on the apparently systematic exposure, from east to west, of increasingly lower levels of the upper lithosphere. They propose that fragments of the original top-to-the-west lithospheric detachment fault, now dissected by late stage normal faults, occur both east, and possibly west, of Site 900. Thus, Site 1069 may lie on either an upper plate fault block (of continental crust?) or on the lower plate to this detachment, in which case "mantle material could be found at shallow levels" (Krawczyk et al., 1996). Even so, Krawczyk and Reston (Krawczyk et al., 1996) also predict exposed upper mantle peridotite west of Site 1069.

Site 1069 is situated in the southern Iberia Abyssal Plain in a water depth of 5075 m. The site lies on the north-south seismic line CAM134 over the crest of a relatively flat-topped north-south basement ridge (Figs. 3, 4). East-west seismic profile Sonne-22, on which the original proposed site IBERIA-07A lay, passes 1200 m south of the site (Figs. 3, 5). The east flank of the ridge is underlain by a west-dipping reflector that bounds the west side of the next basement high to the east, and its west flank appears to coincide with a similar re-

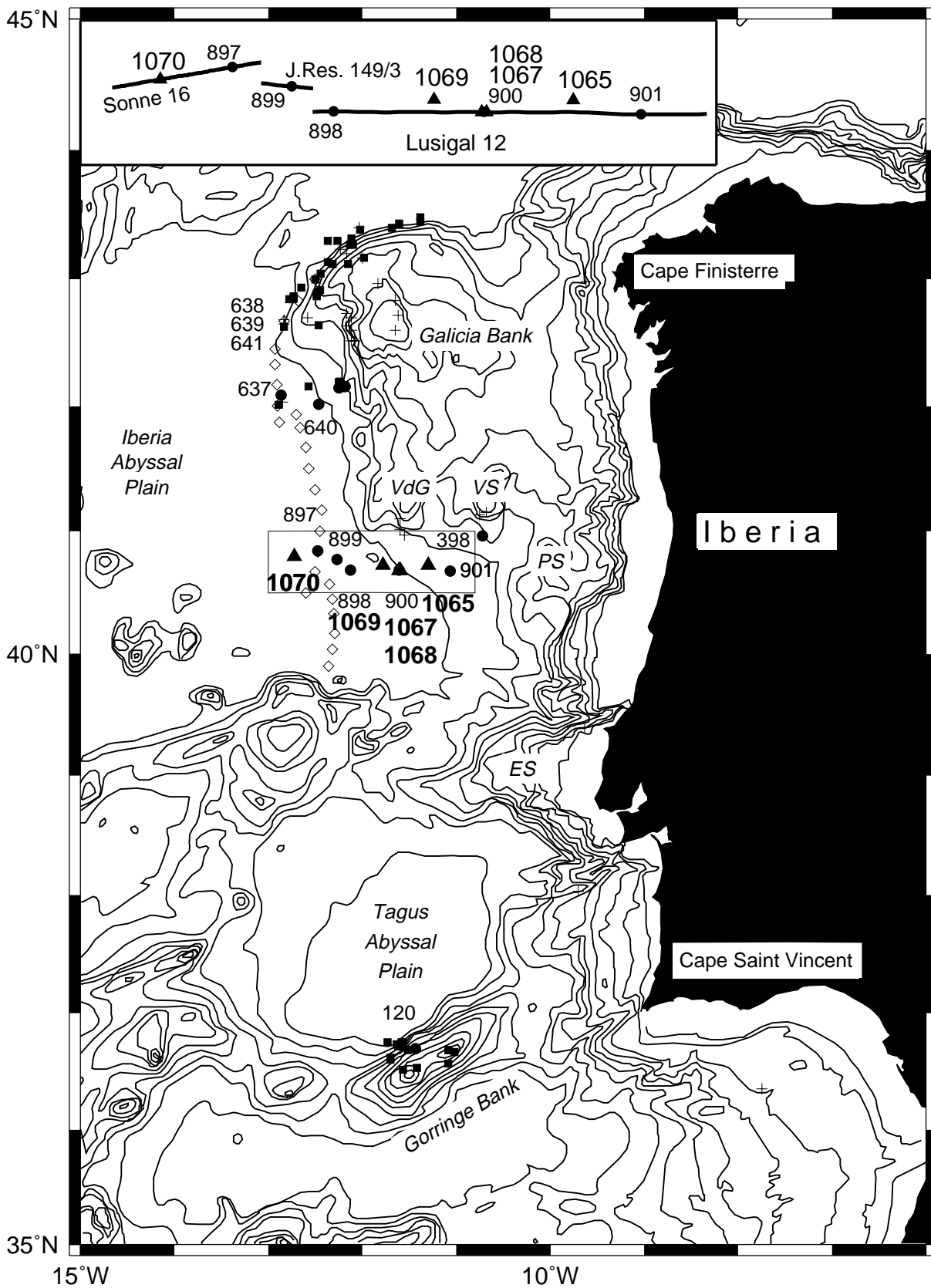


Figure 2. Contoured bathymetric chart of the west Iberia margin. Contours at 500 m intervals. Leg 173 sites are shown by triangles with bold numbers; sites drilled on earlier legs are shown by dots. PS, VS, and VdG correspond to Porto, Vigo, and Vasco da Gama seamounts, respectively. ES denotes the Estremadura Spur. Solid squares and crosses denote rock samples obtained by submersible and dredge, respectively. The inset is a composite of seismic tracks showing the relative locations of Leg 173 and other drill sites.

flector. Both reflectors have the appearance of normal faults. Exactly the same general features are present on the parallel profile CAM144, which crosses the ridge crest 6 km to the north (Fig. 3). A few kilometers southward on the Lusigal-12 line, the high is underlain by a subhorizontal reflector that seems to be the prolongation of the normal fault bounding the next block toward the east. Thus, seismic profiles suggest that the basement ridge is a fault block. Profiles CAM134 (Fig. 4) and Lusigal-12 show that it dies out southward in the OCT. The postrift sediment thickness over the acoustic basement is about 0.86 s TWT (~860 m) thick.

OPERATIONS

Once the location for Site 1069 was reached, a positioning beacon was deployed at 0845 hr on 22 May 1997. A brief remote TV survey was conducted, although the closest subsea cable was estimated to be

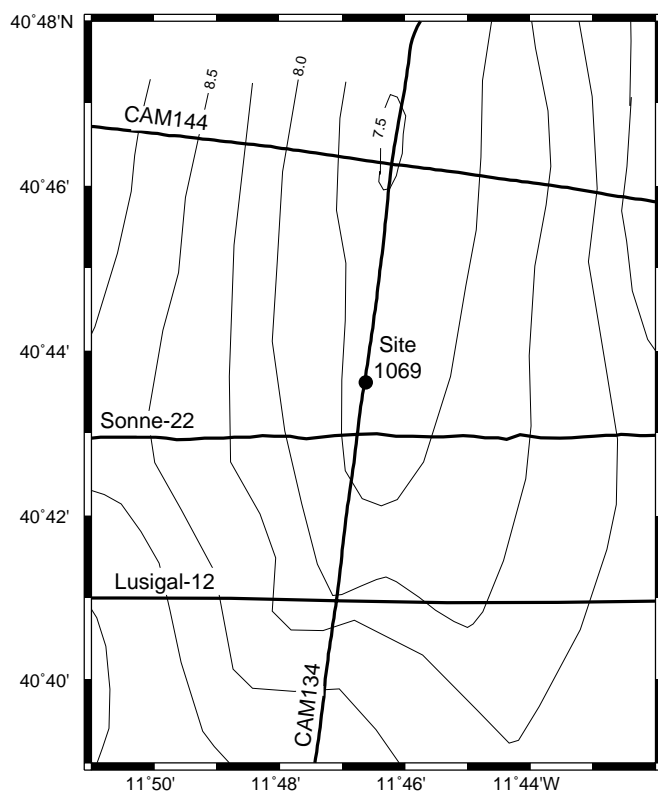


Figure 3. Tracks of multichannel seismic reflection profiles in the vicinity of Site 1069, with contours of two-way traveltime to basement below sea level (contour interval 0.25 s, ~250 m).

at least 11.5 nm away. Hole 1069A was spudded at 1715 hr on 22 May at 5086.0 mbrf with the RCB center bit assembly. The center bit was inspected twice before coring began at 0830 hr on 25 May when a depth of 5804.9 m (718.9 mbsf) was reached (Table 2). Originally, the plan had been to drill to a depth of 810.0 mbsf before initiating coring; however, the steadily decreasing penetration rate (3.4 m/hr) made coring a more attractive option at the shallower depth.

Continuous RCB coring was begun after the center bit was recovered and a core barrel was deployed. Metasedimentary basement rocks were encountered in Core 173-1069A-17R. Penetration proceeded with extremely poor recovery (0–10%) at an average rate of penetration (ROP) of 9.7 m/hr. The ROP was too slow for coring through loose sand and too fast for basement material. To explain the erratic torque ranging from 200–350 amps, lack of fill between connections, and coring times ranging from 35–80 minutes (16.5 to 7.2 m/hr ROP), it is speculated that the unrecovered formation consisted of loosely cemented sands interlayered with harder, more indurated rock. Coring ended at 959.3 mbsf.

Because of the importance of logging the basement section of the hole, extra time was spent making wiper trips and hole conditioning. After an abbreviated first wiper trip (902–593 mbsf), the top drive had to be picked up and a center bit dropped at a depth of 795 mbsf. High torque during reaming was noted from 887 mbsf to the bottom of the hole at 902 mbsf. After coring was completed at a total depth of 959 mbsf, a second complete wiper trip was made to ~100 mbsf. Then the pipe was run back to 773.0 mbsf, where the top drive was picked up and a center bit deployed. It took 4.0 hr to ream back to bottom. A third wiper trip was made to a depth of 767.0 mbsf. On the return trip, an obstruction was encountered at 800 mbsf. The hole was reamed to bottom from this point using the top drive and a center bit. Pump pressure was elevated during the last 15 m. As on the previous wiper trip, sepiolite mud was circulated once total depth was reached. In total, 23 hr was spent in making the three wiper trips, including the mud sweeps. When the center bit was recovered after the last wiper trip, 0.41 m of silty sand and a gray clay ball were found inside the core barrel that had been intruded through the 1-cm-diameter center bit jet. This material was curated as Core 26G, a “ghost” core, and came from an interval extending from 767 to 959 mbsf.

Circulation was immediately lost when the bit was released and the pipe became plugged with back-flow material. The pipe was pulled back to a depth of 862 mbsf, which was the originally intended pipe placement for logging. While attempting to set back the top drive, the pipe was taking 20,000 lb weight, forcing the driller to pull additional pipe back to 800 mbsf. The pipe was then pulled further to 776 mbsf to enable logging of the deepest sedimentary section.

Wireline logging proceeded with the triple combination logging suite, consisting of HNGS/APS/HLDS/DIT/TLT. This tool string was unable to pass a point only 1–2 m beyond the open-ended pipe. After working the tools for a while without success, the effort was abandoned and the tools were recovered. The drill string was advanced 11 m to a depth of 788 mbsf without giving any indication of an obstruction in the hole, and the pipe was then pulled to a depth of

Table 1. Predictions about the nature of the crystalline basement under Site 1069.

Ocean/continent transition model	Prediction	References
Very slow seafloor spreading	Oceanic basalt, oceanic gabbro, serpentinized peridotite	Sawyer, 1994
	Absence of continental crust	Whitmarsh and Miles, 1995 Whitmarsh and Sawyer, 1996
Dismembered continental crust	Continental crust, synrift intrusives or extrusives	Whitmarsh and Miles, 1995 Whitmarsh and Sawyer, 1996
Tectonically exposed (“unroofed”) upper mantle	Serpentinized mantle peridotite, underplated gabbros	Beslier et al., 1995
		Beslier et al., 1996 Krawczyk et al., 1996 Pickup et al., 1996 Whitmarsh and Miles, 1995
2. Lithospheric detachment fault	Upper plate continental crust or lower plate mantle	Krawczyk et al., 1996

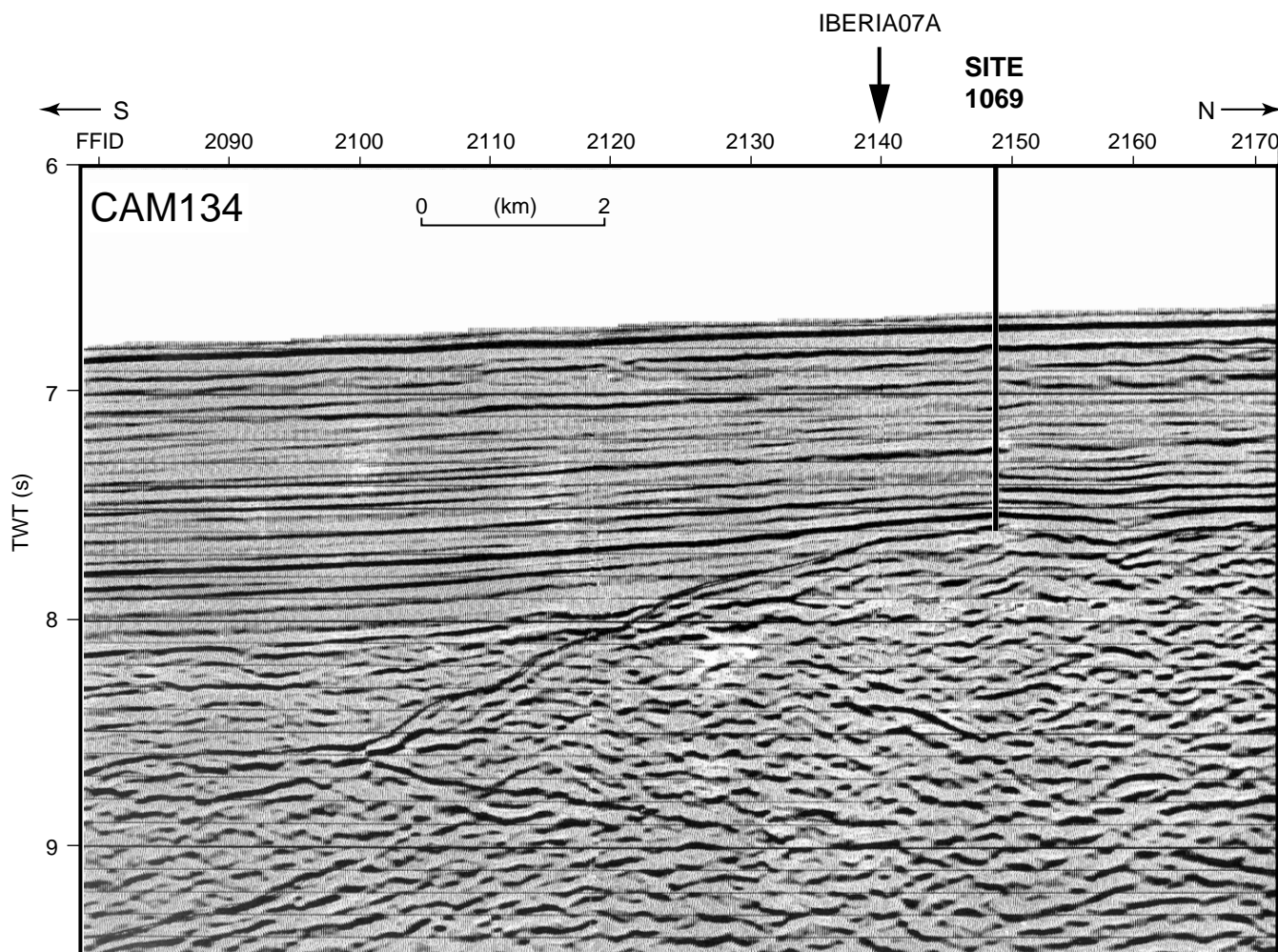


Figure 4. Multichannel seismic reflection profile CAM134 across Site 1069. The profile was collected during *Discovery* cruise 215 in 1995 (Minshull, 1995). Proposed site IBERIA-07A lay at the intersection of this profile and profile Sonne-22.

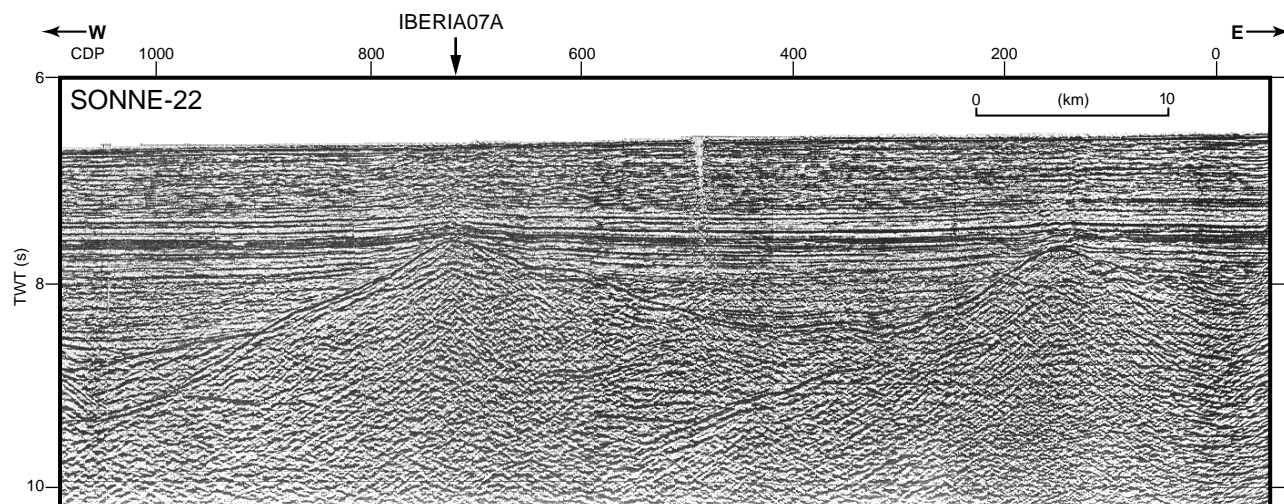


Figure 5. Multichannel seismic reflection profile Sonne-22 across proposed site IBERIA-07A, 1200 m south of Site 1069 (the line was processed by S.L.B. Pickup; courtesy of K. Hinz). Note the fault-block-like natures of the high under Site IBERIA-07A and of the next basement high to the east.

Table 2. Site 1069 coring summary.

Core	Date (May 1997)	Time (GMT)	Interval (mbsf)	Length cored (m)	Length recovered (m)	Recovery (%)
Drilled from 0.0 to 718.8 mbsf						
173-1069A						
1R	25	1330	718.8-728.4	9.6	4.84	50.4
2R	25	1635	728.4-738.1	9.7	3.51	36.2
3R	25	2000	738.1-747.7	9.6	3.55	37.0
4R	26	0045	747.7-757.4	9.7	3.57	36.8
5R	26	0345	757.4-767.1	9.7	2.18	22.5
6R	26	0730	767.1-776.8	9.7	7.14	73.6
7R	26	1045	776.8-786.4	9.6	7.80	81.3
8R	26	1320	786.4-796.0	9.6	6.90	71.9
9R	26	1610	796.0-805.6	9.6	5.91	61.6
10R	26	2000	805.6-815.3	9.7	9.48	97.7
11R	27	0420	815.3-825.0	9.7	5.92	61.0
12R	27	0910	825.0-834.7	9.7	8.32	85.8
13R	27	1220	834.7-844.4	9.7	7.02	72.4
14R	27	1540	844.4-854.0	9.6	7.78	81.0
15R	27	1900	854.0-863.6	9.6	5.27	54.9
16R	27	2300	863.6-873.3	9.7	4.46	46.0
17R	28	0145	873.3-882.9	9.6	0.92	9.6
18R	28	0415	882.9-892.5	9.6	0.15	1.6
19R	28	0730	892.5-902.0	9.5	0.09	0.9
20R	28	1640	902.0-911.6	9.6	0.19	2.0
21R	28	1940	911.6-921.3	9.7	0.44	4.5
22R	28	2220	921.3-930.9	9.6	0.25	2.6
23R	29	0055	930.9-940.1	9.2	0.03	0.3
24R	29	0420	940.1-949.7	9.6	0.09	0.9
25R	29	0700	949.7-959.3	9.6	0.08	0.8
26G	29	2330	767.0-959.3	0.0	[0.41]	[0.2]
Cored totals				240.5	95.89	39.9
Drilled				718.8		
Total				959.3		

Note: Ghost Core 26G was recovered from 767.0 to 959.3 mbsf during a wiper trip.

An expanded version of this table with individual section lengths is on CD-ROM, back pocket, this volume.

102 mbsf. While pulling pipe to this position, back flow was observed coming from the drill pipe at a depth of ~651 mbsf. Barite-weighted gel mud was spotted in the pipe at a depth of ~564 mbsf and this solved the back-flow problem. The hole was filled with sepiolite mud and rig-up for logging began. The triple combination logging suite was again run, this time reaching a depth of 764 mbsf. Logging was conducted up from that point. Surprisingly, the hole was in good shape and the caliper logs showed a hole only slightly out of gauge (12–14 in). The second logging run consisted of the NGT, SDT, and FMS. These tools were able to reach the same depth (780 mbsf); however, a tool fault made the FMS inoperable and the tools had to be pulled out of the hole. At 0600 hr, 31 May, rig down was completed and wireline logging operations in the hole were concluded. The pipe was pulled clear of the seafloor at 0615 hr and the positioning beacon was released and recovered at 0845 hr. The pipe trip was completed, and the ship was secured for transit to Site 1070 (proposed site IBERIA-10A). Departure from the site began at 1445 hr 31 May 1997.

LITHOSTRATIGRAPHY

A 155-m-thick sedimentary succession was cored in Hole 1069A. Coring continued for a further 85.5 m, over which recovery was extremely poor (<3%), but the drilling rate was very rapid. Pieces of metasedimentary rock, which may be large clasts from a sediment possessing a soft matrix (clay or sand), were recovered over this deeper interval.

The sedimentary succession above the pieces of metasedimentary rock consists of a middle Eocene to upper Campanian turbidite-hemipelagite succession, overlying upper Berriasian to ?lower Valangin-

ian nannofossil chalk and ~10 cm of ?Tithonian clay (disturbed by drilling). The thin clay is underlain by Upper Jurassic conglomerate (recovered only as pieces) that contains clasts of shallow-water limestones and metasedimentary rock.

A simplified summary of the lithostratigraphy cored at this site and other Leg 173 and Leg 149 sites is shown in Figure 6. The middle Eocene to upper Paleocene succession drilled at this site is lithologically very similar to that of the same age encountered at three sites situated 15–17 km to the east (ODP Sites 1068, 900, and 1067). It is assigned, therefore, to the lower part of Subunit IIB as defined at Site 900. The lower Paleocene to upper Campanian succession at Site 1069 is characterized by an increase in the frequency, proportion, and thickness of sandstone lithologies within the turbidite-hemipelagite-contourite succession and so is designated as Subunit IIC.

The Lower Cretaceous 2.4-m-thick nannofossil chalk at Site 1069 is assigned to Unit IV. Although it is lithologically dissimilar to the Lower Cretaceous deposits in Unit IV at Sites 897 (Shipboard Scientific Party 1994a), 899 (Shipboard Scientific Party, 1994c), and 1068 (“Site 1068” chapter, this volume), it does show evidence of mass wasting in its slumped and fractured lower part and so, in this respect, is similar to Unit IV at these Leg 149 sites. The nannofossil chalk comprising Unit IV is interpreted as a slump overlain by pelagic drape preserved in a small depression near the summit of the acoustic basement ridge imaged on seismic lines.

The ~10 cm interval of Upper Jurassic (?Tithonian) clay at Site 1069 is lithologically similar to sediments of the same age drilled at Sites 901 (Shipboard Scientific Party, 1994e) and 1065 (“Site 1065” chapter, this volume). The limestone clasts within the pieces of conglomerate recovered beneath the Upper Jurassic clays are composed of lithologies similar to Tithonian–Berriasian carbonates recovered at Site 639 (Shipboard Scientific Party, 1988) and to clasts occurring within the conglomerates in Subunit VA at Site 1065. Therefore, the clay and limestone conglomerates are designated as Subunit VA at Site 1069. As explained later in this section, pieces of metasediment in Cores 173-1069A-17R to 25R may be samples of clasts from a sedimentary formation possessing a soft matrix that was not recovered in the cores, and so they are designated as Subunit VB.

Rotary coring (RCB) was employed in Hole 1069A, resulting in moderate recovery of the sediments in Units II (62%) and IV (46%) and very poor recovery of Unit V (<10%). Coring began within Unit II at 718.8 mbsf, and terminated at 959.3 mbsf. Figure 7 summarizes the core recovery, lithologies, and ages of the lithostratigraphic units recognized in Hole 1069A. The ages, lithologic compositions, overall colors, facies and depositional environments, boundary depths, and cored intervals of Units II, IV, and V are summarized in Table 3.

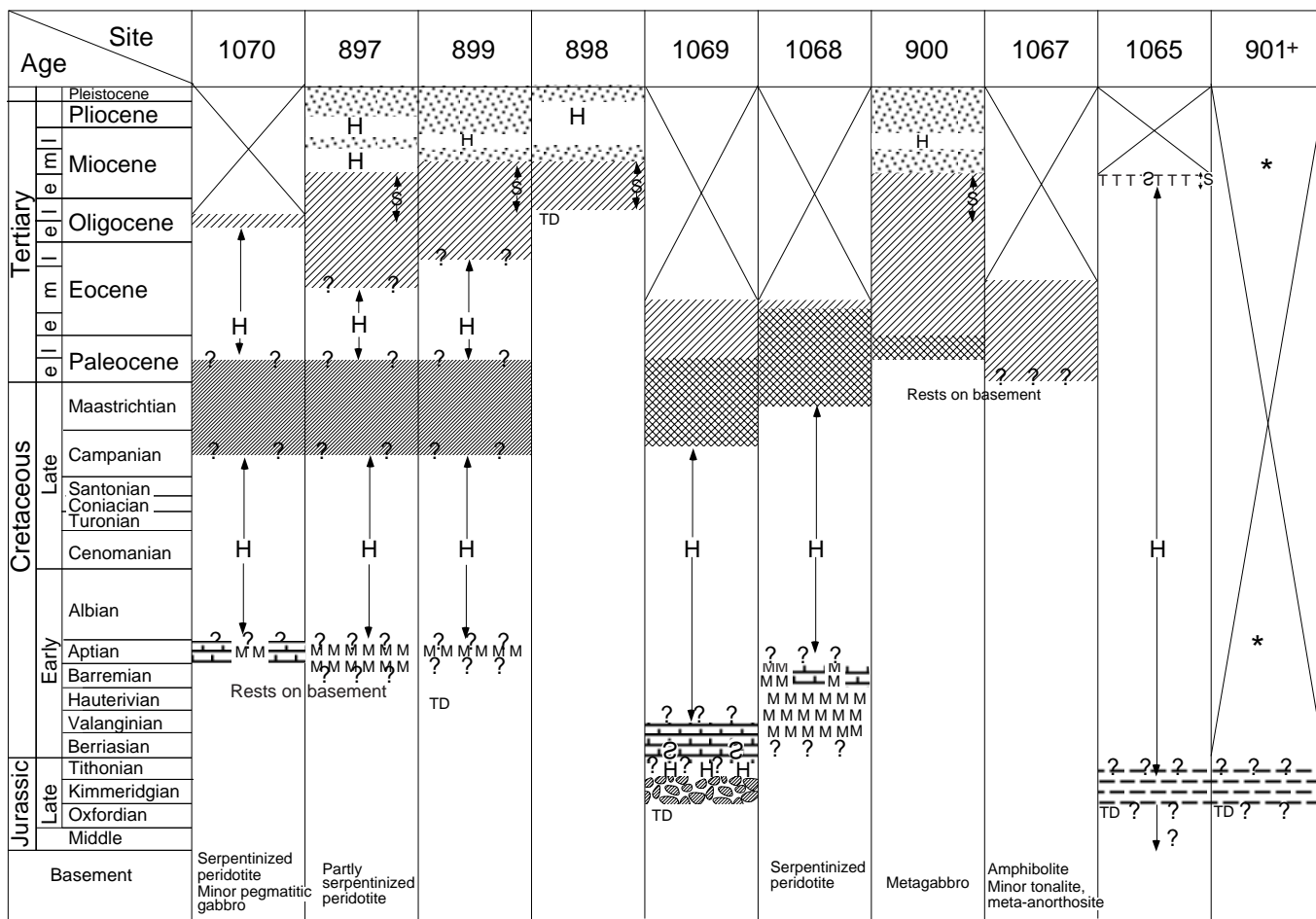
Unit II

Interval: 173-1069A-1R-1, 0 cm, through 173-1069A-16R-2, 44 cm
Depth: 718.8–865.54 mbsf
Age: middle Eocene to late Campanian

General Description

Recovery averaged 62% and ranged from 22.5% to 97.7% over the 147-m-section cored. The sediment is generally firm to hard, and core disturbance is typically limited to slight or moderate fracturing. Slight biscuiting occurs in Core 173-1069A-3R.

The four lithologic motifs shown in Figure 8 are end-members of a spectrum of lithologic associations and thickness variations observed in Unit II. These motifs are almost identical, with the exception of Motif 1, to those described in the “Lithostratigraphy” section of the Site 1068 chapter, this volume. Consequently, descriptions are only given here of features in Unit II unique to Site 1069.



		Lithostratigraphic Units			Lithostratigraphic Units
	Siliciclastic turbidites and nannofossil pelagites [■]	I		Nannofossil chalk	IV
	Nannofossil chalk	II		Mass flow deposits: Olistostromes (Sites 897, 899) Serpentinite breccias (Site 1070, 899) Amphibolite, etc. breccias (Site 1068)	
	Thin motifs* Carbonate turbidites and noncarbonate hemipelagites		III		Metasediment and shallow-water limestone pieces (? clasts)
	Thick motifs* (15-100 cm)	III			Clay, claystone with thin sandstones and conglomerates
	S Siliceous allochems				
	Red brown claystones (with sandstones and conglomerates at base at Sites 897, 899)				

Not cored S Slumps H Hiatus TD Total depth *, +, ■ See caption

Figure 6. Simplified summaries of stratigraphic successions cored at Leg 149 and Leg 173 sites. Unit III is almost barren of fossils and so its age is very uncertain. + = Unit V as shown in Site 901 was designated by Shipboard Scientific Party (1994e) as Unit II, following the normal ODP practice of numbering units sequentially downhole; * = a washed core recovered Miocene nannofossil ooze and a 5-mm-thick layer of gray clay of Aptian age. Solid square = nannofossil pelagites dominant at Site 900. Solid circles = "Motifs" refers to types of upward-darkening sequences shown in Figure 2 of the "Site 1068" chapter and Figure 8 (this chapter). The cross-hatched symbols on the summary chart indicates that both thin (Motif 2) and thick (Motif 1) sequences are present.

Leg 173 Hole 1069A

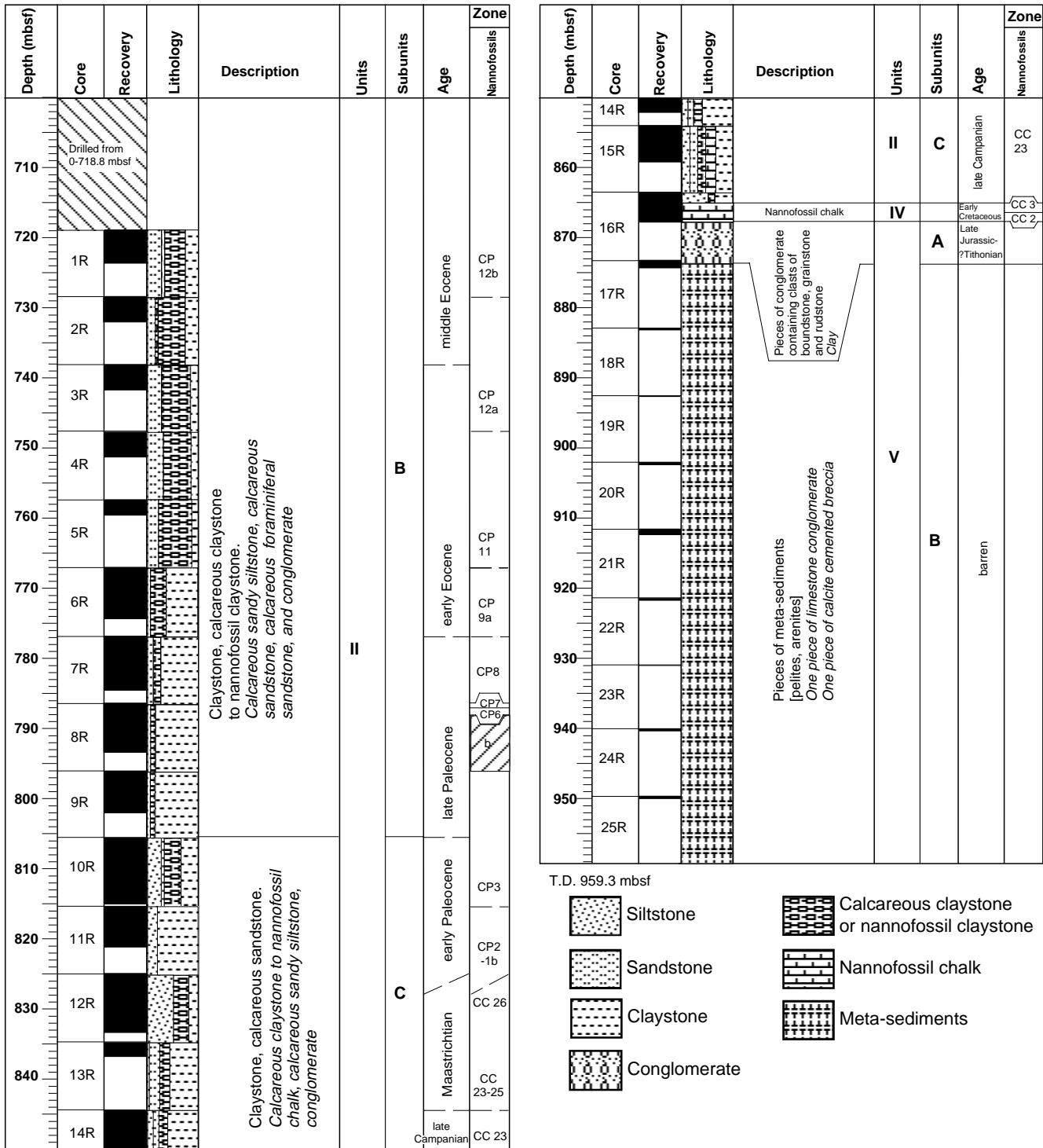


Figure 7. Summary lithostratigraphic column for Hole 1069A. Minor lithologies are listed in italics.

Leg 173 Hole 1069A

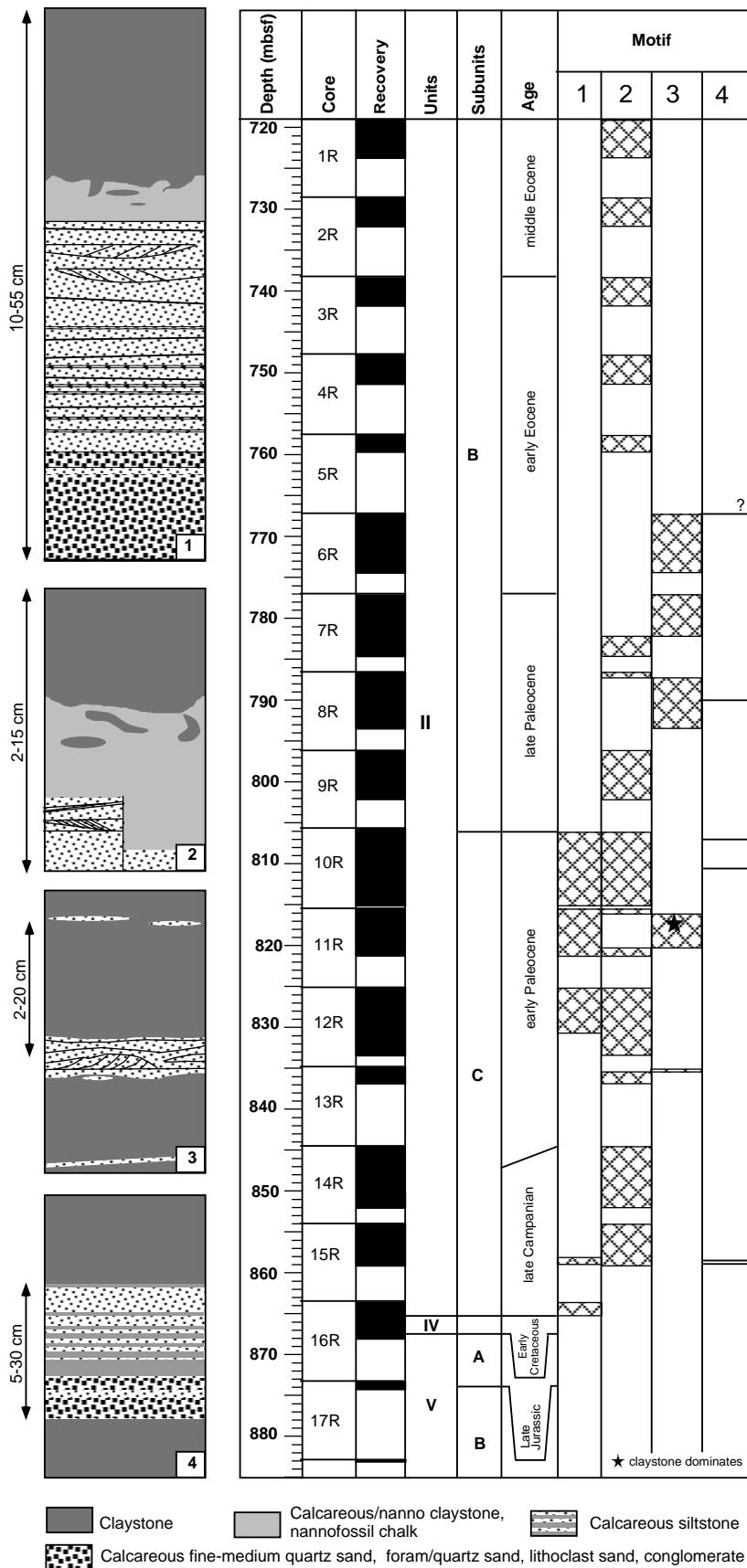


Figure 8. Lithologic motifs and their distribution in lithostratigraphic Unit II at Site 1069. The four motifs shown on the left side of the figure are idealized end-members of a spectrum of lithologic associations observed in the cores. Motifs 1 and 2 are variants of upward-darkening sequences. Motif 1 is much thicker than the others (Fig. 10B, C), and dominated by either (1) foraminiferal sands, (2) carbonate sands, (3) calcite-cemented siliciclastic sandstones, or (4) lithic sandstones and conglomerates. These lithologies may rest directly on the claystone of the underlying motif, or be underlain by thin laminae or thin to medium beds of calcareous sandy siltstone containing parallel, wavy, lenticular, or cross-laminae. Motif 2 sequences are up to 15 cm thick and may contain basal intervals of calcareous sandy siltstone up to 6 cm thick (Figs. 9A, B, 10A). The sandy siltstone lithology is absent in some Motif 2 sequences (Fig. 9B). Motif 3 does not contain any fine-grained calcareous lithologies: a basal calcareous sandy siltstone interval (<2 cm thick), containing structures similar to those occurring in the same lithology in Motifs 1 and 2, is overlain by brown claystone. Motif 4 also consists of calcareous siltstone/sandstone (5–30 cm thick) intervals that exhibit sharp bases and tops (Fig. 9C, 10C, D). They contain similar structures to those occurring in the coarser basal parts of the other motifs. The right side of the diagram shows the distribution of the four motifs in the cored interval of Unit II. The sandstones of Motif 4 are shown as lines in column 4.

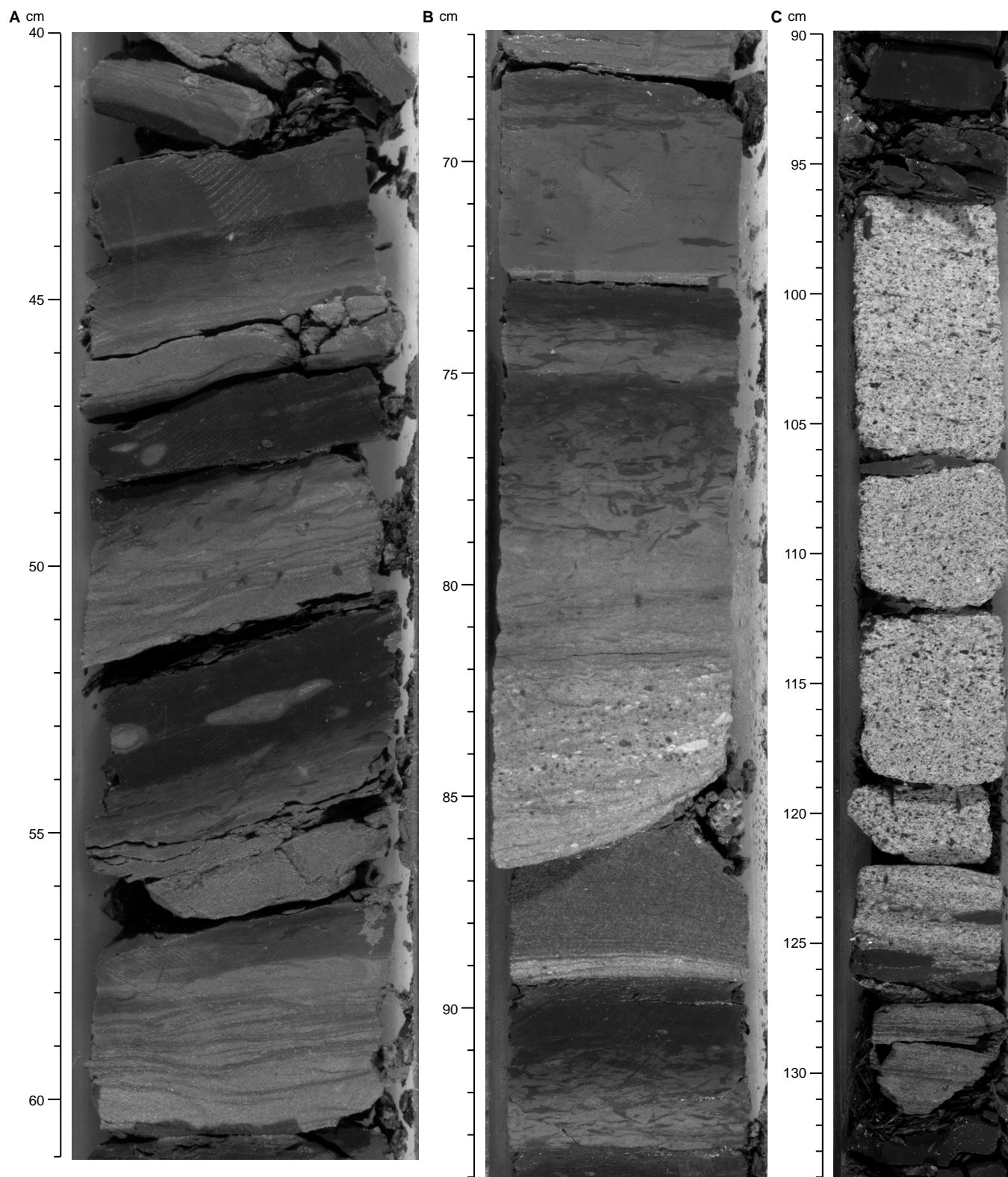


Figure 9. Core photographs of Motifs 2 and 4 in Subunit IIB in Hole 1069A. **A.** Interval 173-1069A-4R-1, 40–61 cm, showing thin Motif 2 upward-darkening sequences containing relatively thick basal calcareous sandy siltstone intervals. Sandy silt-filled burrows occur at 53 cm within hemipelagic claystone; the burrows were probably filled with sediment when the overlying sandy silt was deposited. **B.** Interval 173-1069A-9R-3, 67–94 cm. Motif 2 upward-darkening sequences lacking a basal sandy siltstone interval occur between 90.5–93 and 73–75 cm. The sharp curved contact between a sandy siltstone with horizontal to upwardly convex laminae between ~86–89.5 cm and the overlying normally graded calcareous sandstone was probably caused by core disturbance. The coarser base of the sandstone contains dark clasts of metasediment (pelites and arenites) and lighter colored clasts of shallow-water limestones. **C.** Interval 173-1069A-8R-3, 90–134 cm. A Motif 4 coarse calcareous sandstone showing a sharp top and base and very faint parallel laminae. The clasts' composition is similar to that described in (B).

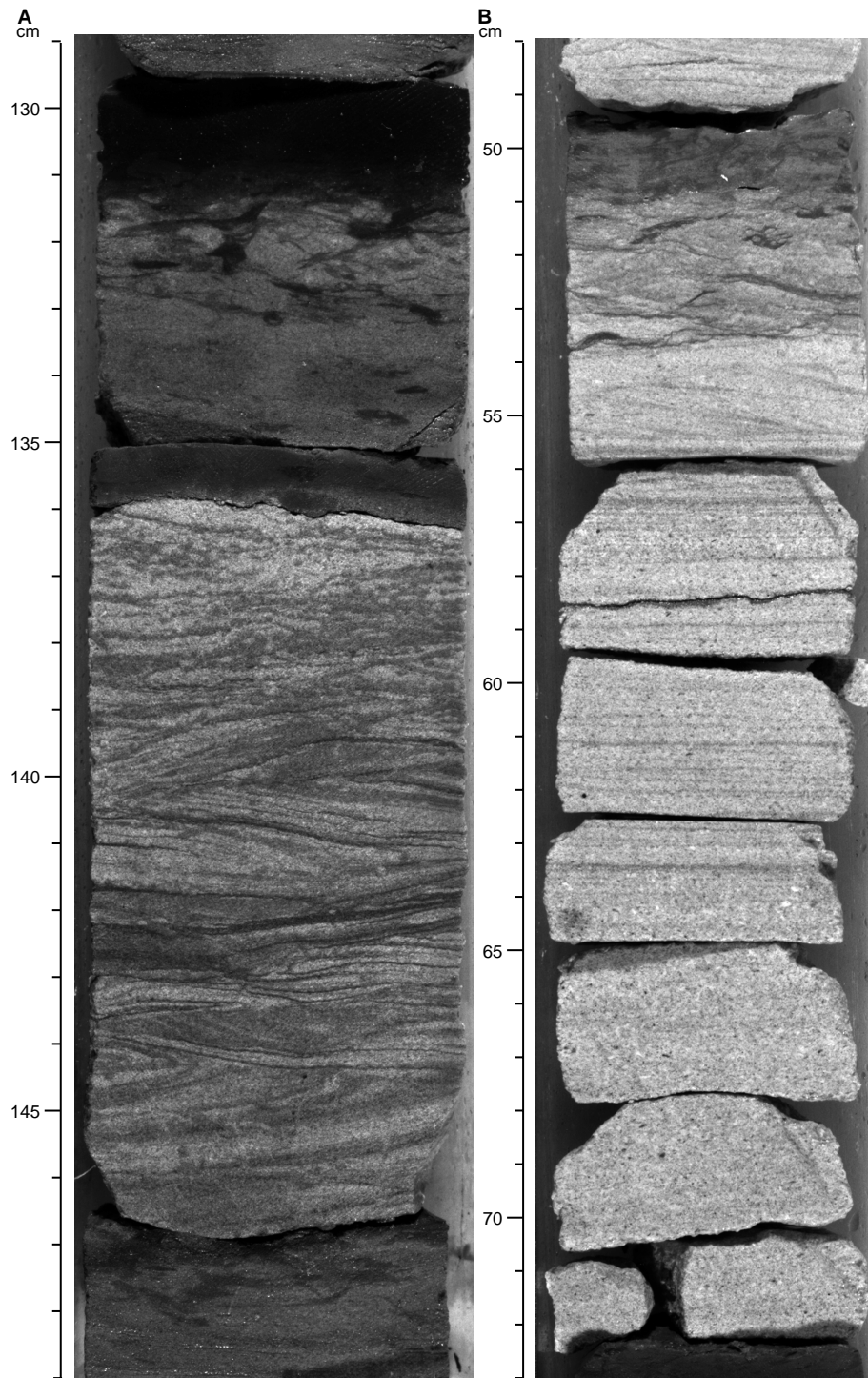


Figure 10. Core photographs of sandstones in Subunit IIC. **A.** Interval 173-1069A-10R-3, 129–149 cm. A sharp-topped Motif 4 sandstone between 136–146.5 cm contains trough cross-lamination (seen oblique to the current flow) overlain by an interval (136–138.5 cm) showing disruption of laminae caused by either burrowers or water escape. The sandstone is overlain by calcareous claystone to nanofossil chalk, above which occurs a Motif 2 upward-darkening sequence (129.5–135 cm). **B.** Interval 173-1069A-10R-5, 48–73 cm. A normally graded coarse lithic carbonate sandstone (identified in thin section as a foraminiferal peloid grainstone) showing turbidite T_a – T_c units. Between 65–72 cm, it is massive to faintly laminated (T_a/T_b), parallel laminated between 55.7–65 cm (T_b), and cross to lenticular laminated (T_c) between 51–54 cm. Lenticular bedding (possibly trough cross-lamination) showing slight bioturbation occurs at the top of the sand bed between 51–54 cm and is also part of the T_c unit. It is overlain by bioturbated calcareous sandstone, above which occurs the base of another sandstone bed (at 49.5 cm). (Continued next page.)

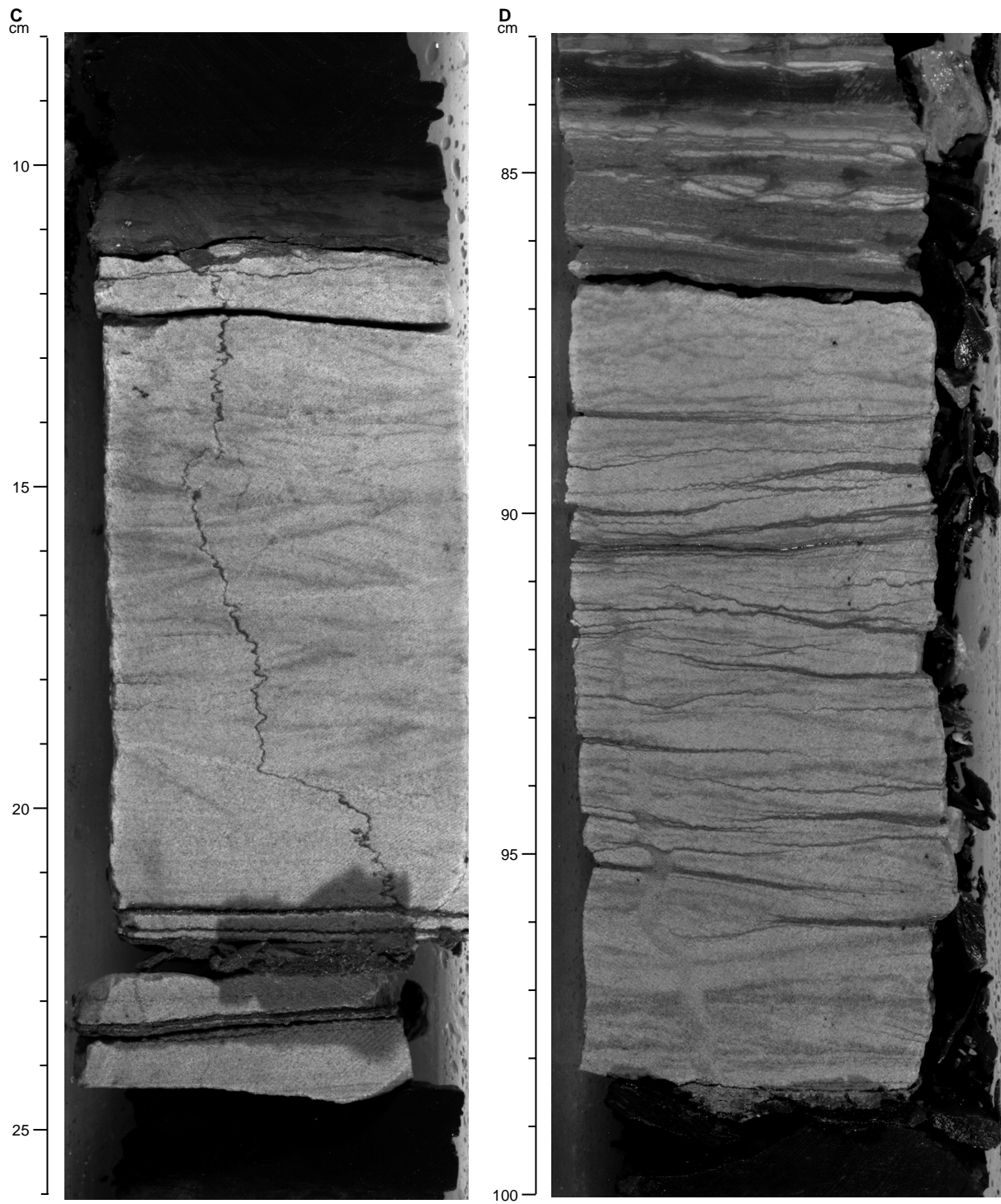


Figure 10 (continued). **C.** Interval 173-1069A-10R-8, 8–26 cm. A sandstone at the base of a Motif 1 sequence shows parallel lamination at the base (20–24.5 cm) overlain by trough cross-lamination. The boundary with the overlying calcareous claystone to nannofossil chalk is slightly gradational, and the fine-grained lithology is burrowed down a few millimeters into the sandstone. The claystone at the top of the sequence extends beyond the photograph a further 3 cm. The sandstone is cut by a stylolite oriented perpendicular to the bedding. **D.** Interval 173-1069A-11R-4, 83–100 cm. A sharp-topped Motif 4 sandstone (86.7–98.2 cm) showing an oblique section through trough cross-lamination, overlain by a disrupted interval (caused by burrowing or water escape). On the left side of the core a vertical slightly sinuous burrow extends from 92 cm to the base of the sandstone.

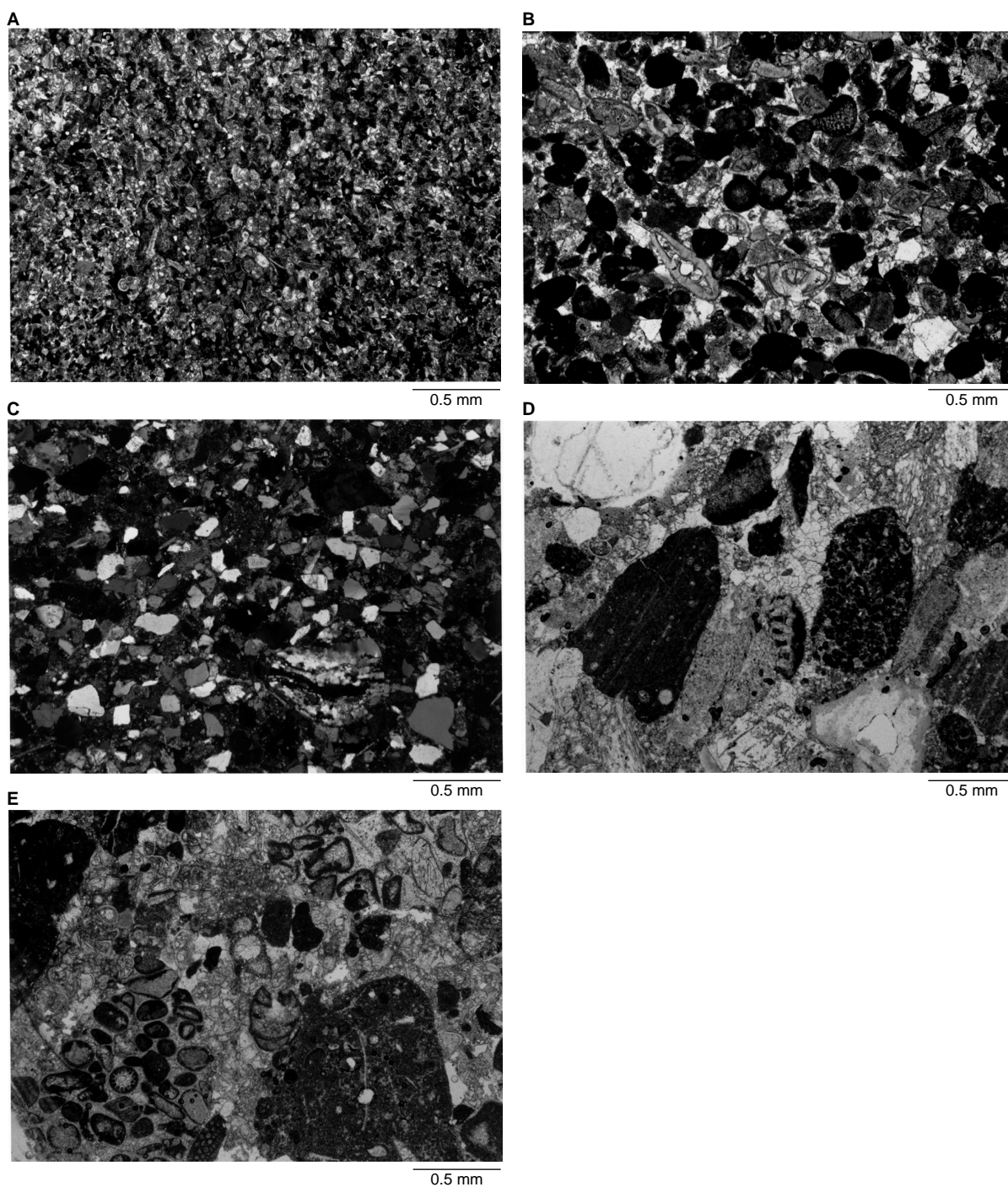


Figure 11. Photomicrographs of representative Unit II sand sediments. **A.** Foraminiferal-peloidal packstone/chalk (Sample 173-1069A-11R-1, 41–44 cm, plane polarized light). Planktonic foraminifers occur in a micritic matrix, which also contains rare silt-sized quartz clasts. **B.** Peloidal packstone (Sample 173-1069A-7R-5, 35–38 cm, plane polarized light). The sediment also contains planktonic foraminifers, micrite-coated skeletal fragments, and quartz clasts. **C.** Calcareous siliciclastic sandstone (Sample 173-1069A-15R-4, 17–21 cm, crossed polars). Subangular fine-grained quartz clasts, plus one coarse polycrystalline quartz clast, occur in a sparite cement; the black ovoid-shaped grains are peloids. **D, E.** Fine-grained conglomerate (Sample 173-1069A-13R-2, 50–54 cm). (D) From left to right across the middle of the photograph the following types of clast occur: chalk (micrite) with calcispheres or calcitized *Rhaxella* sponge spicules (the parallel lines are scratch marks on the thin section); a pelite clast shows a flat contact with the chalk clast on the left; a micrite-coated shell fragment occurs to the left of the pelite; above the peloid grainstone clasts are several closely packed pelite clasts. To the right of the grainstone occurs another pelite clast, above and below which are two micrite clasts showing poorly developed cryptalgal structure. At the top left there is a hole in the slide, beneath which occurs a quartz clast, and next to that are planktonic foraminifers. Granular calcite cement occurs in the center. (E) In between three relatively large limestone clasts (intraclast-skeletal grainstone at bottom left; the other two clasts are composed of cryptalgal peloidal micrite) occurs calcite cement and smaller allochems of micritized skeletal debris, thin-shelled planktonic foraminifers and two benthic foraminifers (in the center of the photograph).

similar to that described at Sites 898 (Shipboard Scientific Party, 1994b) and 900 (Shipboard Scientific Party, 1994d), and Sites 1067 and 1068 (this volume). Petrographic studies, therefore, focused on 23 thin sections of the sandy and conglomeratic intervals.

Four types of sandstone are recognized (Fig. 11): (1) foraminiferal sands, (2) carbonate sands, (3) calcite-cemented siliciclastic sandstones, and (4) lithic sandstones and conglomerates. These are end-members of a spectrum of lithologies that may be mixed together in one thin section or bed, or may be juxtaposed in alternating laminae, or grade vertically into one another.

Foraminiferal sands are dominated by whole and/or fragmented planktonic foraminifers 0–3 mm across. Foraminiferal tests are almost all intact when preserved in a micritic (chalky) matrix, but the proportion of fragmented tests increases when peloids and quartz clasts are also present. Light brown phyllosilicate clay-rich lenticles (~1.0 mm wide, 0.15 mm thick) are sometimes concentrated in laminae within varieties containing common quartz clasts. They are most likely small burrows, but the possibility of them being clasts cannot be totally ruled out. Calcite-cemented siliciclastic sandstones contain peloids and other skeletal debris, plus trace to common amounts of quartzose fine sand and silt. Syntaxial cement rims around presumed echinoderm skeletal fragments are a common feature. Glauconite grains up to 0.15 mm were observed in only one thin section of peloidal foraminiferal sandstones in interval 173-1069A-12R-2, 124–127 cm. They appear as dark green clasts in the core and are therefore difficult to distinguish from pelite basement clasts that have the same color, and are commonly present in medium- to coarse-grained sands throughout Unit II.

Carbonate sands consist of calcite-cemented peloidal and intraclastic packstones and grainstones, ranging in grain size from fine to the finer end of coarse sand (<0.7 mm). They also contain trace to common amounts of planktonic and benthic foraminifers, and other skeletal debris (echinoderms and bivalves). Rare clasts composed of single and polycrystalline quartz and pelites are also present.

Most beds of calcite-cemented siliciclastic sandstones contain fine-grained, moderately to poorly sorted, angular to subangular quartz clasts. Peloids and skeletal debris are usually present in rare to common amounts. Calcite microspar forms the cement, and larger calcite crystals commonly occur as syntaxial overgrowths around skeletal fragments. Coarser grained sandstones show a bimodal distribution of siliciclastic clasts. Fine- to medium-grained grains dominate, but coarse sand-sized single and polycrystalline quartz clasts occur, with rare amounts of coarse feldspar clasts, peloids, and skeletal debris. Broken planktonic foraminifers may be present within the coarse calcite cements.

Coarse-grained lithic sandstones and granule conglomerates contain lithic clasts composed of shallow-water carbonate sediments and metamorphic rocks. They are cemented by calcite spar, within which may occur fine quartz sand and/or broken foraminifer tests. Carbonate clasts include cryptalgal boundstones containing a variety of encrusting organisms, peloid and intraclast grainstones, bivalve debris, echinoderm plates (almost always overgrown by syntaxial cement rims), and rare coated grains and oncooids. Most of the clasts composed of metamorphic rock are fragments of pelite, but meta-arenites are also present, and one clast of biotite hornfels was observed in a thin section of Sample 173-1069A-12R-6, 130–134 cm.

Depositional Processes

The interpretation of the upward-darkening sequences as calcareous turbidites overlain by hemipelagic clays given in the site reports for Holes 898A and 900A (Shipboard Scientific Party, 1994d, 1994b) and Holes 1067A and 1068A (this volume) applies to the Unit II sediments in Hole 1069A. However, thick intervals of carbonate mud commonly observed within the upward-darkening sequences in Subunit IIC in Hole 1068A (Motif 1; Fig. 8) are not present in the Unit II succession cored in Hole 1069A. Nonetheless, in the latter hole Sub-

unit IIC does contain significantly thicker (as much as 50 cm thick) Motif 1 sequences than the “normal” Motif 2 upward-darkening sequences (Motif 1 in Figs. 8, 10). This is because their basal sand interval is much thicker, which indicates that some turbidity flows arriving in the area around Site 1069 were carrying a greater proportion of sand-sized material than those feeding the Site 1068 area. This difference may be explained several ways. The thicker, sandier turbidites cored at Site 1069 could be more proximal than the thicker carbonate-mud dominated turbidites encountered in Hole 1068A. Alternatively, local sea-bottom topography (influenced by basement highs and the differential compaction of sediments around and above them) could have affected the proportions of fine and coarse sediments deposited by the flows. Another possibility is that the turbidity flows transporting sediment could have originated in different areas: the sediment supplied from one area was largely carbonate mud (Motif 1 at Site 1068), whereas that from the other area was sand (Motif 1 at Site 1069).

The petrographic composition of the sands in Motifs 1, 2, and 4 at Site 1069 indicates that there were three different sources of sediment: (1) planktonic foraminifers concentrated by current winnowing subsequent to settling to the ocean floor as planktonic “rain”; (2) siliciclastic quartz and lithic (metasediments) sand derived from exposed basement rocks; (3) exposures of lithified shallow-water limestones.

The sharp tops to some of the sands within Motif 4 upward-darkening sequences and the concentration of planktonic foraminifers in the sands at the base of turbidites suggests some reworking by contour currents.

Unit IV

Interval: 173-1069A-16R-2, 44 cm through 16R- 3, 123 cm.

Depth: 865.54 to 867.83 mbsf

Age: ?early Valanginian to late Berriasian

General Description

Unit IV is 2.3 m thick and occurs only in Core 16R (Fig. 12). The boundary between Subunit IIC and Unit IV occurs at Section 173-1069A-16R-2, 44 cm (865.54 mbsf) and is defined at the first occurrence of dusky yellow nanofossil chalk of Unit IV. The contact with Unit IV is sharp, but there is no difference in dip between the two formations (Fig. 13).

The upper Berriasian to ?lower Valanginian nanofossil chalk is dusky yellow at the top and changes to mottled dusky yellow to light olive brown below Section 173-1069A-16R-3, 45 cm. Slightly inclined bedding is indicated by faint irregular color bands that dip ~10°–20°. These are sometimes cross-cut by subhorizontal laminae, which are probably products of diagenesis. Isolated shell fragments (<1 cm long) occur in Section 173-1069A-16R-2 (Fig. 13A). Microfaults occur in interval 173-1069A-16R-2, 95–126 cm. In interval 173-1069A-16R-3, 46 to 122 cm, the nanofossil chalk is mixed with sand- and gravel-sized extraformational clasts similar in composition to the pieces of limestone conglomerate and metasediment occurring in Subunit VB. Over the same interval, the sediments are disturbed by brecciation and slumping (see “Structural Geology” section, this chapter, and Fig. 13B). The deformation could have been caused by drilling disturbance but, given that the core is in several coherent pieces (one of which is 20 cm long), it was more likely produced by sediment slumping. The occurrence of thin deformed layers of sand and gravel within the slumped interval supports this conclusion.

Depositional Processes

The nanofossil chalk of Unit IV at Site 1069 is a pelagic deposit occurring on a slightly inclined slope near the summit of a ridge in the acoustic basement (Fig. 14). The top of the acoustic basement is

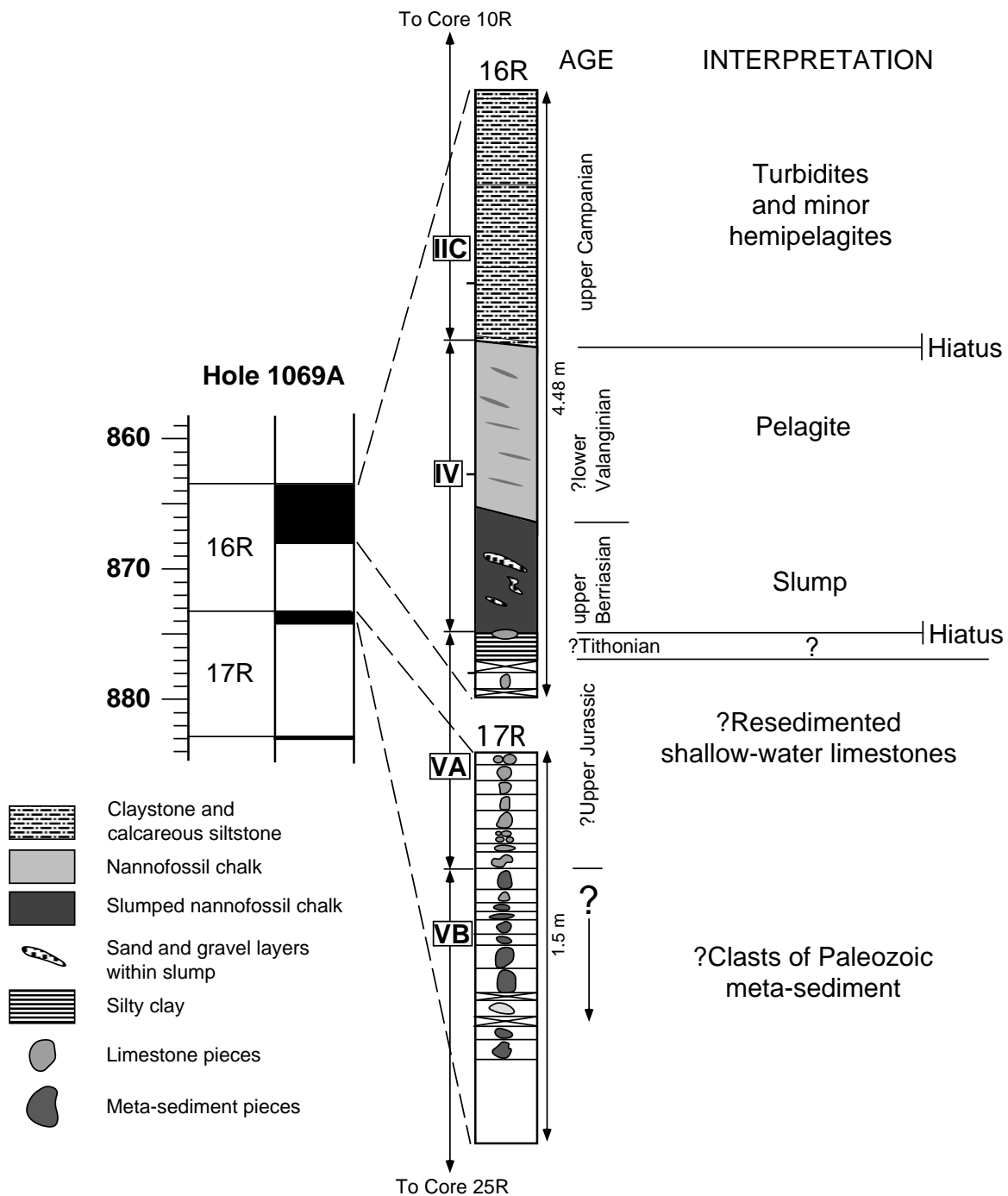


Figure 12. Summary of the relationships between Units II, IV, and V in Cores 173-1069A-16R and 17R. The left side of the diagram is an extract from Figure 7 showing core depths (mbsf) and recovered intervals (shown black). The right-hand column shows the key features present in Cores 16R and 17R. Note that (1) the sketches summarizing the content of the two cores are drawn at different scales, (2) the width of the cores is exaggerated, and (3) the shapes of the pieces of limestone and metasediment are only approximate.

presumed to coincide with the top of Unit V. The occurrence of a slumped interval at the base of Unit IV suggests that initially the sediments accumulated on a slight slope, became unstable and slumped downslope, picking up loose clasts of limestone and metasediment from the underlying Unit V that are now incorporated within the slump.

But why at Site 1069 is there only a pelagic drape of Berriasian to Valanginian age? If, as suggested by Wilson et al. (1996, see below),

Hauterivian/possible Valanginian to Turonian sediments accumulated at lower elevations around the basement high (Fig. 14), why were no pelagites, or any other types of sediment, preserved at this site until the late Campanian? The answer may be that the pelagic sediments filled a small depression that is too small to image seismically. Once such topographic irregularities had been smothered by pelagic sediments, no small depressions would remain, and so later sediments would be transported basinward by gravity-driven transport processes.

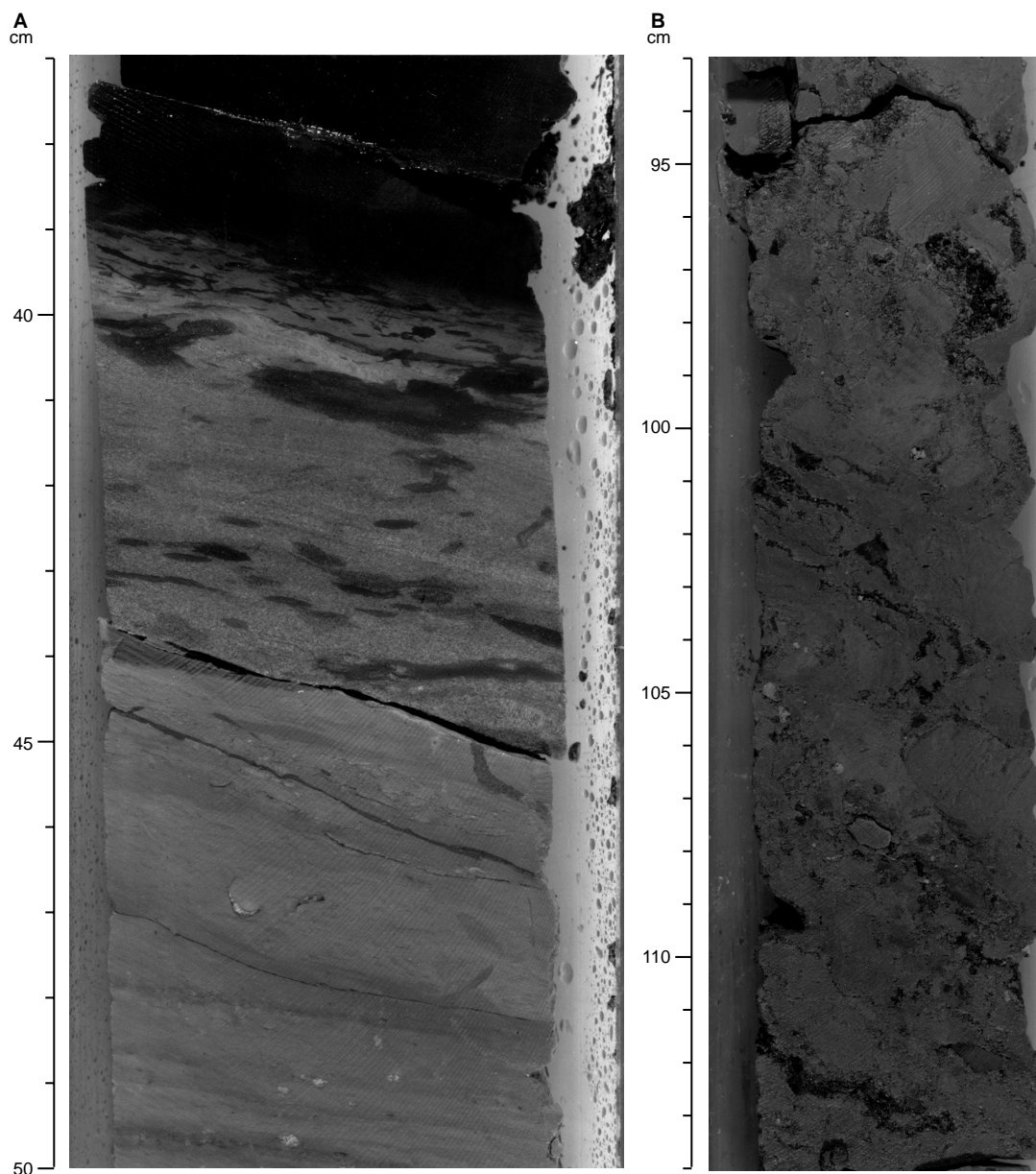


Figure 13. Core photographs of Unit IV in Hole 1069A. **A.** Interval 173-1069A-16R-2, 37–50 cm. The boundary between Subunit IIC and Unit IV dips at $\sim 20^\circ$ and occurs on the left side of the core at 43.7 cm. The core is broken into two pieces that fit together precisely across the boundary; as shown, they are slightly displaced. A Motif 2 upward-darkening sequence lacking a basal sandy interval occurs above the boundary. Below it are bioturbated nanofossil chinks within which occur two shell fragments at 47 cm, and color banding that is more gently inclined than the $\sim 20^\circ$ dip of the bedding. **B.** Interval 173-1069A-16R-3, 93–114 cm. Brecciated nanofossil chalk, possibly deformed by slumping, containing thin layers of sand- and granule-sized clasts of limestone and metasediments.

es or eroded by bottom currents. Deposition would only have resumed at Site 1069 when sediments filled the deep basin to the west of the acoustic basement ridge and onlapped its summit area (Figs. 5, 14).

The occurrence of the purely pelagic sediments of Unit IV constrains the age of the topography of the top of the acoustic basement in the Site 1069 area: it must have been created before the late Berriasian. This conclusion has wider implications. This is because in the Leg 149/173 area the sedimentary cover imaged on seismic sections shows reflection convergence and onlap onto basement highs indicating that it passively onlapped a pre-existing topography that may have been formed as early as the Valanginian (Fig. 14); there is no evidence of deformation (apart from differential compaction between

basement highs and lows) until the middle Miocene (Wilson et al. 1996). The existence of upper Berriasian to ?lower Valanginian nanofossil chalk near the top of the basement high in the Site 1069 area is consistent with Wilson et al.'s (1996) suggestion that the main rifting episode that created the basement topography probably occurred "early in the Valanginian and after the Tithonian". The evidence from Hole 1069A suggests that this was a pre-late Berriasian event.

Unit V

Interval: 173-1069A-16R-3, 123 cm, through 25R-1, 44 cm
Depth: 867.83–959.3 mbsf

Age: Subunit VA: Late Jurassic (?Tithonian); Subunit VB: barren

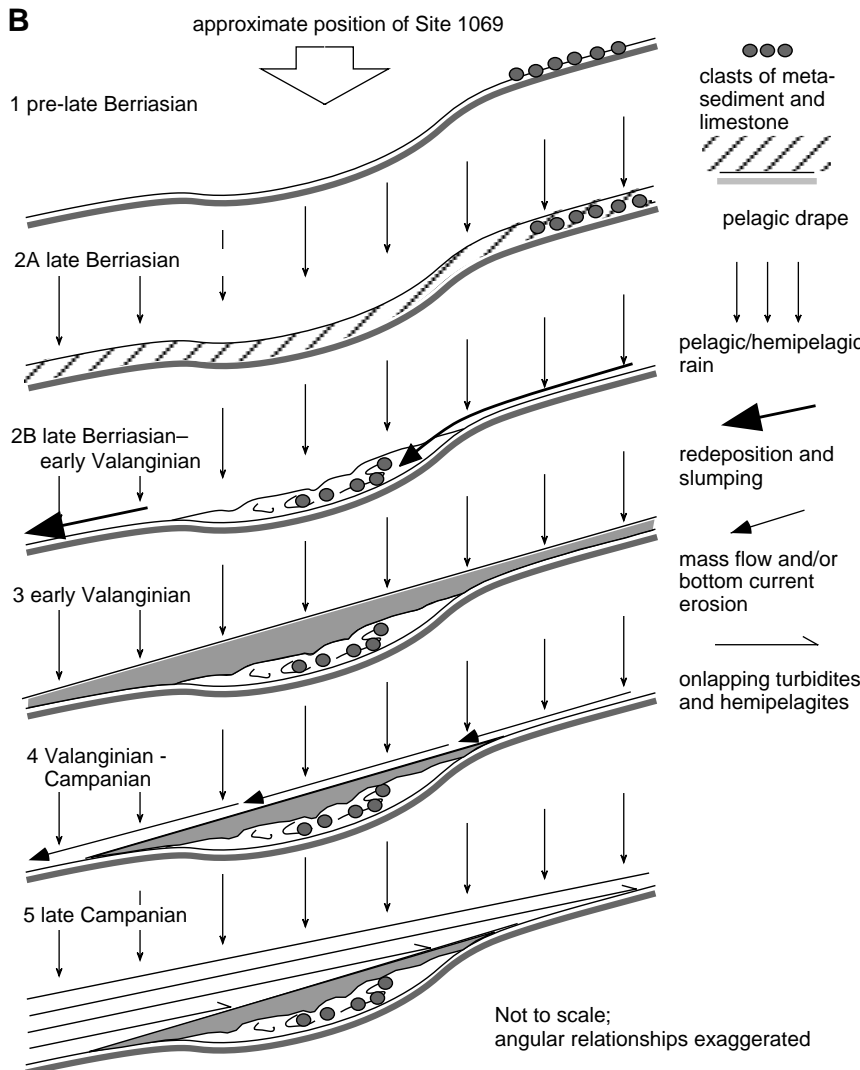
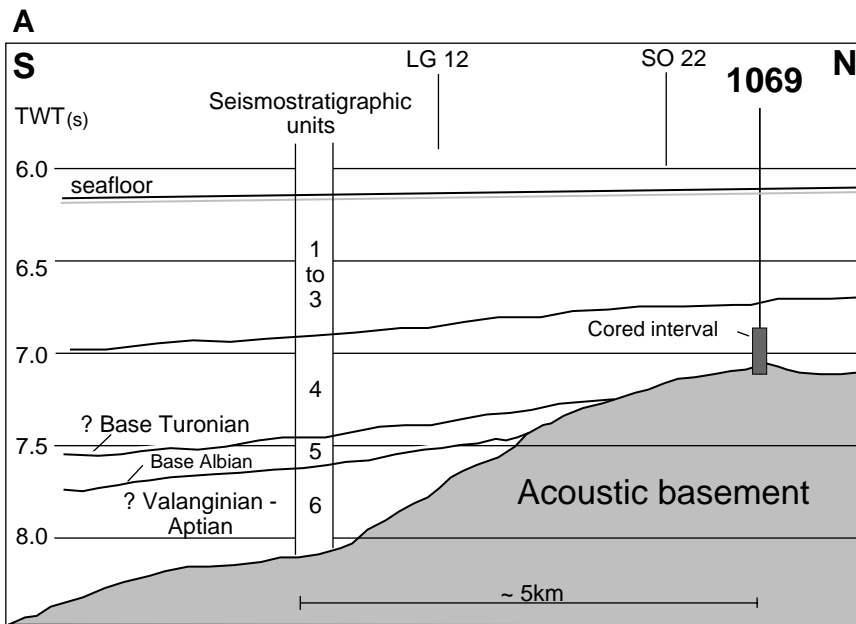


Figure 14. The setting and possible origin of the upper Berriasian–lower Valanginian pelagic drape cored in Hole 1069A. **A.** Interpretation of part of seismic line CAM 134 (which is shown in Fig. 4), showing the relationship between the cored interval in Hole 1069A and the Lower Cretaceous sediments draping acoustic basement. The intersection of east-west seismic lines is shown: LG12, and SO22 (shown as Fig. 5). The seismostratigraphic units and ages of the bases of those occurring in the Cretaceous are from Wilson et al. (1996, fig. 3C). Note that the acoustic basement beneath Site 1069 is ~1600 m higher than that beneath the “Seismostratigraphic units” column on the diagram. Further discussion is in the text. **B.** Drawings illustrating how upper Berriasian–lower Valanginian sediments might have been preserved beneath Site 1069, whereas no further retention of sediments occurred until upper Campanian sediments onlapped the acoustic basement high. The drawings show how a postulated small depression on the flanks of the gently inclined summit area was filled with sediment (by pelagic drape and slumping) during late Berriasian to early Valanginian time (steps 1, 2A, 2B, 3). This sediment fill effectively smoothed the topography so that any later pelagic sediments were removed by mass-wasting processes or erosion by bottom currents (step 4) until late Campanian time when sediments onlapped the slope (step 5).

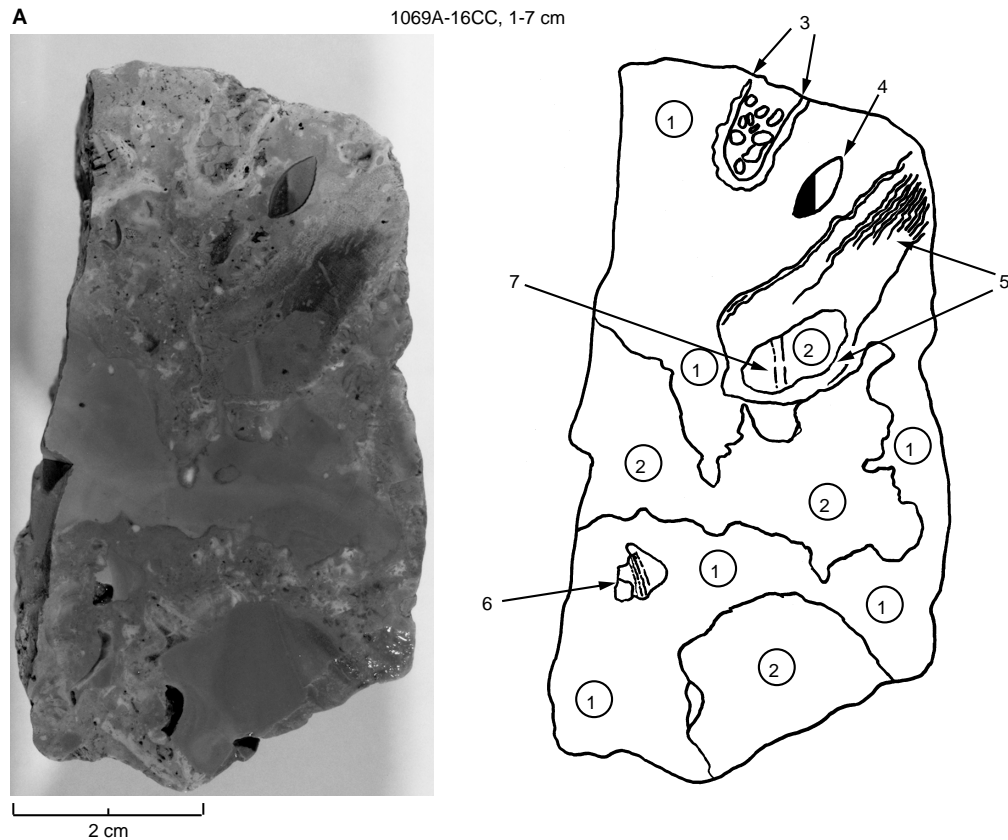


Figure 15. Photographs of cut and polished surfaces and a thin section of limestone pieces from Subunit IVA, Hole 1069A. A. Sample 173-1069A-16R-CC (archive half). Key to labels on the sketch of key features: 1 = heterogeneous boundstone with skeletal fragments (including some chaetitid sponges) and peloids; 2 = cavities within the boundstone filled with carbonate mud (peloidal in places); 3 = possible boring lined with encrusting organisms and filled with peloidal/intraclastic grainstone; 4 = bivalve (possibly a borer) with a geopetal fill of carbonate mud overlain by calcite spar indicating that at the time the mud filling was deposited, top was to the left; 5 = a chaetitid calcisponge in which the internal structure has been neomorphosed to micrite towards the lower left of the photograph; 6 = cavity within (1) partially filled with carbonate mud within which laminations are slightly oblique to the top of the geopetal mud fill of 4; 7 = internal carbonate mud sediment within 5 showing layering parallel to top of geopetal mud fill of 4. (Continued next page.)

Recovery of Unit V sediments was very poor (<3%). The boundary between Unit IV and Unit V occurs at interval 173-1069A-16R-3, 123 cm (867.83 mbsf), and marks the first occurrence of gray hemipelagic/pelagic clay containing ?Tithonian-age nannofossils. Unit V is divided into two subunits on the basis of the lithologic composition of curated pieces of rock recovered in Cores 173-1069A-17R to 25R. The boundary between Subunits VA and VB is placed at the first occurrence of metasediment pieces in the core at Section 173-1069A-17R-1, 44 cm (between Pieces 8 and 9 at 873.74 mbsf).

Subunit VA

At the top of the subunit a 10-cm-thick interval of medium dark gray clay occurs (interval 1069A-16R-3, 123–133 cm). A series of very light gray to very pale orange shallow-water limestone pieces were recovered in the basal interval of Section 173-1069A-16R-CC and at the top of Section 17R-1 (Fig. 12). A light gray to white carbonate pebble occurs at the boundary with Unit IV and may either have been emplaced during drilling, or be part of the overlying slumped interval. A 7-cm-long piece of boundstone was recovered in the core catcher of Core 16R. It consists of an organically built framework within which cavities are filled by internal sediments, and it contains a “spirit level” structure fill within a bivalve fragment in which the sparite/micrite boundary is vertical (Fig. 15A). This indicates that it is a transported clast (or part of a larger clast) and not a sample of an in situ organic build-up.

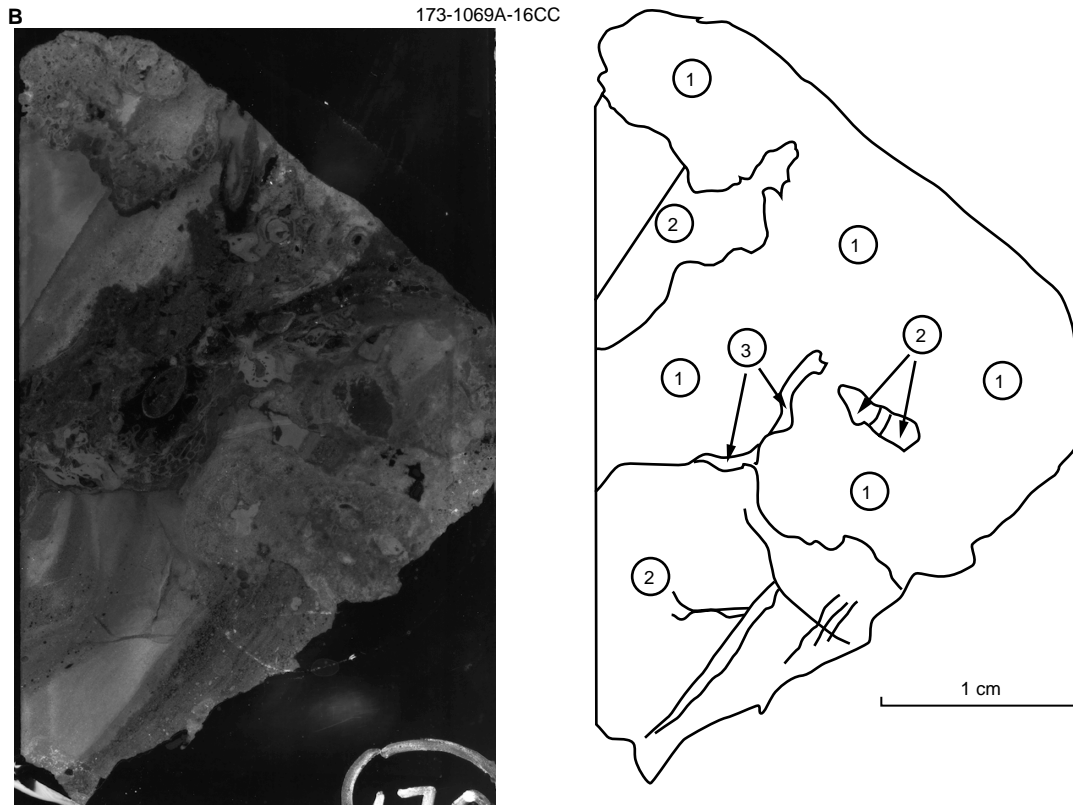
The pieces of limestone in Core 173-1069A-17R consist of conglomerates in which occur clasts of grainstone, boundstone, and rudstone (Fig. 15C). The clasts are predominantly allochems and carbonate lithoclasts including coated grains, oncoids, skeletal debris, cryptalgal fragments, chaetitid calcisponges and other frame-building organisms, and occasional clasts of peloid grainstone.

Subunit VB

The nature and origin of this subunit was the subject of much discussion and speculation among members of the shipboard scientific party. This was because of the paradoxical situation in which only very poor recovery (<3%) of hard metasediments was achieved, yet each of the nine cores was drilled unusually quickly (25–80 minutes). This high drilling rate suggests that a large proportion of the rock column that was drilled consisted of soft friable material.

In Core 173-1069A-17R, a small limestone piece (Piece 10), similar to those occurring in Subunit VA above, occurs between pieces of metasediment, as does a piece (Piece 18) containing smaller (<1.5 cm) clasts of metasediment and limestone cemented by calcite and dolomite (Fig. 16). Several pieces of dark gray to black slightly fissile shaly material, containing some silt- and coarse sand-sized pyrite crystals were recovered in Cores 173-1069A-21R (Pieces 8 and 10) and 24R (Piece 3).

The metasediment pieces recovered from Subunit VB range in length from 2 to 17 cm. The surfaces of most of them are damaged by



C 173-1069A-17R-1, Piece 2



Figure 15 (continued). **B.** Negative photograph of a thin section taken from the lower part of the working half of the limestone piece in the core catcher of Core 16R. In the sketch of key features: 1 = heterogeneous boundstone with skeletal fragments; 2 = cavities filled by micritic internal sediments; 3 = calcite cement fringe (?after aragonite) that grew before cavity was totally filled with internal sediment. **C.** Sample 173-1069A-17R-1 (Piece 2 [working half]). Grainstone to rudstone containing darker subrounded clasts of metasediments. The two large (~1 cm) irregular lighter colored clasts near the top of the photograph are composed of heterogeneous boundstone containing a variety of encrusting organisms and peloids and intraclasts. A coated skeletal fragment occurs 2.5 cm from the bottom, and is surrounded by intraclasts and coated grains (a few of which have metasediment nuclei). The slightly darker irregular clasts towards the bottom left are fragments of chaetitids, as is the roughly ovoid-shaped fragment one centimeter to the right of the large coated skeletal fragment.

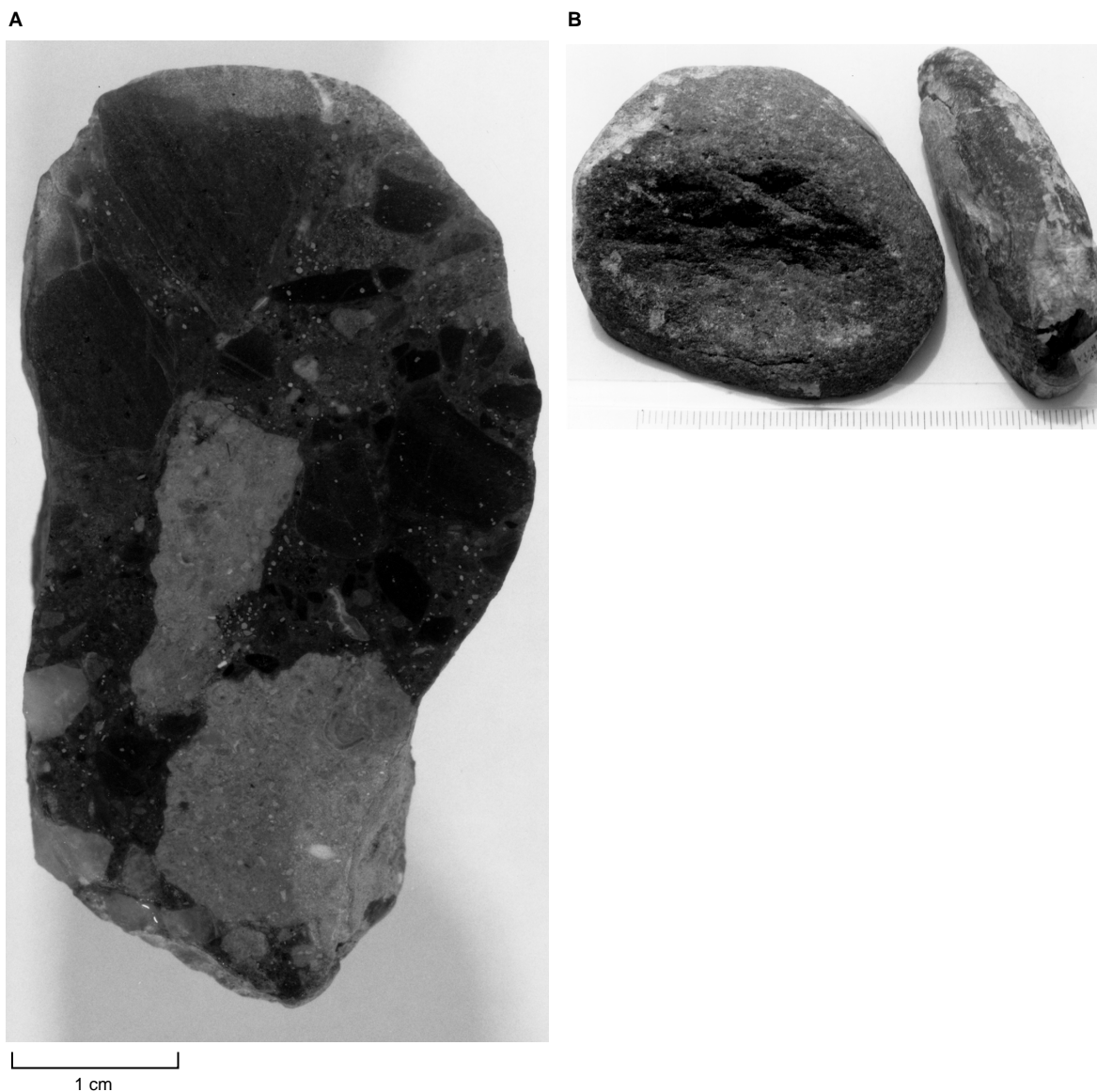


Figure 16. Pieces from Subunit VB, Section 173-1069A-17R-1. **A.** Polished surface of Piece 18 (archive half). The two lighter colored clasts are limestone. The upper one is composed of heterogeneous boundstone material, and the lower one is a poorly sorted peloidal-intraclastic grainstone. The darker clasts (which range in size down to sand grains not visible in the photograph) are composed of metasediments (pelites and meta-arenites). **B.** Possible sedimentary clasts composed of metasediments. The disoid shape of Piece 12 (on the right) is controlled by the foliation, and its rounded and smooth surface is only partially damaged by drilling. The surface of Piece 13 is rounded and relatively smooth, and undamaged by the inserts of the drill bit. The scale shows 1-mm intervals.

drilling, but two of them in particular (Samples 173-1069A-17R-1, [Pieces 12 and 13]; Fig. 16B) have shapes and surface textures that suggest that they may be large clasts. Piece 13 is well rounded and its surface is relatively smooth, the only roughness being at the micro-scale and related to the size of its constituent crystals and its foliation. Piece 12 is flat, its shape being controlled largely by foliation: parts of its rounded edges show the same kind of smooth “finish” as exhibited by Piece 13.

Does the poor recovery of pieces of metasediment indicate wide spacing between layers or clasts of these rocks? The rapid drilling rate suggests that it does and that the material not recovered is soft: either unlithified sand, fissile shale, or pelites shattered by cataclasis. Experience at Site 1065 showed that plastic clay is slow to drill through, so this lithology is not likely to have been present. Only slight brittle deformation is present in the pieces of metasediment.

This is not consistent with the hypothesis that the missing soft material could be tectonically brecciated pelites (see “Structural Geology” section, this chapter). The occurrence of three pieces of shaley material supports the hypothesis that fissile shale might occur between the hard metasediments, but it seems strange that more of such material was not recovered. A “ghost core” (Core 173-1069A-26G) obtained during wiper operations prior to logging Hole 1069A contains unlithified coarse lithic sand mixed with nannofossil-rich fine-grained sediment. A high proportion of the clasts in the sand are composed of the same kind of metasediments that occur in Subunit VB—much higher than in any of the sands present higher in the hole in the cores of Unit II. This sand sample can be used as evidence to support the case for Subunit VB being composed dominantly of a similar sediment. But the material in the ghost core could have been collected from anywhere between 767 mbsf (within Subunit IIB) and the bottom of the

hole, and so could be a sample of coarser unlithified sands that were not recovered elsewhere from Subunit IIC.

Sedimentary Processes

No precise environmental interpretations can be given for the sediments of Unit V, as it was not possible to observe facies relationships.

The limestone pieces in Core 173-1069A-17R show clear evidence of the redeposition of debris from a slightly older or contemporaneous deposit of boundstones, rudstones, and grainstones. Variscan metasedimentary basement clasts were also transported together with the carbonate debris. The association of carbonate and basement clasts is similar to that seen in the thin turbiditic intervals occurring in the Tithonian succession at Site 1065. The comments made in the "Lithostratigraphy" section, "Site 1065" chapter, this volume, are therefore appropriate to Subunit VA at Site 1069:

"The presence of slate and meta-arenite lithoclasts in the conglomerates indicates exposure and erosion of Variscan basement rocks, presumably to the north in the Vasco da Gama Seamount area. The lithoclasts of shallow-water limestones exhibiting lithologies similar to those recovered during Leg 103, described by Jansa et al. (1988), suggest that limestones slightly older than Unit V were being eroded, or that contemporaneous carbonate buildups located on tectonic highs were shedding debris into the area around Site 1065. The latter scenario is similar to that described by Leinfelder and Wilson (1989, in press) for Kimmeridgian sediments filling the Arruda Sub-basin 30 km to the north of Lisbon."

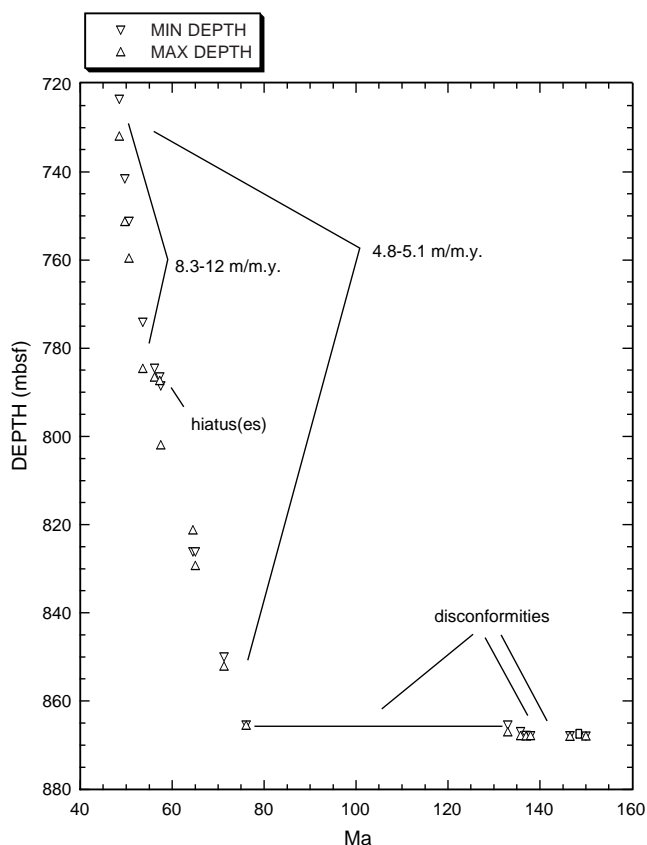


Figure 17. Age-depth plot for Site 1069 (see Table 4 for datums used).

The pieces of metasediment (Fig. 16) recovered in Core 173-1069A-17R to 25R exhibit features (see "Igneous and Metamorphic Petrology" and "Structural Geology" sections, this chapter) that match very well with descriptions of Variscan basement rocks collected from a deep fault escarpment on the western side of Galicia Bank (Mamet et al., 1991). Here, Variscan basement rocks are overlain by Tithonian dolomites, a comparable stratigraphic juxtaposition to that drilled in Hole 1069A, although at this site all the material appears to have been resedimented.

If it is assumed that the pieces of metasediment in Subunit VB are pebble- and cobble-sized sedimentary clasts and are scattered throughout (as isolated clasts, or occasional layers of clasts) a succession of shales, then a debris flow origin is likely. But if a soft unlithified sand comprises the greater proportion of the succession, then there are probably only two possible origins for the subunit. It could have been deposited in (1) the distal part of a sand-rich alluvial fan, or (2) it was deposited by high concentration turbidity flows (cf. Facies A1.4 disorganized pebbly sand of Pickering et al. [1989]). The absence of any red coloration on the surfaces of both the supposed clasts and the sand-sized clasts in the ghost core, and the lack of any pieces of well-lithified carbonate soil horizons that characterize Upper Jurassic and Lower Cretaceous fluvial sediments exposed in the Lusitanian Basin (Hill, 1989; Hiscott et al, 1990) suggests that a fluvial origin is unlikely. However, submarine fan and slope channel deposits associated with resedimented shallow-water carbonates do occur in the Upper Jurassic of Portugal (Leinfelder and Wilson, 1989, in press; Ravnås et al., in press).

BIOSTRATIGRAPHY

A variety of rocks representing strongly contrasting paleoenvironments, ranging in age from Late Jurassic to middle Eocene, were cored at Site 1069A. The transition from a Jurassic restricted, interior clastic basin to an open marine, shelf-slope depth carbonate margin is documented by attendant changes in the microfaunas and nannofloras and is consistent with the concept of continental rifting of the West Iberia margin during latest Jurassic–earliest Cretaceous time. No continuous record is provided, however, of the post-Valanginian subsidence of the basin to abyssal depths because an ~55 m.y. hiatus separates Valanginian shallow-water, nannoconid chalks from an overlying uppermost Campanian deep-water turbidite/hemipelagite sequence. Local correlations and implications of these changes in paleoenvironments are briefly mentioned below.

Table 4. Calcareous nannofossil datums used to construct the age-depth plot in Figure 17.

Biozones	Biostratigraphic datums	Age (Ma)	Core, section, interval (cm)	Min. depth (mbsf)	Max. depth (mbsf)
CP12b	b <i>R. inflata</i>	48.5	1R-CC, 24-26	723.62	731.89
CP12a	b <i>D. subloboensis</i>	49.7	3R-2, 119-120	740.80	751.24
CP11	t <i>T. orthostylus</i>	50.6	4R-CC	751.24	759.6
CP9a	t <i>T. contortus</i>	53.6	6R-CC, 14-17	774.2	784.6
CP9a	b <i>T. contortus</i>	53.6	6R-CC, 24-26	774.2	784.6
CP8a	b <i>D. multiradiatus</i>	56.2	7R-CC, 21-24	784.6	786.5
NP8	b <i>H. riedelii</i>	57.3	8R-1, 9-11	786.5	787.3
CP6	b <i>D. mohleri</i>	57.5	8R-2, 70-71	788.6	801.9
CP1b	b <i>C. tenuis</i>	64.5	12R-1, 120-122	826.2	821.2
	t Cretaceous spp.	65	12R-3, 134-136	826.2	829.3
CC23a	t <i>B. constricta/ Q. trifidum</i>	71.3	14R-4, 111-113	850	852.1
	b <i>Q. trifidum</i>	76.1	16R-2, 38-41	865.5	865.5
	t <i>C. deflandrei</i>	133	16R-2, 44-45	865.5	867
	b <i>C. oblonga</i>	135.8	16R-3, 42-43	867	867.8
	t <i>U. granulosa</i>	137	16R-3, 43-45	867.8	867.9
	b Valanginian	138	16R-3, 123	867.9	867.8
	t Tithonian	146.6	16R-3, 129	867.9	868
	b Tithonian	150	16R-CC, 13-15	868	867.9

Note: b = bottom; t = top.

The age-depth plot for this site (Fig. 17; Table 4) is based on less well-constrained data than for the previous two sites in that only core-catcher samples were examined for the most part, thus uncertainties caused by the sampling interval are larger. Compared to the previous two sites, there are some similarities, with high sedimentation rates indicated for the uppermost lower Eocene to the lowermost middle Eocene (roughly 48.5–49.5 Ma) and relatively low rates indicated for the lower Eocene (50–54 Ma), where carbonate dissolution was intense because of deposition close to and below the CCD. There also appear to be hiatuses in this part of the section.

Sedimentation rates increased again in the Paleocene section (55–65 Ma), where nanofossils were abundant and quite well preserved in some intervals, but not in others. The Paleocene section is somewhat thicker here than at the previous site, probably because there are more turbidites in the section (see “Lithostratigraphy” section, this chapter). There are, however, many carbonate-barren intervals and probably a number of minor hiatuses.

A major discontinuity representing over 55 m.y. of time separates the uppermost Cretaceous interval from the Lower Cretaceous. Other discontinuities representing short intervals of time have been identified in the Lower Cretaceous cores, as indicated elsewhere in this section.

Calcareous Nanofossils

The calcareous nanofossil succession at this site was dated primarily from core-catcher samples except for the Mesozoic sediments in Core 173-1069A-16R, which were examined in greater detail. The sequence began exactly as at Site 1068, that is, in the middle Eocene *Rhabdosphaera inflata* Subzone (CP12b of Okada and Bukry, 1980; upper NP14 of Martini, 1971). Also as at the previous site, the next core (173-1069A-2R) belongs to Subzone CP12a (NP14) and contains the first appearance datum (FAD) of *Pseudotriquetrorhabdulus inversus*. Sample 173-1069A-3R-CC was barren, but Sample 173-1069A-3R-2, 119–120 cm, indicates that this core can also be assigned to Subzone CP12a, which spans the lower/middle Eocene boundary. From there the nanofossil zones and subzones follow more or less consecutively to the middle Paleocene, although there are many barren samples within the sequence.

As with the previous cores in this hole, Cores 173-1069A-4R and 5R are short, resulting in poor recovery; they can be assigned, however, to the *Discoaster lodoensis* Zone CP11 (NP10). Sample 173-1069A-6R-CC contains well-developed *Tribrachiatius bramlettei* along with *Discoaster diastypus* and, therefore, belongs to the earliest Eocene *Tribrachiatius contortus* Zone CP9a (NP10). As this was the first reasonably full core recovered at this site, detailed study may show that Subzone 9b is represented higher up in this core.

Sample 173-1069A-7R-CC is a sandy, calcite-cemented turbidite with a reduced number of moderately preserved nanofossils, but it does contain large (14 µm) *Ellipsolithus macellus*, *Fasciculithus bobii*, *Coccolithus robustus*, and *Discoaster multiradiatus*, the latter being the basal marker for the uppermost Paleocene Zone CP8 (NP9). Sample 173-1069A-8R-1, 9–11 cm, is characterized by *Heliolithus riedelii*, *Discoaster splendidus*, *Discoaster limbatus*, and *F. tympaniformis*, and is assigned to Zone CP7 (NP8). Starting within the same core section, Samples 173-1069A-8R-1, 87–90 cm, and 8R-2, 70–71 cm, contain *Discoaster mohleri* (basal marker for Zone CP6; = NP7 and lower NP8) along with *Fasciculithus tympaniformis*, *Coccolithus robusta*, *Heliolithus kleinpellii*, and large *Braarudosphaera bigelowii*, a dissolution-susceptible form whose presence suggests that all of the material in this part of the section has been reworked from shallower depths by turbidites. This presumption is confirmed by the presence of the large Lower Cretaceous taxon, *Nannoconus steinmannii*, which was observed sporadically throughout the Cenozoic column recovered at other Leg 173 sites.

The large number of barren samples encountered in this portion of the hole also suggests that much of the calcareous material introduced by turbidites has been emplaced below the carbonate compensation

depth (CCD). In particular, the next set of samples taken downcore were all barren (Samples 173-1069A-8R-2, 117–118 cm; 8R-4, 89–90 cm; 8R-5, 62–63 cm; and 8R-CC). The top of the next core is essentially barren as well; thus, at the time of writing Zones CP4 and CP5 have not been accounted for. Sample 173-1069A-9R-CC contains lithologies of three different colors, of which the dark brown is barren and the tan and green contain abundant nanofossils. These are assigned to Zone CP3 (NP4) based on the presence of the secondary marker *Fasciculithus ulii* in the absence of *F. tympaniformis*. Preservation of placoliths is best in the tan layer because of less diagenetic overgrowth.

Sample 173-1069A-10R-6, 0–4 cm, is dated as uppermost Zone CP3 (NP4) based on the presence of *Prinsius martinii* in the absence of *Fasciculithus tympaniformis*, *F. magnus*, and *Prinsims dimorphosus*. The core catcher of Core 10R does contain *Fasciculithus magnus* (≤20 µm wide) and is assigned to the middle to lower part of the same zone.

Brown, gray, and very light gray sediments in Sample 173-1069A-11R-CC contained nanofossils, an indication that the site may have lain above the CCD for a brief interval during the early Paleocene. The presence of *Cruciplacolithus intermedius* and 8-µm-long *Coccolithus pelagicus* in the absence of *C. subpertusa* and *Prinsius dimorphosus* indicate Zones CP1b–CP2 (NP2–3). The same assemblage is detected in Sample 173-1069A-12R-1, 118 cm, along with complete *Braarudosphaera bigelowii* and thoracosphaerid fragments in spite of dilution by large numbers of Cretaceous coccoliths. The latter two taxa can be taken as tracers of Tertiary material for the purpose of trying to locate the Cretaceous/Tertiary (K/T) boundary. Trace numbers of *Braarudosphaera* along with thoracosphaerid fragments, were detected downcore to Sample 173-1069A-12R-3, 135 cm. The actual K/T boundary, however, has been obscured by the emplacement of numerous turbidites and could not be better defined.

The uppermost Cretaceous index taxa *Micula murus* and *Ceratolithoides kamptneri* were present in Samples 173-1069A-12R-1, 118 cm, and 12R-6, 76 cm, respectively, indicating the presence of the upper Maastrichtian Zone CC26. Sample 173-1069A-12R-CC was barren and 13R-CC could not be assigned an age within the Maastrichtian because of the apparent absence of *Lithraphidites quadratus* within the section. The presence of *Quadrum sissinghii*, *Q. trifidum*, and *Broinsonia parca constricta* in the absence of *Eiffelithus eximius* suggests an age of latest Campanian for Samples 173-1069A-14R-4, 112–113 cm, through 173-1069A-16R-2, 33–41 cm. Normally, this assemblage should be confined to Zone CC23a. However, the prevalence of reworked taxa within this multicolored sequence suggests caution in that all of the boundaries for this and the adjacent subzones are based on last occurrence datums. Reworking could extend the distributions of the index taxa upsection. However, the assemblage can be no older than Zone CC22a, the base of which is the first occurrence datum of *Quadrum trifidum*.

In Section 173-1069A-16R-2, the turbidites and hemipelagites of Subunit IIC are separated from the underlying yellowish Lower Cretaceous chalk of Unit IV by a major hiatus (Fig. 12). The upper portion of the chalk is dominated by nannoconids within a matrix of nannoconid/micrantholith skeletal debris. The assemblages include *Nannoconus steinmannii*, *N. bermudezi*, and *Cyclagelosphaera deflandrei*, which together suggest an age of early Valanginian. This portion of the chalk is separated by an intraformational hiatus at Section 173-1069A-16R-3, 44 cm, from a lower unit that has undergone redeposition and/or slumping with the incorporation of older clastic grains and occasional pebbles (Figs. 13, 14). Sample 173-1069A-16R-3, 45 cm, yielded a few specimens of *Umbria granulosa*, whereas Sample 173-1069A-16R-3, 93 cm, contained rare *Tubodiscus jurapelagicus*, *T. verenea*, few *Rhagodiscus nebulosus*, *Nannoconus steinmannii*, common *Lithraphidites carniolensis*, *Crucicellipsis cuvillieri*, and abundant *Assipetra infracretacea*. Together, these indicate an age within the late Berriasian according to Bergen (1994). Upon further analysis clasts in this lower chalk unit may yield a variety of ages within the Berriasian.

The yellow chalk is underlain by an Upper Jurassic black silt, disturbed by coring, which marks the top of lithostratigraphic Unit V. The nannoflora includes *Stephanolithion bigotii* and *Diazomatolithus galicianus*; at present, the latter species is known to date only from the Tithonian of Site 901 (de Kaenel and Bergen, 1996). The uppermost Jurassic index fossil present at the top of the section at Site 1065, *Conusphaera mexicana minor*, however, has not been observed at this site; therefore, a possible Tithonian age is tentative at the time of writing. A light gray streak of nannofossil ooze in Sample 173-1069A-16R-3, 129 cm, yielded a more diverse assemblage than seen in the Jurassic at either Site 901 or Site 1065, and included some of the more delicate, less dissolution-resistant forms such as abundant *Stradnerlithus sexiramatus*, *Tetrapodorhabdus coptensis*, and *Axopodorhabdus cylindratus*.

Core 173-1069A-16R represents a succession of quite different paleoenvironments, beginning with the environmentally restricted upper Jurassic black silt that has only a limited nannoflora greatly diluted by fine clastics. Only the streak of nannofossil ooze mentioned above indicates a brief incursion of more open marine conditions to what was presumably a relatively shallow, interior continental basin. A major change of environment is witnessed by the deposition of the upper Berriasian chalk. The contact between it and the underlying upper Jurassic is marked by large limestone clasts. The consistently high diversity of the Berriasian nannoflora in all samples examined indicates a more open connection to the sea than previously and is consistent with major rifting and basin development at this time; deposition was well above the CCD. The fact that the upper Berriasian was redeposited (as described above) shortly after its deposition indicates further disturbance, perhaps from continued tectonic activity. An examination under a binocular microscope of these chalk samples taken for nannofossil analysis reveals a yellow stain on what was previously a grayish carbonate (the color of which is still seen in some of the chalk pebbles). These stains might suggest subaerial weathering. Exposure and weathering of this Berriasian material, however, did not leach out the nannofossils at this site, but may have done so at Site 1065, where a carbonate-free yellow siltstone pebble and a piece of ironstone were recovered from the interval between the Miocene and Upper Jurassic, an interval for which possible subaerial exposure and weathering has also been suggested (see "Biostratigraphy" section, "Site 1065" chapter, this volume).

Above the disconformity at Section 173-1069A-16R-3, 44 cm, the chalk is relatively undisturbed, except by minor compaction

faults and a slight tilt to the bedding. The nannoflora is quite different from the diverse flora immediately below, being dominated by nannoconids, an assemblage thought to be indicative of relatively shallow-water, outer shelf-slope, open marine environments. A similar yellow nannoconid limestone of this age was cored on Galicia Bank at Site 639 (Applegate and Bergen, 1988), and may have been widespread throughout this region wherever water depths and environments were suitable. Significantly, this lower Valanginian nannofossil assemblage is somewhat similar to the one that forms the carbonate matrix of the breccia in Cores 173-1068A-15R and 16R at Site 1068. Further shore-based study will be necessary to better establish the equivalence and correlations of this nannofacies between these sites; however, the Valanginian–Barremian emplacement of the breccia at Site 1068 indicates that tectonic disturbances were still taking place at that time. At Site 1069, however, no such record of breccia emplacement exists; instead, the relatively thin chalk unit is overlain by the much younger upper Campanian turbidites, which were deposited at abyssal depths (Fig. 12).

Planktonic Foraminifers

Paleogene planktonic foraminifers are generally recorded as common and moderately well preserved in the upper part of the sedimentary sequence analyzed from Samples 173-1069A-1R-CC through 173-1069A-4R-CC (Table 5). The assemblages recovered from Samples 173-1069A-1R-CC and 173-1069A-2R-CC are characteristic of latest early Eocene to earliest middle Eocene age, Zones P9–P10. The species present in these samples include *Morozovella aragonensis*, *Acarinina broedermanni*, and *Globigerinatheka senni*. The co-occurrence of species *Acarinina bullbrooki*, *A. soldadoensis*, and *Morozovella aragonensis* in Sample 173-1069A-3R-CC suggests that sediments recorded at this level are no younger than latest early Eocene, Zone P9 in age. A similar assemblage is recorded in Sample 173-1069A-4R-CC. Although Sample 173-1069A-5R-CC contains abundant planktonic foraminifers, the preservation is only poor to moderately good and the only determinable species are *Morozovella aequa* and *Acarinina bullbrooki*. The latter species makes its first evolutionary appearance in Zone P9, latest early Eocene. Below this horizon, in Samples 173-1069A-6R-CC through 173-1069A-8R-CC, planktonic foraminifers are either absent or very poorly preserved.

In Sample 173-1069A-9R-CC, planktonic foraminifers are abundant and moderately well preserved. Species recovered from the sam-

Table 5. Distribution of planktonic foraminifers in Hole 1069A.

Age	Zone	Core, section	Depth (mbsf)	Abundance	Preservation	<i>Acarinina bullbrooki</i>	<i>Morozovella caucasica</i>	<i>Globigerinatheka senni</i>	<i>Globigerina eocaena</i>	<i>Acarinina broedermanni</i>	<i>Globigerina frontosa</i>	<i>Morozovella aragonensis</i>	<i>Acarinina soldadoensis</i>	<i>Acarinina pentacamerata</i>	<i>Morozovella aequa</i>	<i>Morozovella conico truncata</i>	<i>Acarinina subsp. haerica</i>	<i>Globotruncana ventricosa</i>	Indeterminate spp.	Reworked
middle to early Eocene	P10-P9	1R-CC	723.62	F	M			F		R										
middle to early Eocene	P10-P9	2R-CC	731.89	C	M	R	R	R	R	R										C
early Eocene	P9	3R-CC	741.63	R	P							R	R							R
early Eocene	P9	4R-CC	751.24	C	M	R						R	R	R						C
early Eocene	P9	5R-CC	759.55	A	P	R									R					A
		6R-CC	774.22	B																
early Eocene-late Paleocene	P9-P5	7R-CC	784.58	C	P									R						F
		8R-CC	793.27	B																
late Paleocene	P4	9R-CC	801.88	A	P											R				A
		10R-CC	814.95	B																
		11R-CC	821.21	A	P															
late to early Paleocene	P4	12R-CC	833.29	B													R			A
late to early Paleocene	P4	13R-CC	841.52	A	P												R			
Maastrichtian-Campanian		14R-CC	852.09	R	P													R		C
		15R-CC	859.22	B																
		16R-CC	868.04	N/I																
		17-1	874.25	N/I																
		17R-CC	874.32	N/I																
		21R-1	912.2	B																

ple include *Morozovella conicotruncata* indicating an early late Paleocene age for deposition of these sediments. Sample 173-1069A-10R-CC is barren of microfauna larger than 125 μm . Although Tertiary planktonic foraminifers are abundant in Sample 173-1069A-11R-CC, they are so poorly preserved and overgrown that they are barely discernible as such. Sample 173-1069A-12R-CC yielded three specimens of Paleogene planktonic foraminifers, whereas in Sample 173-1069A-13R-CC, Cretaceous forms are common in association with rare Paleocene specimens.

Microfossils are extremely rare in Sample 173-1069A-14R-CC, and only two specimens of Cretaceous planktonic foraminifers have been recovered despite prolonged searching through the residue. Sample 173-1069A-15R-CC is barren of microfauna and Sample 173-1069A-16R-CC is so small that it has been retained for shore-based palynological investigation. Samples 173-1069A-16R-1, 145–149 cm, 173-1069A-16R-2, 87–91 cm, and 173-1069A-16R-3, 26–29 cm, were found to be barren of planktonic foraminifers.

Benthic Foraminifers

Calcareous benthic foraminifers from the size fraction 125–500 μm , when present, are recorded as generally rare to few throughout the section analyzed from Samples 173-1069A-1R-CC through 173-1069A-15R-CC, although they are common in Samples 173-1069A-4R-CC, 173-1069A-6R-CC and 173-1069A-9R-CC. In the smaller-size fraction, 63–125 μm , common to abundant, moderately well-preserved calcareous benthic foraminifers are present in all samples with the exception of Samples 173-1069A-3R-CC, 173-1069A-7R-CC, 173-1069A-12R-CC, which contain only rare specimens, and Samples 173-1069A-8R-CC, 173-1069A-14R-CC, and 173-1069A-15R-CC, which are barren. The extremely fossiliferous assemblages often recovered in this small size fraction are interpreted as reworked as the sediments are considered to be turbiditic.

Agglutinated foraminifers are present in all samples analyzed (i.e., Samples 173-1069A-1R-CC through 173-1069A-15R-CC), with the exception of 173-1069A-14R-CC and 173-1069A-15R-CC, which are barren. The persistent occurrence throughout the interval from Core 173-1069A-1R through 15R of species such as *Ammodiscus* spp., *Bathysiphon* spp., and *Glomospira* spp., which are typical of deeper water habitats, together with the sporadic occurrences of calcareous foraminifers and the lithologic characteristics, suggest that these sediments were deposited in a fully marine environment at, probably, abyssal depths subject to periodic fluctuations of the CCD. Samples 173-1069A-16R-2, 87–91 cm, and 173-1069A-16R-3, 26–29 cm, contain assemblages of agglutinated foraminifers dominated by abundant *Ammodiscus* spp., together with a few calcareous benthic foraminifers, common inoceramid prisms, and common mollusc fragments. These latter assemblages are characteristic of an outer shelf/upper bathyal, oceanic environment.

PALEOMAGNETISM

Magnetic measurements were taken at 5-cm intervals on the archive-halves of cores from Hole 1069A, using the pass-through cryogenic magnetometer, as described in the “Paleomagnetism” section, “Explanatory Notes” chapter (this volume). After measuring the NRM, sections were progressively AF demagnetized using 10 mT steps, starting at 10 mT and ending at 60 mT. Forty-one additional discrete samples, taken from the working halves of the core, were progressively AF and thermally demagnetized to determine directional stability and to check the reliability of the measurements from the archive halves. The volume magnetic susceptibility was measured at 3-cm intervals on most of the cores from Hole 1069A.

Remanence and Susceptibility of Sedimentary Units

Hole 1069A has been divided into three lithostratigraphic Units (II, IV, and V; see “Lithostratigraphy” section, this chapter). Downhole variations of magnetic intensity and susceptibility are analogous to, and appear to reflect lithologic changes of, other Leg 173 sites. Unit II, a mixture of brownish-red claystone and hemipelagic gray sandstone, produced roughly parallel patterns of alternating high and low intensities and susceptibilities. The high and low peaks generally correlate with the turbidite layering (Fig. 18). In general, lows correspond to the hemipelagic gray sandstone and conglomerate at the base of the turbidite sequences and highs correspond to the brown claystone overlying the turbidite sequences. However, Subunit IIB has slightly lower magnetic intensities (3.5×10^{-4} to 0.1 A/m) that show a greater variation (approximately three orders of magnitude, ranging from 7×10^{-5} to 4×10^{-2} A/m) than Subunit IIC. Conversely, the magnetic susceptibility values of Subunit IIB are more closely clustered than those of Subunit IIC (Fig. 18). Based on lithologic descriptions (see “Lithostratigraphy” section, this chapter) the boundary between Subunits IIB and IIC has been placed at 805.8 mbsf within Core 173-1069A-10R. As shown in Figure 18, the magnetic intensity and susceptibility data suggest a change occurs slightly higher in the section at approximately 800 mbsf, in the bottom third of Core 1069A-9R. This may represent an initial subtle increase in the carbonate sand content that becomes more obvious downhole.

The characteristic brown bed and the associated peaks in NRM intensity and volume susceptibility, previously observed at Leg 173 Holes 1067A and 1068A, and during Leg 149 at Site 900 (Shipboard Scientific Party, 1994d), were also observed in Hole 1069A. This intensity and susceptibility spike is found in Core 173-1069A-7R at a depth of about 776 mbsf. This further suggests that this brown bed may be used as a stratigraphic marker for correlation of the lower Eocene sediments of the Iberia Abyssal Plain. So far we have been unable to relate the significance of this observation to the sediment mineralogy or regional paleoceanographic conditions.

Sediment Magnetostratigraphy

Pass-through measurements of the archive halves of the cores indicate several possible polarity reversals between 738 and 854 mbsf (Fig. 19). Further measurements and progressive demagnetization results from corresponding discrete samples confirm these polarity changes. Figure 20 exhibits typical AF and thermal demagnetization behavior of these sediments. Also illustrated in Figures 19 and 20 is the component of drilling-induced magnetization (inclinations greater than 70°) that is not always as effectively removed by AF demagnetization. Thermal demagnetization methods proved to be more effective for determining stable magnetic directions of the sediments.

Preliminary biostratigraphic (see “Biostratigraphy” section, this chapter) and paleomagnetic results indicate that the sediments span Eocene through the Upper Jurassic. During this time interval there were several magnetic polarity reversals (see the revised time scale of Berggren et al., 1995). However, because of the discontinuous deposition and partial core recovery, it may not be possible to construct a complete magnetostratigraphy. Such an evaluation will be done as a shore-based study.

Magnetic Results from Unit IV

Pass-through measurements of Unit IV, a Berriasian to Valanginian nannofossil chalk (see “Biostratigraphy” and “Lithostratigraphy” sections, this chapter), show steep NRM inclinations. From 863 to 865 mbsf, Unit IV inclinations become progressively less steep with

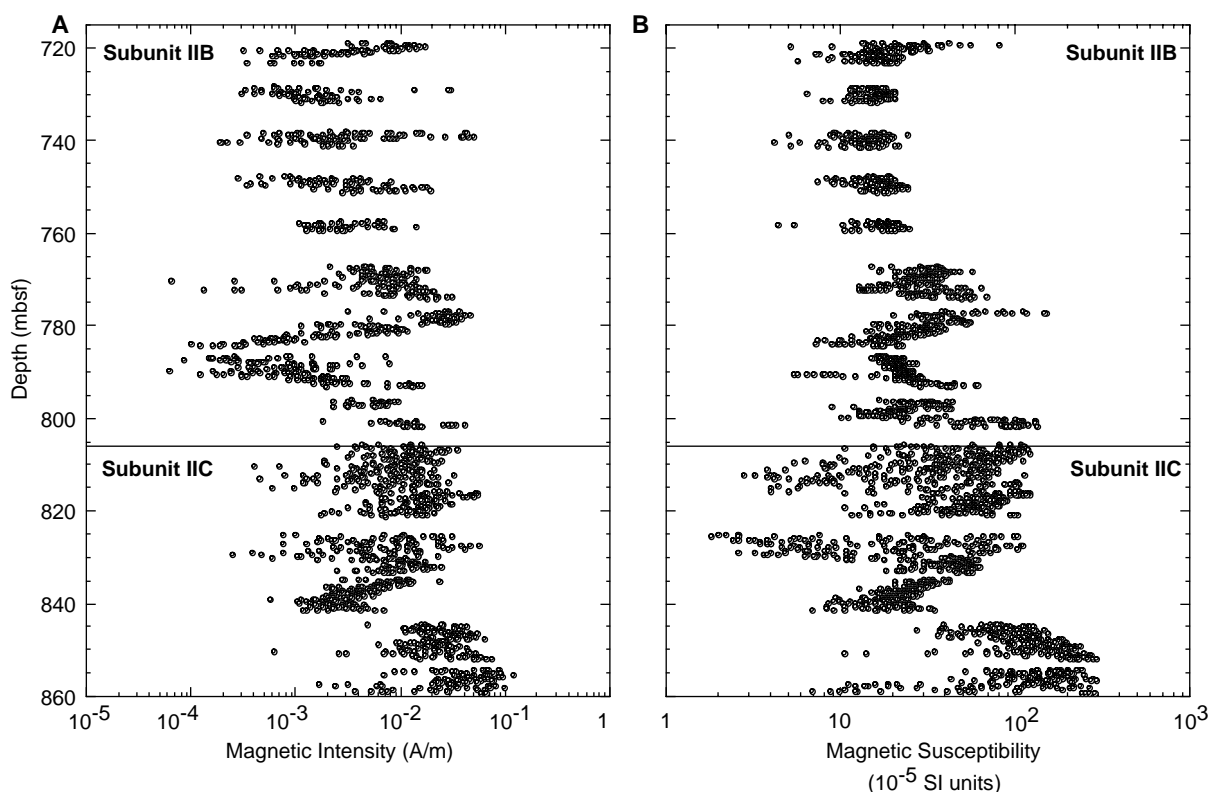


Figure 18. Plot of (A) remanent magnetization intensity (A/m) and (B) magnetic susceptibility (10^{-5} SI units) showing downhole variations in Hole 1069A. In general, lows correspond to the hemipelagic gray sandstone and conglomerate at the base of the turbidite sequences and highs correspond to the brown claystone overlying the turbidite sequences.

increasing AF demagnetization. This suggests that the top of Unit IV may be reversely magnetized. Shore-based thermal demagnetization experiments will be conducted to further test this preliminary observation. The remainder of Unit IV, 865 to 870 mbsf, appears to have a normal polarity.

Magnetic Results from Unit V

Unit V has been divided into two subunits. The lithology of this unit is unclear because of poor core recovery. Pieces of conglomerate containing clasts of boundstone, grainstone, and rudstone comprise Subunit VA; meta-arkosic wacke and metasilstones compose Subunit VB (see “Lithostratigraphy” section, this chapter). Pieces of meta-arkosic wacke from Subunit VB (Section 173-1069A-17R-1, [Pieces 10 through 14]) have a patina and subrounded to subangular shapes that have not been totally abraded by the roller cone drill bit, suggesting that Subunit VB is a conglomerate deposit. A conglomerate test, on minicores drilled out of pieces from Unit V (Sections 173-1069A-17R-1 [Pieces 9, 15, 16, and 21], and 1069A-21R-1 [Pieces 4 and 5]) was performed to test the conglomerate origin for Subunit VB. The selected pieces are sufficiently long that they demonstrably could not have rotated along any axis in the core barrel but Z (see “Paleomagnetism” section, “Explanatory Notes” chapter, this volume). NRMs and thermal demagnetization measurements yield stable magnetic directions, with both positive and negative inclinations, representing at least 50° variation between pieces (Fig. 21). These results indicate that the pieces were not coherently magnetized, further supporting the belief that Unit V is a conglomerate deposit with the pieces having existed as isolated clasts.

IGNEOUS AND METAMORPHIC PETROLOGY

Acoustic basement was first encountered in Core 173-1069A-17R (873.7 mbsf) within lithostratigraphic Unit V (see “Lithostratigraphy” section, this chapter) and continued to the bottom of the hole (959.3 mbsf). The core recovery was extremely poor (<5%), and the total length of core recovered was about 2 m. Core 173-1069A-17R included limestone (Pieces 1 through 8 and 10; see “Lithostratigraphy” section, this chapter); the rest of Core 173-1069A-17R and Cores 173-1069A-18R through 25R are meta-arkosic wacke and metasilstone.

General Lithologic Description

Meta-arkosic wacke and metasilstone were recovered as hard subangular to rounded pieces, which varied in diameter from 2 to 9 cm. Most are grayish black (N2) to medium dark gray (N4), but some are greenish black (5GY 2/1) to dark greenish-gray (5G 4/1). The meta-arkosic wacke is fine- to medium-grained, including relatively coarse-grained (<2 mm) metasandstone (Core 173-1069A-17R-1 [Piece 16]), and very fine-grained metasilstone (e.g., Core 173-1069A-19R-1 [Piece 2]). The metasediments consist of 10%–40% plagioclase, 30%–70% quartz, 1%–15% chlorite, and 5%–40% sericite. Most samples have pale tabular crystals which, in thin section, are subhedral altered ilmenite and/or dolomite porphyroblasts. Many samples also contain accessory pyrite, which occurs as isolated crystals, veins, and stylolites, and in hollow structures that may represent deformed burrows or fossils. A few samples also contain thin

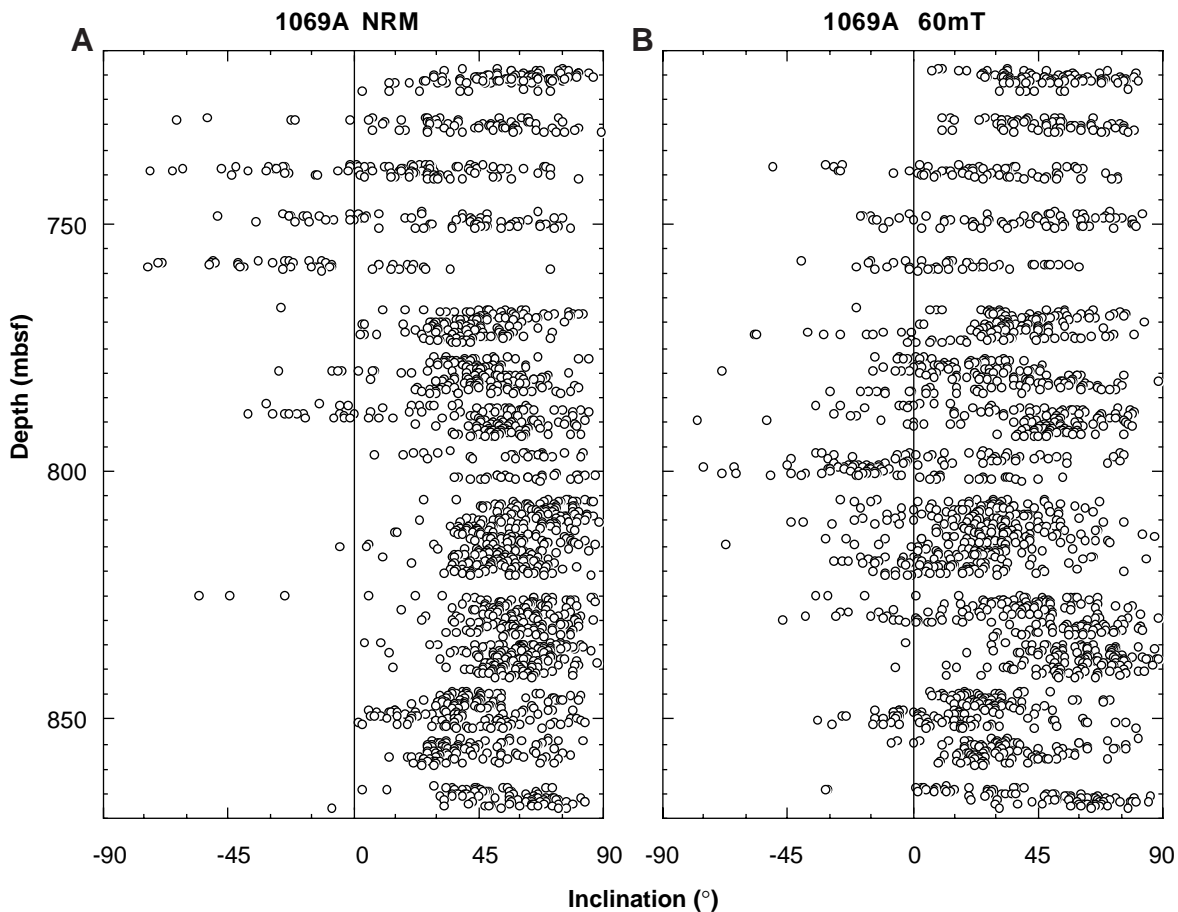


Figure 19. Diagrammatic representation of NRM inclinations (A) before and (B) after 60-mT AF demagnetization from pass-through measurements on the archive halves of the cores, indicating several possible polarity reversals. The drilling-induced magnetization component is characterized by steep inclinations greater than 70°.

quartz veins. These are most common in Section 173-1069A-25R-1. All pieces are foliated and many show relict bedding or lamination. The foliation intersects relict bedding at high angles in some pieces (e.g., Samples 173-1069A-21R-1 [Pieces 2 and 3]; see “Structural Geology” section, this chapter).

Petrography

Six thin sections were cut from a series of low-grade metasedimentary rocks cored in Hole 1069A. The rocks are classified as greenschist or subgreenschist facies meta-arkosic wackes and metasilstones containing varying amounts of quartz, plagioclase, muscovite, sericite, chlorite, ilmenite, tourmaline, chalcopyrite, and pyrite. Two of the thin sections (from intervals 173-1069A-20R-1 [Piece 2, 5–10 cm], and 173-1069-23R-1 [Piece 2, 1–3 cm]) contain substantial dolomite. Major textural and mineralogical features of the thin sections are summarized in Table 6.

Textures

All of the samples contain some original sedimentary textures: specifically, variably altered original detrital material (plagioclase, muscovite, quartz) in which the clastic origin of the particles (angular to subangular grain shapes) is evident (Fig. 22). The classification of

the rocks is based, in part, on the characteristics of these original grains. In the metasilstones, the rocks are composed largely of mineral grains smaller than 0.05 mm. The meta-arkosic wackes are coarsely grained, but particle size is still typically 0.2 mm or less. The abundance of plagioclase fragments relative to identifiable rock fragments dictates the use of the term “arkosic wacke” (Pettijohn et al., 1972).

Original bedding or lamination is preserved in several samples (e.g., Sample 173-1069A-21R-1 [Piece 2, 5–10 cm], also see “Lithostratigraphy” section, this chapter). In addition, at least one sample (Sample 173-1069A-21R-1 [Piece 2, 5–10 cm]) contains what appear to be pyritized fossils (first noted by Gus Gustafson; Fig. 23).

Metamorphic fabrics include deformed quartz, neoblastic growth of fine-grained (mostly <0.01 mm) phyllosilicates (sericite and chlorite), and a metamorphic foliation, commonly at a high angle to bedding. In all samples, the foliation is defined, in part, by preferred orientation of neoblastic phyllosilicates. In most samples, some original detrital minerals, especially quartz, are also oriented parallel to the foliation. This effect is particularly evident in the finer grained rocks (intervals 173-1069A-19R-1 [Piece 1, 1–3 cm], and 173-1069-23R-1 [Piece 2, 1–3 cm]). In pyrite-rich samples, the foliation is also marked by elongate masses of pyrite and by very thin (<0.05 mm), pyrite-rich veins or stylolites. Ilmenite (either porphyroblastic or detrital sedimentary) is randomly oriented or very weakly aligned with

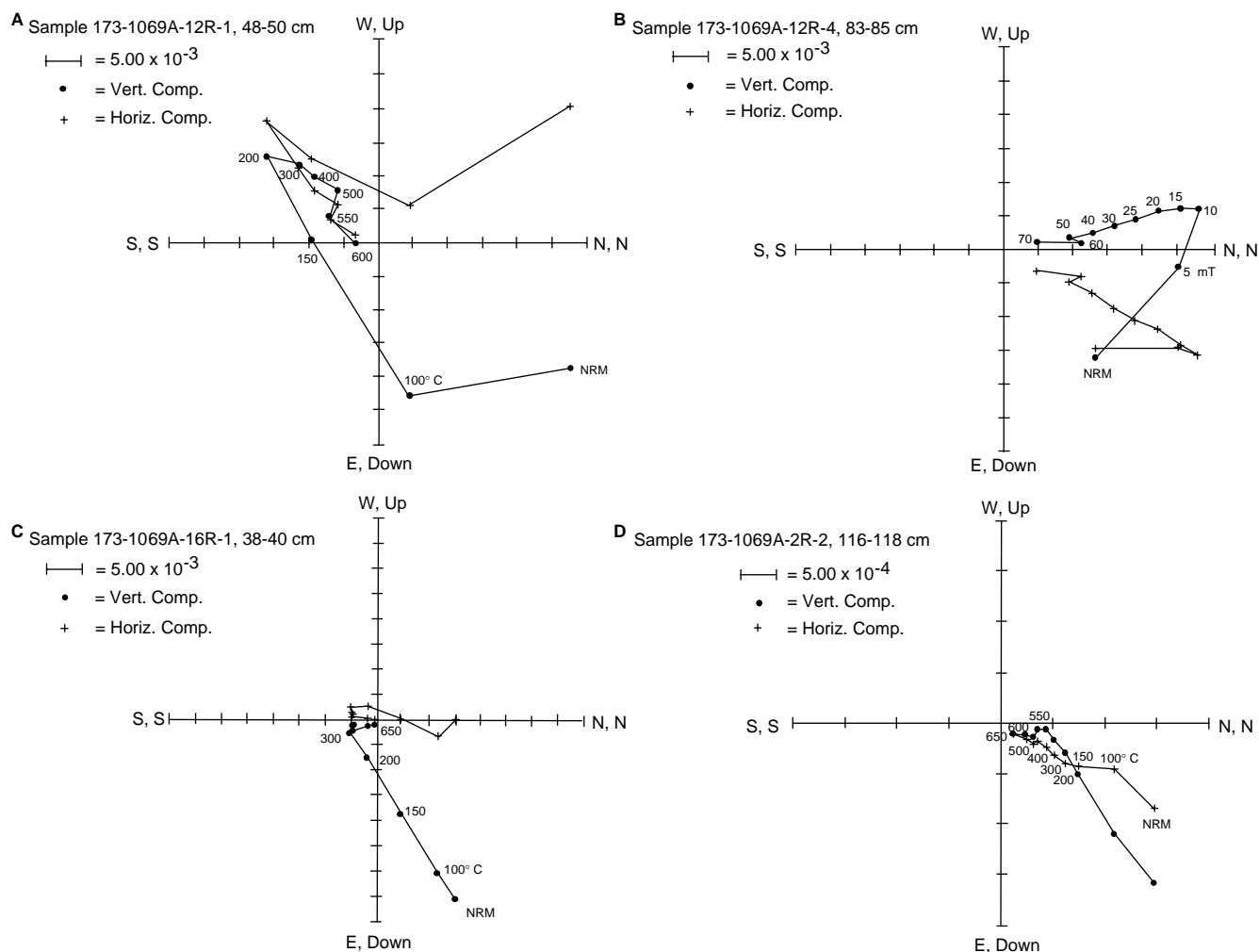


Figure 20. Representative vector end-point diagrams showing the results of thermal and AF demagnetization of reversely magnetized discrete samples (A and B) and normally magnetized discrete samples (C and D). Crosses and diamonds represent the projection of the magnetization vector end points on the horizontal and vertical planes, respectively. The declinations have not been corrected in this figure (see “Paleomagnetism” section, “Explanatory Notes” chapter, this volume).

foliation or bedding. In some samples (e.g., from thin section #172, interval 173-1069A-21R-1 [Piece 2, 5–10 cm]), mica growth appears to have taken place preferentially in pressure shadows associated with ilmenite grains and/or masses of pyrite.

Mineralogy

Quartz occurs in all samples as silt- to sand-sized, angular to subangular, elongate to equant grains. It is the commonest mineral in most samples, ranging in mode from 30%–70% (but see discussion of plagioclase below). Some relicts of the detrital character of the quartz are evident in most samples. In the coarsest rocks (e.g., interval 173-1069A-17R-1 [Piece 16], 84–88 cm), large, detrital quartz grains are largely intact. In the metasilstones, however, most quartz is aligned parallel to the foliation, probably reflecting pressure solution (see “Structural Geology” section, this chapter).

Plagioclase occurs in all samples as silt- to sand-sized, angular to subangular, detrital grains. It is generally recognized by albite or pericline twin forms. Its apparent mode ranges from 10%–40%. Because

untwinned plagioclase is difficult to distinguish from quartz (especially in the metasilstones), these modes must be considered minima.

A very fine-grained, highly birefringent phyllosilicate is a major constituent (10%–40%) of all samples. This material is tentatively identified as sericite. Sericite occurs in the interstices between the felsic detrital grains, in pressure shadows associated with the opaque minerals, and as a partial replacement of plagioclase. Sericite, in large part, defines the metamorphic foliation. Muscovite (<5%) occurs in relatively large (up to 0.4 mm) grains that are probably detrital. This muscovite is often kinked and/or partially replaced by chlorite.

Very pale green chlorite is less abundant than sericite, rarely making up more than 5% of the rock (15% in Sample 173-1069-23R-1 [Piece 2, 1–3 cm]). It is very rare to absent in Sample 173-1069A-20R-1 (Piece 2, 5–10 cm). It is most easily recognized by its anomalous, brownish interference colors. Fine-grained chlorite has an occurrence similar to sericite. Chlorite also occurs as a partial replacement of (detrital?) muscovite. Some relatively large masses of chlorite may represent former detrital muscovite.

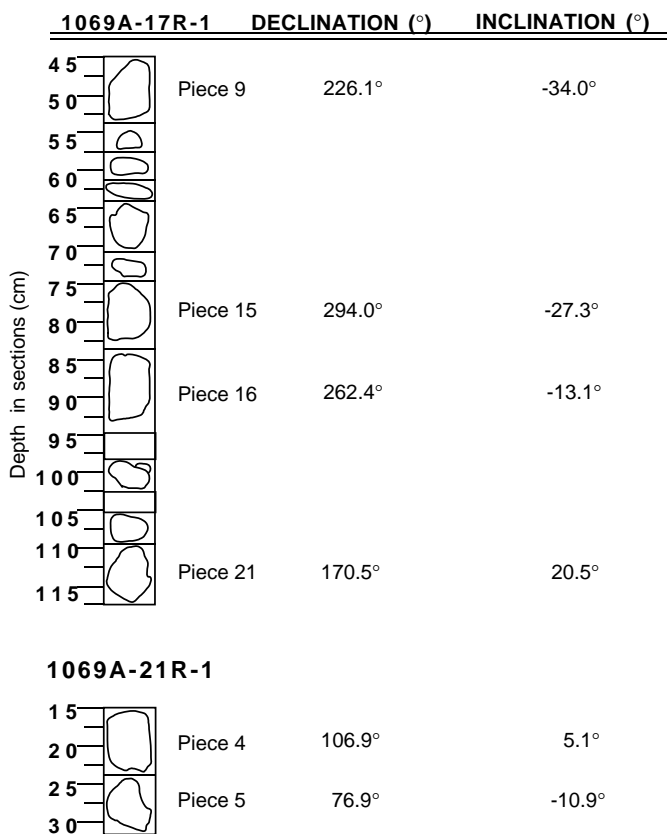


Figure 21. Results of a conglomerate test, on minicores drilled out of pieces from Subunit VB (Samples 173-1069A-17R-1 [Pieces 9, 15, 16, and 21]; 173-1069A-21R-1 [Pieces 4 and 5]) Diagram shows general outline shapes of the clasts. The scatter in the inclinations indicates that the pieces are not coherently magnetized, supporting the belief that Unit V is a conglomerate deposit; declination and inclination were measured in the core reference frame (see “Paleomagnetism” section, “Explanatory Notes” chapter, this volume). The declinations have been corrected to account for an error in the cryogenic magnetometer software (see “Paleomagnetism” section, “Explanatory Notes” chapter, this volume).

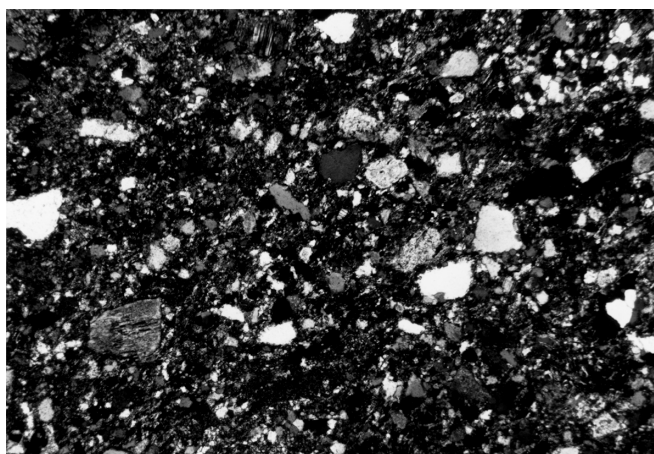
Dolomite occurs in Samples 173-1069A-20R-1 (Piece 2, 5–10 cm), and 173-1069A-23R-1 (Piece 1, 1–3 cm). In the former, it makes up a large part of the rock (20%–30%) and may have been part of the original diagenetic mineral assemblage. In this sample, the dolomite is often aligned with the plane of foliation. In Sample 173-1069A-23R-1 (Piece 1, 1–3 cm), dolomite occurs as subhedral to euhedral crystals that appear to be porphyroblasts.

Pyrite occurs as irregular masses, thin stylolites or veins, and in vugs (hollow structures which sometimes contain quartz). Pyrite is common in two of the samples (about 2%–5% in Samples 173-1069A-20R-1 [Piece 2, 5–10 cm], and 173-1069A-21R-1 [Piece 2, 5–10 cm]) and occurs as a trace phase (<<1%, very small [<0.01 mm] crystals) in the other thin sections. It is also abundant in many hand samples from Cores 173-1069A-17R to 25R. Several of the vugs are divided by pyritic “bridges” into two or more compartments. In one case (Fig. 23) this compartmentalized, hollow structure appears to be a deformed, pyritized fossil gastropod or foraminifer. More commonly, however, the pyrite vugs are deformed to the point where their original structure cannot be ascertained. Given the well-developed metamorphic foliation seen in these rocks (often defined by alignment of the pyrite vugs), it is likely that the open space in the pyrite vugs is a secondary feature and reflects the dissolution of the phase (carbonate?) that originally occupied the cores of the structures.

Table 6. Thin-section observations on metasediments from Subunit VB.

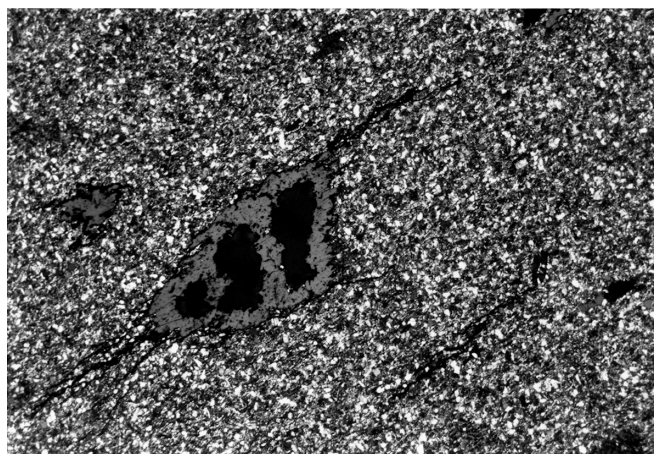
Core, section, piece, interval (cm)	Rock name	Comments
173-1069A-17R-1, 16, 84-88	Meta-arkosic wacke	Leucoxene after ilmenite.
17R-1, 15, 78-81	Meta-arkosic wacke	Leucoxene after ilmenite.
19R-1, 1, 1-3	Metasiltstone	Sericite-rich (40%).
20R-1, 2, 5-10	Meta-arkosic wacke	Pyrite-rich, 20%-30% dolomite, 10%-20% carbonaceous matter in sericite-poor, dark bed. Chlorite rare to absent throughout.
21R-1, 2, 5-10	Meta-arkosic wacke	Pyrite-rich fossils.
23R-1, 1, 1-3	Metasiltstone	Leucoxene after ilmenite, 5% dolomite, 25% sericite, 15% chlorite-rich.

Note: Unless noted, the mineral assemblage is quartz-plagioclase-muscovite-tourmaline-ilmenite (detrital) and sericite-chlorite-ilmenite(?) (metamorphic).



1 mm

Figure 22. Photomicrograph of detrital quartz and feldspar grains, Sample 173-1069A-17R-1 (Piece 16, 84–88 cm). Largest grains ~0.4 mm.



1 mm

Figure 23. Photomicrograph of pyritized fossil gastropod(?) (reflected light), Sample 173-1069A-21R-1 (Piece 2, 5–10 cm). Fossil is 1.5 mm long.

Ilmenite constitutes up to 5% of the thin section mode and is most abundant in the pyrite-free thin sections. The ilmenite is variably, sometimes pervasively, replaced by a fine-grained, highly birefringent mineral interpreted as “leucoxene” (a poorly defined mixture of cryptocrystalline Fe- and Ti-oxides). In hand sample, the heavily re-

placed ilmenites present the aspect of large (up to 1 mm) tabular, whitish masses that superficially resemble plagioclase laths. In thin section, the ilmenite/leucoxene occurs as subhedral, tabular grains containing inclusions of detrital minerals. Some of the ilmenite in Samples 173-1069A-17R-1 (Piece 16, 84–88 cm), and 173-1069A-20R-1 (Piece 2, 5–10 cm), may be detrital.

A dark region (bed?) in Sample 173-1069A-20R-1 (Piece 2, 5–10 cm), contains a substantial amount (10%–20%) of an unidentified opaque substance that may be carbonaceous material.

Accessory phases include tourmaline and chalcopyrite. Tourmaline occurs as small (<0.1 mm), pleochroic greenish-brown crystals that are probably detrital. Small amounts of chalcopyrite are associated with pyrite.

Discussion

The apparently stable coexistence of dolomite + sericite + quartz indicates that metamorphic grade in these rocks is lower greenschist to subgreenschist (Powell and Holland, 1989). This is consistent with the fine grain size and apparent sericitic nature of the metamorphic white mica and the overall preservation of sedimentary textures in these rocks.

In situ rocks closely resembling the Hole 1069A metasediments have been reported from the northwest margin of Galicia Bank, ~300 km north of Site 1069. There, the rocks are described as weakly metamorphosed, sericite- and chlorite-cemented sandstones intercalated with dolomitic rocks and siliciclastic volcanic rocks (Mamet et al., 1991). These rocks are locally fossiliferous, yielding Devonian to Carboniferous ages, and, like the rocks at Site 1069, are overlain by unmetamorphosed Tithonian sediment. If Hole 1069A was drilled through the same formation as exists northwest of Galicia Bank, then the basement high drilled at Site 1069 is composed, at least in part, of continental crust. On the other hand, strong paleomagnetic and other arguments can be made that the metasediments in Hole 1069A are clasts of continental material in a sedimentary breccia or conglomerate that are derived from local(?) continental outcrops (see “Lithostratigraphy” and “Structural Geology” sections, this chapter), in which case the petrological arguments for continental basement under the site are weaker.

STRUCTURAL GEOLOGY

Hole 1069A passed through 155 m of weakly deformed middle Eocene to Upper Jurassic sediments (lithostratigraphic Units II and IV, and Subunit VA) and then penetrated 85.6 m into the acoustic basement from which pieces of folded and foliated low-grade metasediments were recovered. These are interpreted as a clastic deposit, Subunit VB (see “Lithostratigraphy” section, this chapter).

Structural Observations in Unit II, Unit IV, and Subunit VA

A significant change in the true dip of bedding occurs within Subunit IIB at about 760 mbsf (Fig. 24; Table 7 on CD-ROM, back pocket, this volume). Above 760 mbsf, the dip is more variable and steeper (between 5° and 28°; Fig. 25); below, it is less variable and significantly shallower (between 0° and 18°; Fig. 25). In the lower part of Subunit IIC steeper values were again measured. The change in dip at 760 mbsf appears to be abrupt. It is probably related to tectonic deformation.

Deformation structures observed in the core include faults, stylolites, and slump folds. The fault planes dip between 11° and 72°, slickenside lineation is mostly parallel to the dip, and the slip sense, where it can be observed, is normal. Faults are rare in Cores 173-1069A-1R through 13R (719–844 mbsf) and were observed in only seven intervals. In Cores 173-1069A-14R, 15R, and 16R (844–873

mbsf), faults are more common and were found in nine intervals. The faults indicate a slight extensional deformation of Units II and IV. Stylolites were observed only in Core 173-1069A-10R of Subunit IIB (see Fig. 10, “Lithostratigraphy” section, this chapter). The orientation of the stylolites indicates subhorizontal compression. They may have formed during a post-Paleocene compressional tectonic event (e.g., middle Miocene Betic compression). Folds, most likely formed as slump folds in soft sediments, were observed only at the base of the sediments (intervals 173-1069A-14R-1, 60–65 cm, and 173-1069A-14R-2, 120–125 cm). Slumping and microfaulting are pervasive in the lower part of Unit IV (interval 173-1069A-16R-3, 80–123 cm; see Fig. 13B, “Lithostratigraphy” section, this chapter).

Overall, deformation structures are rare in the upper part of Unit II, more common in the lower part of Subunit IIC and even more common in Unit IV. In Subunit VA no deformation structures are visible because of the types of recovered rock (clay disturbed by drilling and limestone pieces).

Structural Observations in Metasediments of Subunit VB

Hole 1069A penetrated 85.6 m into acoustic basement from which foliated meta-arkosic wackes, metasiltstones, and dolomitic meta-arkose were recovered. The nature of this basement, whether in place or redeposited as a conglomerate or breccia, is problematic.

Bedding and foliation (cleavage) can be recognized on the cores and in thin sections (Fig. 26). Sedimentary bedding is outlined by variations in composition and by the orientation of large (up to 0.4 mm), often kinked, detrital muscovite grains (partly replaced by chlorite) and by some of the large opaque grains. The orientation of the bedding is variable in the few oriented pieces that were recovered. Under the microscope, the foliation is defined by the orientation of small grains and aggregates of white mica (sericite) and chlorite (<0.05 mm), elongate quartz grains, some dolomite crystals and elongate ilmenite grains, and anastomosing seams of fine-grained, altered pyrite (Fig. 26). In five pieces, the orientation of the foliation could be measured. It dips between 0° and 40° (average 19.4°). The foliation is typically oriented at 45° to 70° to the bedding, but can also be perpendicular or subparallel to the bedding. In Sample 173-1069A-23R-1, 1–3 cm, the foliation is at a high angle (70° to 90°) to the bedding and the latter outlines an open fold, with the foliation parallel to the axial plane of this fold. In Sample 173-1069A-17R-1, 61–63 cm, the angle between foliation and bedding is only about 10° (Fig. 27). Figure 28 shows the relations of opaque minerals with bedding and foliation in a thin section from interval 173-1069A-21R-1, 5–10 cm. The foliation is at an apparent angle of 70° to the bedding. The three hollow objects consisting of pyrite probably represent pyritized fossils, the shape of one of them suggesting a gastropod or foraminifer. These objects were apparently rotated to become parallel with the foliation. Thin, anastomosing stringers of partly altered pyrite also lie parallel to the foliation. These may represent either pyrite that was relatively enriched along the foliation by dissolution of the other constituents of the rock, or pyrite veins. A third type of opaque object is represented by poikiloblastic, euhedral, 1- to 2-mm-long ilmenite porphyroblasts partly replaced by leucoxene. During metamorphism these grew in part parallel to the foliation, and in part parallel to the bedding of the arkosic wacke.

Some larger quartz grains, feldspar grains, and rock fragments have pressure shadows parallel to the foliation that are filled by sericite, chlorite, and fine-grained quartz (0.03–0.05 mm), and have often grown in optical continuity with the larger quartz grain. Many quartz grains show undulatory extinction, some also show subgrain formation at their boundaries. Higher-temperature deformation structures, e.g., polygonal quartz with triple junctions, are only observed in detrital rock fragments and are therefore older than the metasediments.

Structures indicative of brittle deformation, such as fractures, catclastic zones, or veins, are very rare in the metasediments of Subunit VB. Only minor veins of calcite were observed in thin section and in

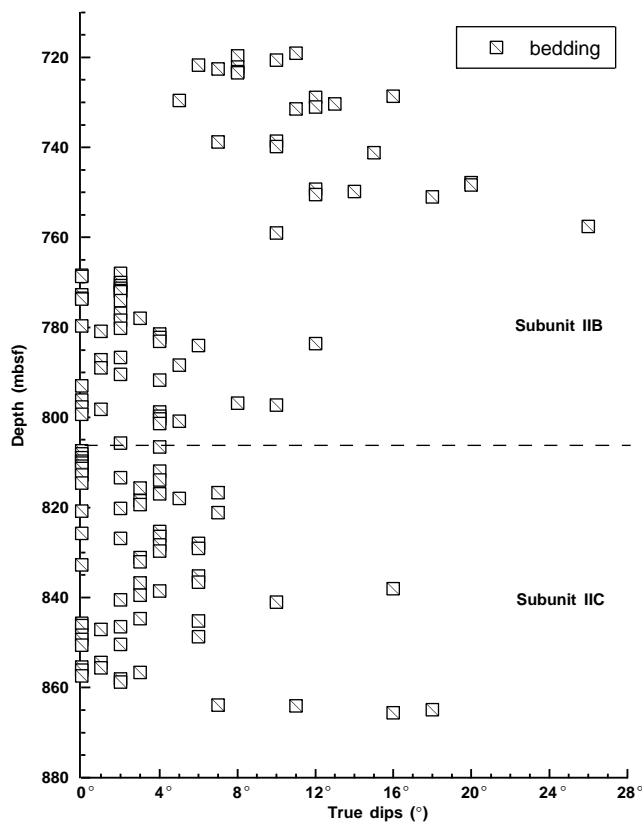


Figure 24. Dip of bedding vs. depth for sediment in Subunits IIB and IIC

Sample 173-1069A-21R-1 (Piece 9). This is in marked contrast to the basement rocks recovered in Holes 1067A and 1068A, and to the basement clasts found in the breccias (Unit IV) of Hole 1068A, where brittle structures are ubiquitous.

The overall observations and mainly the occurrence of anastomosing stringers of opaque minerals parallel to the foliation, indicate that the deformation of the basement rocks was dominated by pressure solution. Crystal plastic deformation played only a minor role (undulatory extinction in quartz), indicating a maximum temperature of ~300°C (see also “Igneous and Metamorphic Petrology” section, this chapter). The foliation represents an axial planar slaty cleavage or schistosity related to folding. This type of deformation is typical of low-grade metamorphic slate belts, such as those which occur in parts of the Variscan orogen.

Orientations of Foliation and Magnetization in the Metasediments

Most of the metasediments recovered from Hole 1069A are small, unoriented pieces (“rollers”). However, five pieces are long enough to have retained their original orientation before coring, and in these the orientation of the foliation and the stable component of magnetization were measured in the core reference frame (see “Paleomagnetism” section, this chapter), in an attempt to answer the question whether the metasediments are in place or resedimented. In addition, foliation and magnetization of one “roller” were measured in an arbitrary reference frame. The results displayed in Table 8 are equivocal but allow some inferences to be drawn.

As mentioned above, the foliation has a generally shallow dip (five measurements range from 0° to 40° with an average of 19.4°). The same applies to the inclination of the stable component of magnetization (5.1° to 34.0°, average 18.1°). Both negative and positive inclinations occur. The angle between the foliation plane and the magnetization vector is variable but is generally low to intermediate (between 4° and 34°, average 18.7°). These observations suggest that

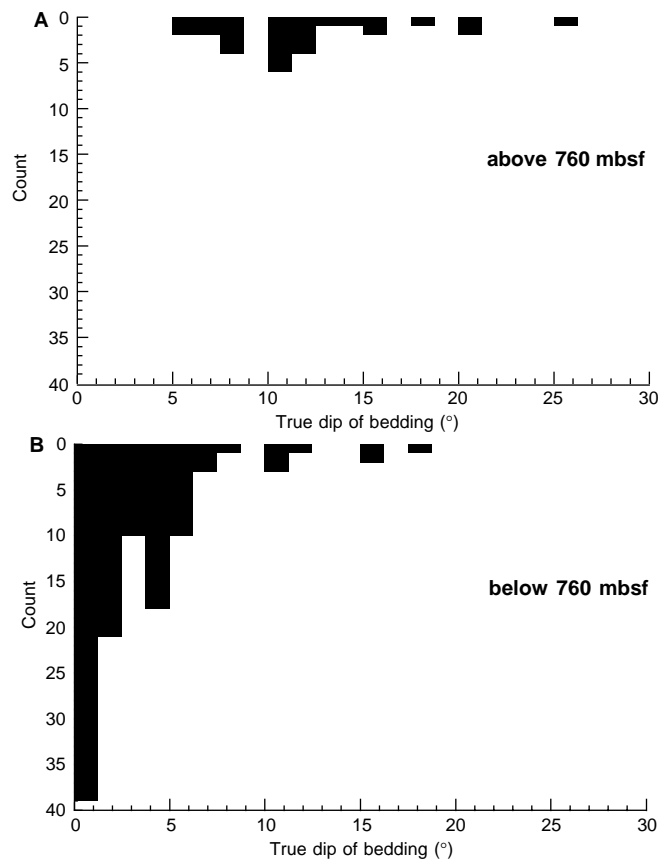


Figure 25. Histograms showing the true dip of bedding measured: (A) above 760 mbsf, and (B) below 760 mbsf.

the metasediments do not represent a breccia deposit, because in this case, the inclination of the different pieces should be randomly distributed, or alternatively, if the magnetization postdated the deposition, should be uniform and, if Cretaceous or Jurassic in age, steeper than observed. The relatively uniform and shallow foliations and inclinations can be explained in two ways: (1) the metasediments are pre-Jurassic in age and are in place; or, (2) the metasediments were redeposited in such a way that the foliations and inclinations became shallowly oriented.

Several of the metasedimentary pieces are moderately to well-rounded pebbles or cobbles (see “Lithostratigraphy” section, this chapter), which favors the second explanation. The presence of both positive and negative magnetic inclinations argues against the first explanation. Subunit VB probably represents a conglomerate with pebbles and cobbles from a source area exposing low-grade metamorphic rocks. The low angle between foliation and magnetization may be explained by synkinematic reorientation or growth of the minerals bearing the magnetization (e.g., the ilmenite grains parallel to the foliation observed in thin section, see above). During their transport the pebbles were rounded to ellipsoidal shapes as in, for example, Sample 173-1069A-17R-1 (Pieces 12 and 13; see Fig. 16B, “Lithostratigraphy” section, this chapter; Fig. 27), with the plane containing the longest and intermediate axes of the ellipsoid (x-y plane) oriented parallel to the foliation, as is often observed in river deposits in slate belts. The pebbles and cobbles were then deposited with the x-y plane in a preferentially shallow orientation (e.g., imbricate structure in fluvial conglomerates).

Conclusions

The absence of a pervasive brittle overprint in the recovered metasediments is not compatible with these rocks forming a strongly

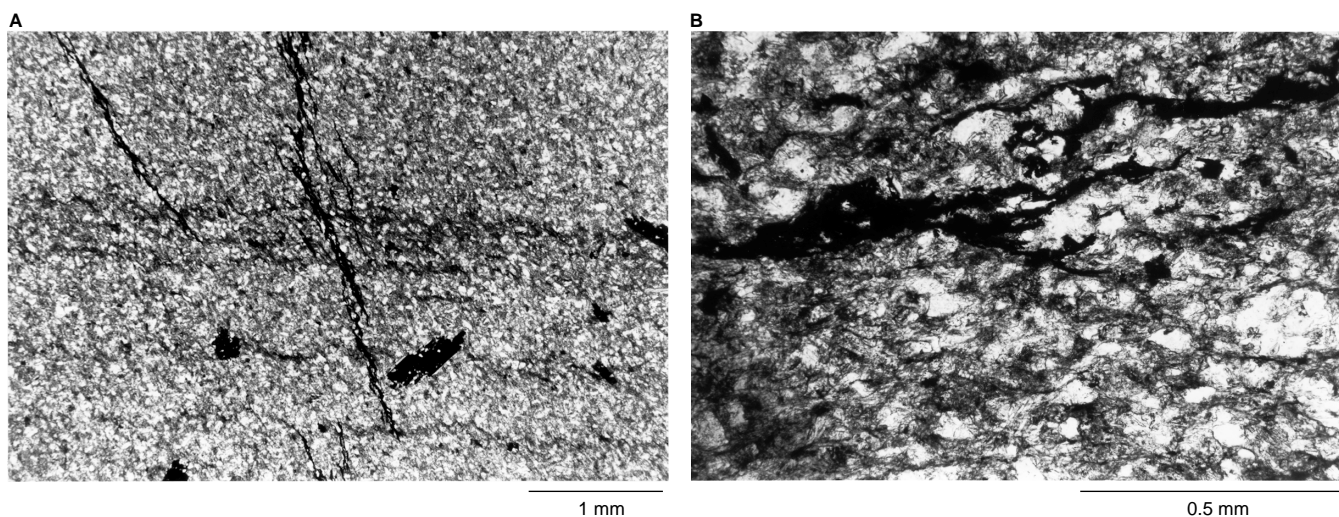


Figure 26. **A.** Thin-section photomicrograph showing bedding (horizontal) and foliation (dipping steeply to the right) in meta-arkosic wacke from Sample 173-1069A-21R-1, 5–10 cm. Opaque objects are ilmenite porphyroblasts and stringers of altered pyrite parallel to the foliation. **B.** Photomicrograph showing the character of the foliation in the same sample as (A). The foliation is defined by elongate quartz crystals deformed by pressure solution, by the alignment of small mica and chlorite grains, and by anastomosing pyrite stringers.

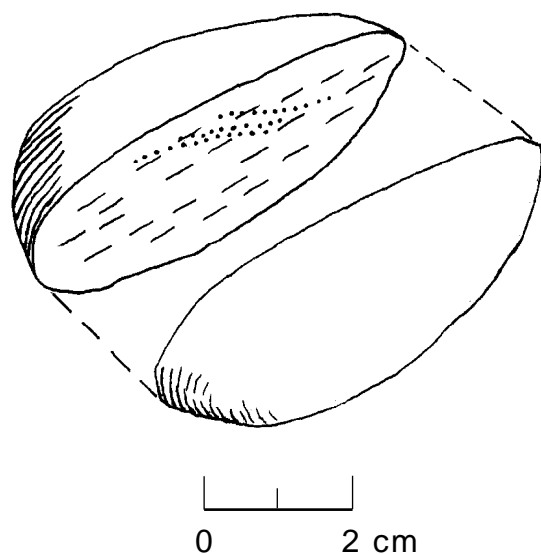


Figure 27. Sketch of foliation (dashed) and bedding (dotted) in a pebble of metasediment from Subunit VB. Foliation is at a low angle to the bedding. The pebble is well-rounded and has an ellipsoidal shape with the shortest axis of the ellipsoid normal to the foliation, as is typically observed in conglomerates formed from foliated rocks. Sample 173-1069A-17R-1, 61–63 cm.

tectonized continental basement. Therefore, these rocks are very likely redeposited. As discussed above, they may represent a fluvial or deltaic deposit. The homogeneous character of the pieces indicates a restricted source area. Similar, weakly metamorphosed rocks of Paleozoic age occur in the area of Galicia Bank further north, directly overlain by rocks of Tithonian age (Mamet et al., 1991), which indicates that these rocks were exposed at the surface in pre-Tithonian time. Thus, a likely assumption is that the meta-arkosic wackes are reworked basement clasts derived from the southern margin of Galicia Bank and deposited as a conglomerate in pre-latest Jurassic time, before the deposition of the pre-rift, Tithonian(?) Subunit VA. The presence of the prerift sedimentary Subunits VA and VB on the basement high at Site 1069A indicates that the basement high represents a block of continental crust.

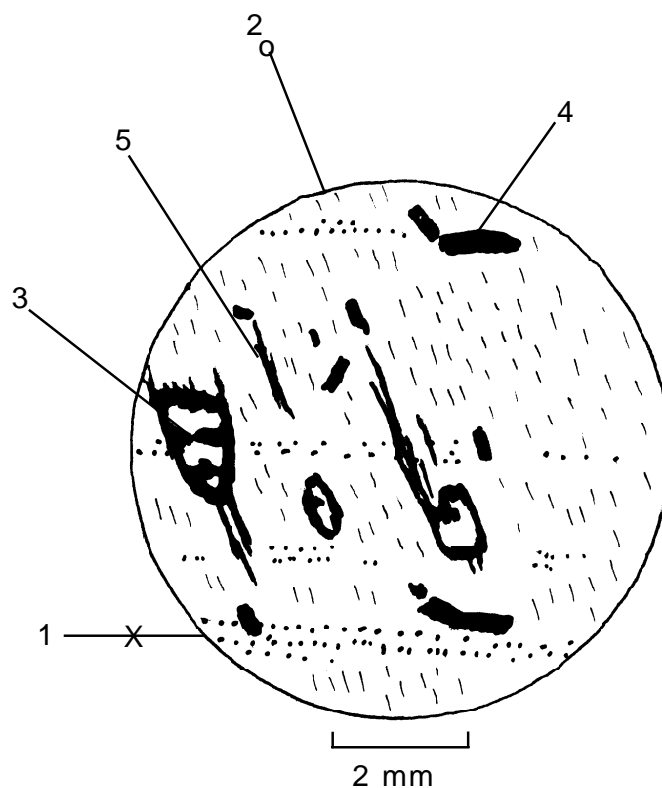


Figure 28. Sketch of relations between bedding, foliation, and opaque objects observed in thin section (interval 173-1069A-23R-1, 1–3 cm). 1 = bedding, 2 = foliation, 3 = pyritized fossil (gastropod or foraminifer), 4 = poikiloblastic, euhedral, 1- to 2-mm-long ilmenite porphyroblasts partly replaced by leucocoxene, and 5 = thin, anastomosing stringers of partly altered pyrite.

ORGANIC AND INORGANIC GEOCHEMISTRY

Concentrations of carbonate, organic carbon, and total nitrogen in sediments from Hole 1069A were measured on one to three samples per core throughout the cored interval (718.8–959.3 mbsf). Routine

Table 8. Measurements of foliation and stable component of magnetization in the meta-arkosic wackes, metasilstones, and dolomitic meta-arkose.

Core, section, piece	Depth in section (cm)	Foliation azimuth/dip (°)	Stable component of magnetization (declination/inclination) (°)	Angle between foliation and stable component (°)
173-1069A-				
17R-1 (Piece 9)	51	000/00	226.1/-34.0	34
17R-1 (Piece 15)	80	090/15	294.0/-27.3	13
17R-1 (Piece 16)	90	090/40	262.4/-13.1	26
21R-1 (Piece 4)	20	196/11	106.1/5.1	4
21R-1 (Piece 5)	26	130/31	76.9/-10.9	28
17R-1 (Piece 21; roller)	113	090/85	170.5/20.5	7

Note: The declinations used here were corrected to account for an error in the cryogenic magnetometer software (see "Paleomagnetism" section, "Explanatory Notes" chapter, this volume.)

measurements were also made of headspace gas compositions as part of the drilling safety program. Four interstitial water samples were squeezed from the sediments in the interval from 729.2 to 829.4 mbsf. Sediments from below this depth were too lithified to make interstitial water sampling possible.

Inorganic and Organic Carbon

Concentrations of carbonate carbon in sediments at Site 1069 vary from 0.1% to 11.4%, equivalent to CaCO_3 concentrations (assuming that all the carbonate is present as pure calcite) of 0.7% to 95% (Table 9). The cored sedimentary sequence at Site 1069 consists of upward-darkening units of basal siltstone/sandstone overlain by calcareous claystone and capped by claystone (see "Lithostratigraphy" section, this chapter). The CaCO_3 contents of sediments from these three different lithologic types within individual upward-darkening sequences are shown in Figure 29. In general, there is considerable overlap in carbonate contents of the basal siltstones and sandstones and the overlying calcareous claystones. In contrast, the dark claystones that typically form the caps of the upward-darkening sequences have much lower CaCO_3 contents, varying from 1.5 to nearly 20%. This pattern is consistent with the interpretation that the basal siltstone and sandstone and overlying calcareous claystone were deposited near or below the CCD by turbidity currents carrying carbonate-rich material from shallower depths, whereas the dark claystones represent hemipelagic sediments.

Concentrations of organic carbon are mostly below detection in sediments from Site 1069. However, a single sample from Unit V (Sample 173-1069A-21R-1, 46–48 cm) contains 0.33% organic C and has a C/N value (4.1) that indicates a predominantly marine source for the organic matter. This sample is a dark gray clay that may represent the matrix of a breccia that was very poorly recovered from the lowermost part of Hole 1069A (see "Lithostratigraphy" section, this chapter).

Headspace Gas Measurements

In Hole 1069A, methane concentrations in headspace gases were very low in the interval from 723.4 to 836.2 mbsf and then increase to as much as 102 ppm near the bottom of the hole (see Table 10; Fig. 30). The sample with the highest methane is the dark gray clay described above as a possible breccia matrix in Unit V. Given the very low organic carbon concentrations in the sediments overlying Unit V, the downward increase in methane concentration in sediments starting at ~850 mbsf is probably a result of upward diffusion of methane from Unit V (Fig. 30).

Interstitial Water

The compositions of four interstitial water samples collected from Hole 1069A are reported in Table 11.

PHYSICAL PROPERTIES

At Site 1069, magnetic susceptibility and natural gamma radiation were measured at 3 and 10 cm intervals, respectively, on all sedimentary cores. No multisensor track (MST) measurements were made on the nine hard rock cores of Subunit VB (173-1069A-17R through 25R) that exhibited limited recovery (<3%) and had no continuous sections. All measurements of velocity used the Hamilton Frame Velocimeter, and results indicate that the Subunit VB cores are within acoustic basement at this site. Index properties of all samples from Hole 1069A included wet and dry mass, bulk density, grain density, porosity, water content, and void ratio. Thermal conductivity experiments were not conducted at this site given the softness or discontinuity of all cores.

Multisensor Track

The magnetic susceptibility and natural gamma radiation of the sediment cores are displayed in Figure 31 and listed in Tables 12 and 13 on the CD-ROM (back pocket, this volume). Generally, above 800 mbsf, in most of Subunit IIB, values of magnetic susceptibility are $<50 \times 10^{-5}$ SI units, with local maxima at about 719 and 777 mbsf. Comparison of individual section susceptibility records with the split core shows that these peaks coincide with very dark brown sediment layers that are on the order of a few centimeters thick. Below 800 mbsf, in the lowest part of Subunit IIB, magnetic susceptibility increases sharply to $\sim 100 \times 10^{-5}$ SI units, and values are more variable until 830 mbsf is reached. Between 835 and 841 mbsf, the values are again $<50 \times 10^{-5}$ SI units. Below 844 mbsf magnetic susceptibility exhibits increasing variability with peaks often $>250 \times 10^{-5}$ SI units. At 864 mbsf, one very dark brown clay layer correlates with a peak that reaches over 900×10^{-5} SI units. In Core 173-1069A-16R (Unit IV), below 866 mbsf, values of susceptibility decrease to $\sim 20 \times 10^{-5}$ SI units.

Natural gamma counts decrease with depth from values of ~70 to ~60 counts per second (cps) in Subunit IIB above 775 mbsf. Activity is more variable between 775 and 830 mbsf, in the lower part of Subunit IIB and the upper part of Subunit IIC. A local maximum of natural gamma activity lies at around 848 mbsf in the lower part of Subunit IIC and peaks reach greater than 70 cps.

Index Properties

The sediment lithology of Subunits IIB and IIC can generally be described as a series of repeating sequences of calcareous sandstone overlain by calcareous claystone (sometimes chalk), and ultimately topped by a low-carbonate claystone. Unit IV consists of nannofossil chalk, whereas samples recovered from basement are mainly hard metasilstone, meta-arkosic wacke, and dolomitic meta-arkose (see "Lithostratigraphy" section, this chapter). Accordingly, we have divided our samples into four lithologic types for purposes of discus-

Table 9. Carbonate, carbon, and nitrogen in sediments from Hole 1069A.

Core, section, interval (cm)	Depth (mbsf)	Inorganic C (wt%)	CaCO ₃ (wt%)	Organic C (wt%)	N (wt%)	Organic C/N
173-1069A-						
1R-3, 74-76	722.54	1.01	8.4	—	0.06	—
1R-3, 78-80	722.58	3.76	31.3	—	—	—
2R-3, 36-38	731.14	0.48	4.0	—	0.06	—
2R-3, 40-42	731.18	2.56	21.3	0.04	0.04	0.9
2R-3, 47-49	731.25	4.43	36.9	—	—	—
3R-2, 73-74	740.33	2.53	21.0	0.04	0.06	0.7
3R-2, 82-83	740.42	4.16	34.7	—	—	—
4R-2, 40-42	749.6	1.44	12.0	—	0.05	—
4R-2, 53-55	749.73	5.14	42.8	—	0.04	—
5R-1, 49-51	757.89	2.89	24.1	—	0.04	—
5R-1, 62-65	758.02	4.57	38.1	—	—	—
6R-1, 5-8	767.15	7.33	61.1	—	—	—
6R-4, 60-61	772.2	1.58	13.2	—	0.06	—
6R-4, 76-77	772.36	0.26	2.2	—	0.06	—
7R-2, 86-88	779.16	0.83	6.9	0.02	0.10	0.2
7R-4, 105-108	782.35	0.48	4.0	—	0.06	—
7R-4, 113-115	782.43	3.02	25.2	0.01	—	—
8R-2, 32-34	788.22	0.31	2.6	0.02	0.05	0.5
8R-2, 103-105	788.93	0.35	2.9	—	0.06	—
8R-3, 97-99	790.37	10.27	85.5	—	—	—
9R-4, 61-62	801.11	0.38	3.2	—	0.06	—
9R-4, 65-66	801.15	3.00	25.0	0.10	—	—
10R-4, 98-99	811.08	7.93	66.1	—	—	—
10R-4, 111-112	811.21	1.86	15.5	—	0.05	—
11R-3, 84-86	819.14	0.49	4.1	—	—	—
11R-3, 104-106	819.34	7.60	63.3	—	—	—
11R-CC, 8-10	821.03	10.35	86.2	—	—	—
12R-4, 67-69	830.17	5.44	45.3	—	0.03	—
12R-4, 83-85	830.33	0.17	1.4	—	0.06	—
13R-3, 82-83	838.52	0.29	2.4	—	0.05	—
13R-3, 91-93	838.61	6.68	55.7	—	—	—
14R-2, 54-56	846.44	0.24	2.0	—	0.05	—
14R-2, 67-69	846.57	0.61	5.0	—	0.03	—
15R-3, 60-62	857.6	9.14	76.1	0.12	—	—
15R-3, 64-66	857.64	2.19	18.2	—	0.05	—
15R-4, 0-2	858.5	0.35	2.9	—	0.07	—
16R-1, 90-92	864.5	3.07	25.6	—	—	—
16R-2, 0-2	865.1	0.19	1.6	0.03	0.55	0.1
16R-2, 72-74	865.82	9.02	75.2	—	—	—
16R-3, 71-73	867.31	2.24	18.6	—	0.06	—
17R-1, 0-2	873.3	11.43	95.2	—	—	—
21R-1, 46-48	912.06	0.09	0.7	0.33	0.08	4.1

Note: — = concentration was below detection limit.

sion. In general, the boundary between some of the sediment types is gradational.

Sample wet bulk density and porosity are plotted vs. depth below seafloor in Figure 32 and are listed in Table 14. In Subunit IIB (above 806 mbsf), claystone porosity appears to increase slightly with depth, from around 35% at the top of the drilled interval to 44% at 790 mbsf. Density of the claystones correspondingly decreases, from 2.10 to 1.95 g/cm³ in this interval. Below 800 mbsf, claystones have porosities around 35% and bulk densities from 2.05 to 2.2 g/cm³. Calcareous claystone and chalk porosities generally vary between 22% and 38% and densities range from 2.15 to 2.35 g/cm³. Sandstones have porosities from 21% to 32% and densities from 2.15 to 2.35 g/cm³ in Subunit IIB. In Subunit IIC, below 806 mbsf, porosities of sandstones (excluding two samples) decrease to <20%. Their bulk densities range from 2.4 to 2.65 g/cm³. The two samples that have higher porosities and lower densities are soft sandstones in the middle part of Subunit IIC. These soft sandstones are poorly cemented by a calcite matrix. Meta-arkosic wackes have very low porosities (<3%) and bulk densities around 2.7 g/cm³. Grain densities of all samples are clustered around 2.7 g/cm³ (Table 14).

Acoustic Velocities

Velocities of the three sedimentary lithologies (claystones, calcareous claystones, and sandstones) and the one basement lithology (meta-arkosic wackes) form distinct sets of measurements (Table 15). With the exception of the sandstones, velocity shows no correlation with sedimentary unit boundaries or depth (Fig. 33); velocity

Site 1069

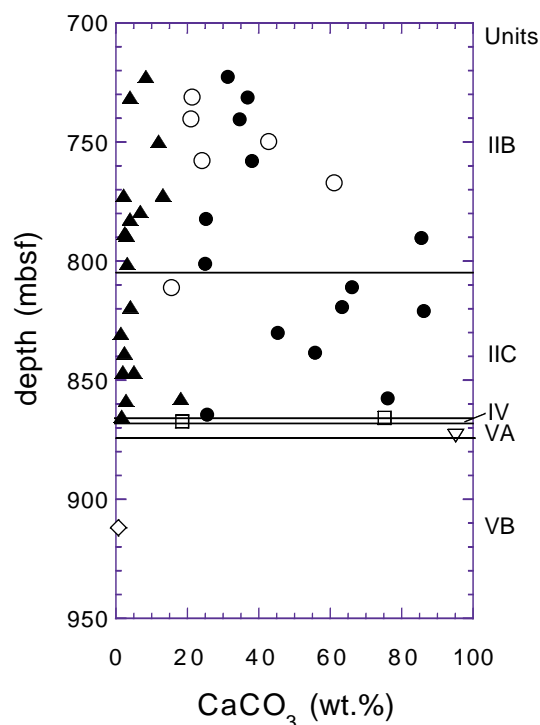


Figure 29. Downhole plot of CaCO₃ in sediments from Hole 1069A. Basal siltstone and sandstone layers from individual upward-darkening sequences are shown as solid circles, overlying calcareous claystones as open circles, and hemipelagic claystone as solid triangles. Unit IV sediments are shown as open squares, clast from Unit VA as an open inverted triangle, and the breccia matrix from Unit VB as an open diamond.

Table 10. Methane and ethane concentrations in headspace gas samples from Hole 1069A.

Core, section, interval (cm)	Depth (mbsf)	Methane (ppm)	Ethane (ppm)
173-1069A-			
1R-4, 37-38	723.37	2.3	—
2R-2, 1-2	729.29	2.8	—
3R-1, 149-150	739.59	2.7	—
4R-2, 0-5	749.2	2.2	—
5R-1, 0-5	757.4	2.2	—
6R-3, 149-150	771.59	2.5	—
7R-6, 52-57	784.32	2.8	—
8R-3, 148-150	790.88	3.2	—
9R-2, 148-150	798.98	3.4	—
10R-2, 0-2	807.1	2.2	—
11R-1, 0-5	815.3	2.6	—
12R-5, 145-150	832.45	2.8	—
13R-1, 149-150	836.19	2.8	—
14R-5, 0-5	850.4	5.2	—
15R-4, 0-4	858.5	19.7	—
16R-2, 0-2	865.1	62.3	—
17R-1, 0-2	873.3	13.8	—
21R-1, 46-49	912.06	101.7	1.6

Note: No heavier hydrocarbons were found in any of the gas samples.

varies generally according to porosity and density (Fig. 34). The sandstone units, which were sampled from Cores 173-1069A-2R through 15R, have velocities that increase with depth from 2600 m/s to 5000 m/s, with the exception of several poorly cemented sand-rich samples (notably a coarse-grained foraminifer sandstone at 848 mbsf). Claystone velocities remain constant with depth at approxi-

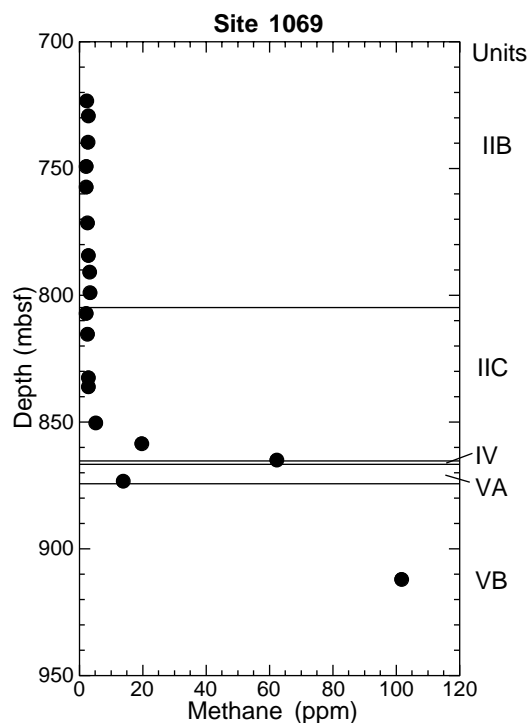


Figure 30. Methane concentrations in headspace gas samples from Hole 1069A.

Table 11. Interstitial water chemistry data for Hole 1069A.

Core, section, interval (cm)	Depth (mbsf)	SO ₄ ²⁻ (mM)	K ⁺ (mM)	Cl ⁻ (mM)	Ca ²⁺ (mM)	Mg ²⁺ (mM)	Na ⁺ (mM)
173-1069A-2R-1, 78-88	729.18	8.7	1.75	522	35.9	26.9	412
6R-3, 0-15	770.10	7.2	1.1	528	37.2	26.4	418
9R-1, 137-150	797.37	5.1	1.44	517	35.8	23.3	419
12R-3, 135-150	829.35	0.75	1.33	450	32.8	13.9	393

mately 2300 m/s, whereas calcareous claystone velocities are more variable with an average of 2500 m/s. Variations in velocities probably reflect varying degrees of cementation and consolidation within the simplified units above. However, velocity differences between lithologies are best explained by porosity variations.

Because of an increase in velocity and density coincident with the appearance of clasts of metasedimentary rocks, the top of acoustic basement is assigned to 874 mbsf within Core 173-1069A-17R. The velocity gradient at this interface, which is poorly constrained given less than 3% recovery in Cores 17R through 25R, is characterized by an increase from ~2500 m/s to ~5000 m/s (Fig. 33). Velocities within Subunit VB show very little deviation from an average of 5300 m/s; although one measurement (Sample 1069A-17R-1, 90 cm) yields a velocity of 4521 m/s. This uncharacteristically low velocity is coincident with a porosity of 3%; all other basement samples have a porosity of ~1%.

DOWNHOLE MEASUREMENTS

After drilling and RCB coring Hole 1069A to a total depth (TD) of 6045 mbrf (959 mbsf), two complete wiper trips were begun at 0700 hr, 29 May 1997, to condition the hole for logging. Additional cuttings were removed from the borehole by circulating sepiolite mud (see "Operations" section, this chapter).

Wireline logging operations began in Hole 1069A at 0500 hr on 30 May 1997. All logging operations were completed 24.5 hours lat-

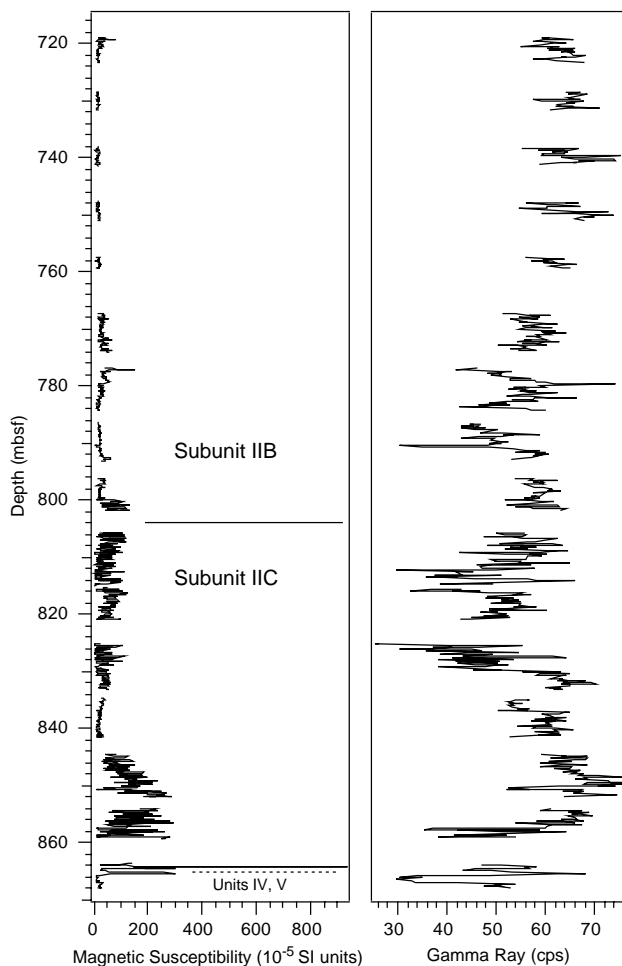


Figure 31. Magnetic susceptibility and natural gamma-ray activity vs. depth in Hole 1069A.

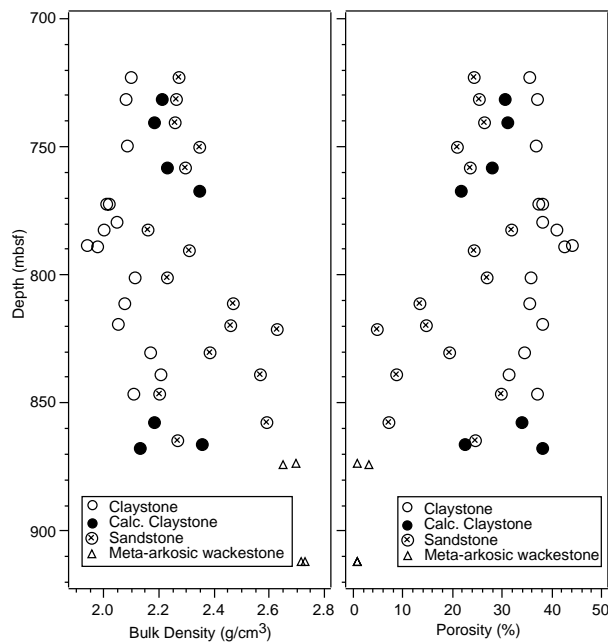


Figure 32. Bulk density and porosity vs. depth in Hole 1069A.

Table 14. Index properties from Hole 1069A.

Core, section, interval (cm)	Depth (mbsf)	Bulk density (g/cm ³)	Grain density (g/cm ³)	Porosity (%)	Water content (% dry mass)	Lithology
173-1069A-						
1R-3, 74-76	722.54	2.1	2.69	36	17	Claystone
1R-3, 78-80	722.58	2.27	2.67	24	11	Sandstone
2R-3, 36-38	731.14	2.08	2.7	37	18	Claystone
2R-3, 40-42	731.18	2.21	2.73	30	14	Calcareous claystone
2R-3, 47-49	731.25	2.26	2.68	25	11	Sandstone
3R-2, 73-75	740.33	2.18	2.7	31	14	Chalk
3R-2, 78-80	740.38	2.26	2.69	26	12	Sandstone
4R-2, 40-42	749.6	2.08	2.7	37	18	Claystone
4R-2, 53-55	749.73	2.34	2.69	21	9	Siltstone
5R-1, 49-51	757.89	2.23	2.69	28	13	Claystone
5R-1, 62-64	758.02	2.29	2.68	23	10	Sandstone
6R-10, 5-8	767.15	2.34	2.71	22	9	Chalk
6R-4, 61-63	772.21	2.01	2.59	37	19	Claystone
6R-4, 76-78	772.36	2.02	2.62	38	19	Claystone
7R-2, 86-88	779.16	2.05	2.68	38	19	Claystone
7R-4, 105-108	782.35	2	2.67	41	21	Claystone
7R-4, 113-115	782.43	2.16	2.69	32	15	Sandstone
8R-2, 32-34	788.22	1.94	2.65	44	23	Claystone
8R-2, 103-105	788.93	1.97	2.67	42	22	Claystone
8R-3, 97-99	790.37	2.31	2.71	24	11	Sandstone
9R-4, 59-61	801.09	2.11	2.71	36	17	Claystone
9R-4, 63-65	801.13	2.23	2.67	27	12	Sandstone
10R-4, 102-104	811.12	2.46	2.69	13	6	Sandstone
10R-4, 110-112	811.2	2.07	2.65	35	17	Claystone
11R-3, 86-88	819.16	2.05	2.68	38	19	Claystone
11R-3, 104-106	819.34	2.46	2.71	15	6	Claystone
11R-CC, 8-10	821.03	2.63	2.71	5	2	Sandstone
12R-40, 67-69	830.17	2.38	2.71	19	8	Sandstone
12R-4, 83-85	830.33	2.17	2.77	34	16	Claystone
13R-3, 81-83	838.51	2.21	2.74	31	14	Claystone
13R-3, 91-93	838.61	2.56	2.71	9	3	Sandstone
14R-2, 55-57	846.45	2.1	2.74	37	18	Claystone
14R-2, 65-67	846.55	2.2	2.69	30	14	Sandstone
15R-3, 60-62	857.6	2.59	2.71	7	3	Sandstone
15R-3, 64-66	857.64	2.18	2.77	34	16	Calcareous claystone
16R-1, 90-92	864.5	2.27	2.67	24	11	Sandstone
16R-2, 72-74	865.82	2.36	2.74	22	10	Chalk
16R-3, 71-73	867.31	2.13	2.81	38	18	Chalk
17R-1, 51-53	873.81	2.7	2.71	1	0.3	Meta-arkosic wacke
17R-1, 90-92	874.2	2.65	2.7	3	1	Meta-arkosic wacke
21R-1, 20-22	911.8	2.72	2.73	1	0.3	Meta-arkosic wacke
21R-1, 26-28	911.86	2.73	2.74	1	0.3	Meta-arkosic wacke

er. Two logging tool strings were run at Site 1069, the triple combination and FMS-sonic (see “Downhole Measurements” section, “Explanatory Notes” chapter, this volume). The primary objective at Site 1069 was to recover logs in the prerift sediments identified as acoustic basement from seismic lines. To achieve this goal the pipe was initially pulled to a depth of 5863 mbrf (777 mbsf); however, from the drilling operations we already believed that the hole had filled to 5949 mbrf (863 mbsf). The first run with the triple combination tool string was unsuccessful as the tool encountered an impassible bridge at 5864 mbrf (778 mbsf), just one meter below the bottom of the pipe. At this point it was decided to spend the remaining time logging the drilled sediment sequence with both triple combination and FMS-sonic tool strings. The pipe was pulled up to 5188 m (102 mbsf) and the triple combination tool string was run into the hole. At 5864 m (778 mbsf) the previously encountered bridge prevented further passage downhole, so a successful uplog was made at a speed of ~600 m/h. The FMS-sonic tool string was then prepared and lowered into the hole. As the tools were run downhole, telemetry errors developed at approximately 200 m below the drill pipe. As the tools were lowered downhole, the Schlumberger engineer attempted to determine what was causing the problems by reconfiguring surface equipment but achieved no improvement. When 778 mbsf was reached, an uplog was started and the FMS calipers were opened. At this point the tool head voltage became erratic and voltage had to be increased drastically to compensate. When measurement current (EMEX) was provided for the FMS, the telemetry system stopped operating altogether. As the tools continued to be pulled to the surface, several attempts were made to close the FMS calipers; none was successful. Finally, the tool was carefully pulled into the pipe with the calipers still open and brought to the surface. Unfortunately, no data were recovered

from the FMS-sonic tool string. An overview of the logging operations can be seen in Tables 16 and 17.

The triple combination tool string included, from top to bottom, the telemetry cartridge, HNGS, APS, HLDS, DITE, and TLT. The data collected by the triple combination is of good quality. All logging data were shifted, from meters below rig floor to meters below seafloor using the driller’s water depth, for preliminary shipboard analysis.

Geophysical Logging Data

Downhole measurements from Hole 1069A provide geophysical and geochemical (U, Th, K) data in the interval 102–778 mbsf (Figs. 35, 36). The overlap between logging data and cores is restricted to the interval 719–770 mbsf (Cores 1R through 6R). The correlation of lithostratigraphic units and logging data made between Holes 900A and 1068A (see “Site 1068” chapter, this volume) can be extended to Site 1069, which is 16 km west of Site 1068.

Between 100 and 145 mbsf, logging data show increasing values downhole for total natural gamma ray (60 to 110 API) and resistivity (0.9 to 1.4 Ω m), and decreasing photo-electric factor (PEF) from 3 to 2.6 barn/e⁻ (Figs. 35, 36). Between 145 and 170 mbsf, the logging data show natural gamma-ray values around 80 API, increasing resistivity downhole from 1.2 to 1.8 Ω m, and PEF, from 2.2 to 3.4 barn/e⁻. This interval correlates well with lithostratigraphic Subunit IC as defined from Hole 1068A logging data (Fig. 37). From 170 to 250 mbsf, total gamma-ray values initially decrease downhole from 100 to 60 API, and then increase to 100 API, while resistivity, density, and PEF measurements all display high values: 1.6 Ω m, 1.9 g/cm³, and 3.4 barn/e⁻, respectively (Figs. 35, 36). This interval correlates

Table 15. Compressional wave velocity data from Hole 1069A.

Core, section, interval (cm)	Depth (mbsf)	Velocity (m/s)	Lithology
173-1069A-			
2R-3, 36	731.14	2277.43	Claystone
2R-3, 40	731.18	2494.16	Calcareous claystone
2R-3, 47	731.25	3010.41	Sandstone
3R-2, 73	740.33	2471.77	Calcareous claystone
3R-2, 78	740.38	2602.62	Sandstone
4R-2, 40	749.60	2325.32	Claystone
4R-2, 53	749.73	2885.74	Siltstone
5R-2, 49	759.39	2449.02	Claystone
5R-2, 62	759.52	3264.01	Sandstone
6R-1, 5	767.15	2737.39	Calcareous claystone
6R-4, 61	772.21	2374.92	Claystone
6R-4, 76	772.36	2379.55	Claystone
7R-2, 86	779.16	2404.15	Claystone
7R-4, 105	782.35	2176.41	Claystone
7R-4, 113	782.43	2728.10	Sandstone
8R-2, 32	788.22	2270.90	Claystone
8R-2, 103	788.93	2291.48	Claystone
8R-3, 97	790.37	3466.12	Sandstone
9R-4, 59	801.09	2305.59	Claystone
9R-4, 63	801.13	2724.23	Sandstone
10R-4, 102	811.12	3697.20	Sandstone
10R-4, 110	811.20	2256.72	Claystone
11R-3, 86	819.16	2364.91	Claystone
11R-CC, 8	821.03	5204.00	Sandstone
12R-4, 67	830.17	3016.96	Sandstone
12R-4, 83	830.33	2205.33	Claystone
13R-3, 81	838.51	2133.94	Claystone
13R-3, 91	838.61	4531.97	Sandstone
14R-2, 55	846.45	2292.15	Claystone
14R-2, 65	846.55	2284.79	Sandstone
15R-3, 60	857.60	5030.96	Sandstone
15R-3, 64	857.64	2377.32	Calcareous claystone
16R-1, 90	864.50	2644.23	Calcareous sandstone
16R-2, 72	865.82	2813.21	Calcareous claystone
16R-3, 71	867.31	2039.55	Calcareous claystone
17R-1, 48	873.78	5609.09	Meta-arkosic wacke
17R-1, 51	873.81	5601.45	Meta-arkosic wacke
17R-1, 79	874.09	5176.91	Meta-arkosic wacke
17R-1, 89	874.19	4521.70	Meta-arkosic wacke
17R-1, 90	874.20	4526.49	Meta-arkosic wacke
21R-1, 20	911.80	5369.43	Meta-arkosic wacke
21R-1, 20	911.80	5638.52	Meta-arkosic wacke
21R-1, 21	911.81	5548.09	Meta-arkosic wacke
21R-1, 26	911.86	5554.14	Meta-arkosic wacke

with lithostratigraphic Subunit IIA, described as nannofossil claystone and nannofossil chalk at Site 900 (Shipboard Scientific Party, 1994d; Fig. 37).

The transition from Subunit IIA to Subunit IIB, inferred at 240 mbsf at Site 1068, occurs at 250 mbsf at Site 1069 (Fig. 37). Between 250 and 375 mbsf, all logging data correlate well between the two sites, but the correlated features lie at a greater depth at Site 1069. In this interval, most values are fairly constant, with the exception of a slight decrease in the total gamma ray from 100 to 90 API and an increase in resistivity from 1.7 to 2 Ω m. Between 375 and 430 mbsf, no correlation can be found between the two sites, as total gamma-ray values increase at Site 1069, whereas they decrease at Site 1068 over the interval (Fig. 37), indicating a difference in lithology between the two sites.

The high gamma-ray values encountered at ~480 mbsf at Site 1068 may be tentatively correlated with the high values reached between 500 and 550 mbsf at Site 1069. Again, a good correlation between Holes 1068A and 1069A appears below 600 mbsf, with almost no differences in depth. As at Hole 1068A, it is quite difficult to define lithostratigraphic units from logging data in the lower part of the hole, mainly because the data display continuous variations (with a wavelength of about 100 m) rather than sudden changes. From core observations, the transition between lithostratigraphic Subunit IIB and Subunit IIC was defined at 730 and 805 mbsf at Sites 1068 and 1069, respectively. However, the logging data features described at 740 mbsf at Site 1068 correlate well with data at 735 mbsf at Site 1069. The lithology of the cores is homogeneous, whereas the logging data exhibit some variations. Such a discrepancy in the depth of the lithostratigraphic subunits described from core and log data may be a result of limited and probably preferential core recovery.

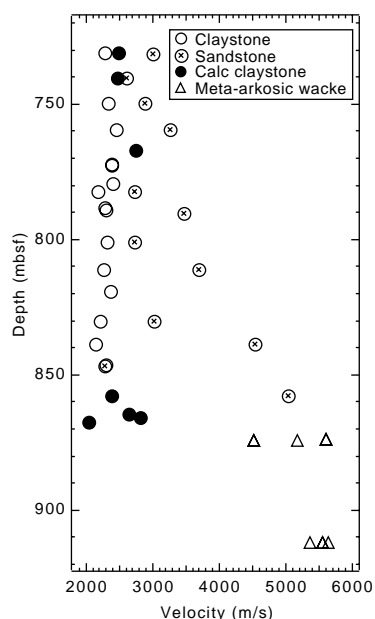


Figure 33. Compressional-wave velocity vs. depth in Hole 1069A.

Variations in the sedimentation rates between Sites 1068 and 1069 inferred from log data, suggest a greater rate during the Miocene at Site 1069, a slightly lesser rate during the upper Eocene, and a similar rate during the middle to lower Eocene, relative to Site 1068.

Finally, a water overpressure encountered at 650 mbsf during the wiper trip may be tentatively related to a 20-m-thick washout interval (670–690 mbsf), where high porosity and low resistivity were recorded.

Borehole Temperature

Figure 38 shows the temperature vs. depth profile for the run of the triple combination tool string from 778 mbsf to the seafloor. The temperature data are unlikely to represent thermal equilibrium between the borehole and the surrounding formation because of the disturbance created during drilling operations associated with fluid circulation. The temperature gradient is relatively constant from the seafloor to about 620 mbsf (up-log); however, these data indicate a low geothermal gradient (17°C/km), which may be because the hole had not reached thermal equilibrium.

SUMMARY AND CONCLUSIONS

Summary

All the cores recovered at this site contain sediments. The cores reveal a long history of deposition, in a great variety of environments, that provides important clues about the development of rifting on the West Iberia margin.

The history of the site began with the deposition of lithostratigraphic Subunit VB. Recovery of this subunit was very poor (<3%), yet the mean rate of penetration of the drill bit while cutting each core was always in the range 7.1–16.3 m/hr (or more precisely, using drilling records, in the range 3–17 min/m). Further, during coring, the bit experienced rapid fluctuations of torque over periods of several seconds. Except for three pieces of dark gray to black, slightly fissile, shaley material recovered from Cores 21R and 24R, the recovered pieces of rock were all pieces of very hard metasediment 2 to 17 cm long. Some pieces exhibit a moderately rounded shape that is evidently influenced by the direction of foliation in the rock. In spite of

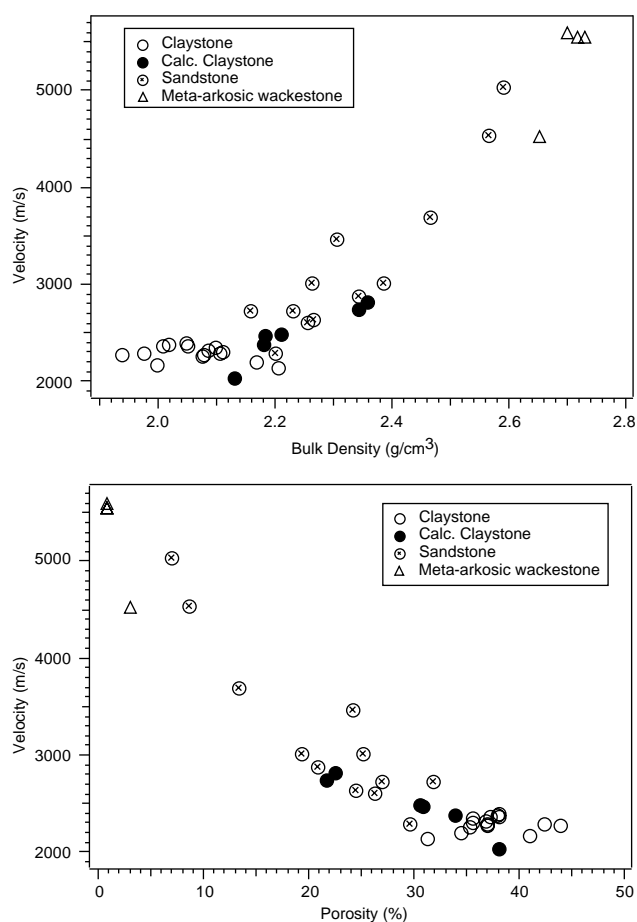


Figure 34. Compressional-wave velocity vs. porosity and density in Hole 1069A.

the abrasion caused by drilling, the original surfaces of the pieces are visible in several cases and this unequivocally suggests that at least these pieces are original clasts that must have existed in a softer matrix that was not recovered in the cores. The clasts are likely to have been about the size of the drill bit in diameter (~10.5 inches) or less because otherwise the rate of penetration would have been significantly slower as larger clasts were drilled through; this was not observed. It seems likely that the torquing was caused by clasts accumulating in the bottom of the hole and temporarily obstructing the bit before being broken up or entering the core barrel.

The clasts themselves are composed of meta-arkosic wackes and metasiltsstones with a metamorphic foliation and minerals typical of lower greenschist to subgreenschist facies. Deformation of the metasediments indicates a probable maximum temperature of ~300°C. In thin section, all samples exhibit original sedimentary textures and some preserve their original bedding or lamination. Vugs exist, one of which may represent a deformed pyritized fossil gastropod or foraminifer. Rocks closely resembling the Site 1069 metasediments, and which have yielded Devonian to Carboniferous fossils, have been reported from the northwestern edge of Galicia Bank (Boillot et al., 1988a; Mamet et al., 1991).

The matrix clearly is a friable material. Candidates include poorly cemented sands (loose sands would have caused the hole to collapse), fissile shale, and pelites shattered by cataclasis. A cataclastic origin is ruled out by the very rare evidence of cataclasis in the clasts. The three pieces of shaley material support the second hypothesis. However, a 40-cm-long ghost core obtained from the interval between 767–959 mbsf during a wiper trip contained unlithified coarse lithic sand with a high proportion of clasts of the same kind of metasedi-

Table 16. Depth parameters at Site 1069 from log and drilling operations.

Tool run	Operation depth	Depth (mbrf)
1	Driller's depth	6045
	Depth reached by tool	5863
	Driller's pipe	5863
	Logger's pipe	5863
	Driller's seafloor	5086
	Logger's seafloor	5087
2	Driller's depth	6045
	Depth reached by tool	5864
	Driller's pipe	5186
	Logger's pipe	5188

ment that occurs in lithostratigraphic Subunit VB, but this could have come from an unsampled interval of sand in Subunit IIC.

Thus, it appears that we cored a formation with pebble- to cobble-sized clasts of metasediment scattered randomly, or in layers, throughout a soft sand or shale matrix. The most favored explanations are that the formation was the distal part of a sand-rich alluvial fan or a high-concentration turbidity flow. Pebbly submarine fan and slope channel deposits occur within the Upper Jurassic of Portugal. Further evidence of the maturity, if not the antiquity, of the deposit is provided by the discovery of 102 ppm methane and 1.6 ppm ethane in headspace gases from the shaley 0.33% organic carbon material in Core 173-1069-21R. This may imply burial in the past under a greater lithostatic overburden than the current 910 m.

In the top few meters of Subunit VB, two occurrences of small pieces of limestone herald the deposition of Subunit VA, which consists of pieces of shallow-water limestone containing clasts of shallow-water carbonate material. So far these rocks are undated, except for one spot sample analyzed for palynology in a subsequent shore-based study which suggests an Upper Jurassic (mid-Kimmeridgian–upper Portlandian) age sediment deposited in a marine environment under a strong terrestrial influence (see “Appendix,” this chapter). They are overlain by only 10 cm of medium dark gray clay in which the Upper Jurassic (?Tithonian) nannoflora has been greatly diluted by fine clastics suggesting deposition in a restricted interior continental basin perhaps in outer shelf depths. A streak of nannofossil ooze within the clay, with a more diverse floral assemblage, indicates that open-water marine conditions were not far away.

The (?Tithonian) clay is possibly overlain by an unconformity, marked by limestone clasts, which separate it from 2.3 m of upper Berriasian to lower Valanginian chalk. The chalk was deposited well above the CCD and possesses a diverse nannoflora indicating a more open connection to the ocean. The lower part of the chalk shows pervasive evidence of slumping and microfaulting and, in places, it is mixed with sand- and gravel-sized extraformational clasts similar in composition to the pieces of limestone conglomerate and metasediment of lithostratigraphic Unit V. The chalk also possesses a slightly inclined bedding that is sometimes crosscut by subhorizontal laminae, probably of diagenetic origin. It is unclear whether the instability in the chalk was simply the result of deposition on a slope or whether it was deposited at a time of tectonic instability and differential vertical movements that included the onset of the subsidence that accompanied the rifting of Iberia from North America at this latitude. If the Unit IV chalk is pelagic drape, then it can be argued that the tectonically generated basement topography had already formed, at least partly, in pre-late Berriasian time, probably in the short hiatus between the Tithonian and late Berriasian.

At this site there was a long ~55 m.y hiatus in deposition between the early Valanginian and the late Campanian representing most of the Cretaceous. The boundary is sharp but without any angular unconformity. It is likely that, because the site is located near the top of a basement high, it was not inundated by abyssal plain turbidites for a long time. Further, the absence of post-early Valanginian pelagic

Table 17. Logging operations at Site 1069.

Date	Time (GMT)	Activity	
5/30/97	5:00	Rig up wireline and triple combination tool string	
	7:30	Run in hole with triple combination (TLT/DIT/HLDS/APS/HNGS)	
	10:00	Pipe depth (PD; 5863 mbrf) reached; no possible progress out of pipe	
	10:35	Tool run back to the seafloor; no data recorded	
	13:00	Tool out of drill string and rig down finished	
	15:00	Pipe lowered to below bridge (5863 mbrf) and pulled back up to 100 mbrf	
	15:00	Rig up triple combination for the second run (TLT/DIT/HLDS/APS/HNGS)	
	16:20	Run in hole to total depth (TD; bridge encountered at 5864 mbrf)	
	19:05	Log up to PD	
	20:20	Tool enters pipe	
	23:00	Rig down finished	
	23:30	Rig up of the FMS-sonic toolstring (FMS/SDT/NGT)	
	5/31/97	1:45	TD reached (5864 mbrf); telemetry problems, tool pulled to the surface
		5:30	Rig down finished; end of logging operations

drapes may be the result of pelagic sediments being transported downslope, and past the site, by gravity-driven processes.

The onset of sedimentation in the late Campanian heralded the beginning of sedimentation in a continental rise/abyssal plain environment that lasted more or less continuously until the present. As at Site 1068, the lithostratigraphic Unit II sediments are a mixture of lighter colored chalk, calcareous claystone, and silty claystone turbidite material that typically get darker upward as the sediment grades into brown to dark greenish gray hemipelagic claystones. This sequence is repeated many times on a scale of tens of centimeters. The sediments contain quite complex permutations of a number of lithologic "motifs". Thicker turbiditic intervals, including calcareous sandstones exhibiting normal grading, are characteristic features of lithostratigraphic Subunit IIC. Thin sections indicate that the sands were probably derived from three different source areas that characteristically provided winnowed foraminiferal tests, siliciclastic quartz, and lithic sand from exposed basement rocks and clasts of limestone from outcrops of lithified shallow-water limestones. The sharp tops to some sands and the concentration of foraminifers at the bases of some turbidites suggest some reworking by contour currents. Deposition was below, or rarely just above, the CCD. The location of the actual Cretaceous/Tertiary boundary is obscured because the sediments have been reworked by turbidity flows.

Post-middle Paleocene sediments are less sandy and the lack of nanoflora (except in reworked turbidite material) indicates deposition below the CCD. Remarkable, but as yet unexplained, peaks in magnetic susceptibility and magnetic intensity occurred in the lowest Eocene and middle Eocene sediments. These peaks correlate with thin black laminae in a dark brown claystone and have been noticed at approximately, if not precisely, the same chronostratigraphic horizon in all Iberia Abyssal Plain cores that contain sediment of this age.

Conclusions

The principal conclusion at this site is that the balance of evidence indicates that the north-south elongated fault block on which it was drilled originally lay in water depths of probably at most a few hundred meters. Between the Late Jurassic (?Tithonian) and the late Campanian, the environment of the site changed from a restricted interior basin to outerself/upper bathyal depths to abyssal depths. By simple isostatic arguments, this indicates a crust ~30 km thick in Late Jurassic times, which, in the complete absence of any evidence for a synrift mantle plume on this margin, is incontrovertible evidence that the block is composed of continental crust. The subsidence during the Cretaceous reflected both synrift tectonic crustal thinning and cooling of the margin.

The implications of this interpretation for the several models of the development of the ocean/continent transition will be discussed elsewhere, but brief reference to Table 1 indicates that revision and combination of some of these models is now required. A further conclusion from this site is that fault blocks in the West Iberia ocean/continent transition that are bounded by seaward-dipping listric normal

faults on seismic sections, as at Site 1069, are more likely to be continental than oceanic, whatever their longitude.

REFERENCES

- Applegate, J.L., and Bergen, J.A., 1988. Cretaceous calcareous nannofossil biostratigraphy of sediments recovered from the Galicia Margin, ODP Leg 103. In Boillot, G., Winterer, E.L., et al., *Proc. ODP, Sci. Results*, 103: College Station, TX (Ocean Drilling Program), 293–348.
- Barron, H.F., 1989. Dinoflagellate cyst biostratigraphy and palaeoenvironments of the Upper Jurassic (Kimmeridgian–basal Portlandian) of the Helmsdale region, east Sutherland, Scotland. In Batten, D.J., and Keen, M.C., (Eds.), *Northwest European Micropalaeontology and Palynology*: Chichester (Ellis Horwood), 193–213.
- Batten, D.J., and Koppelhaus, E.B., 1996. Biostratigraphic significance of uppermost Triassic and Jurassic miospores in Northwest Europe. In Jansonius, J., and McGregor, D.C. (Eds.), *Palynology: Principles and Applications* (Vol. 2): AASP Foundation, 795–806.
- Bergen, J.A., 1994. Berriasian to early Aptian calcareous nannofossils from the Vocontian Trough (SE France) and Deep Sea Drilling Site 534: new nannofossil taxa and a summary of low-latitude biostratigraphic events. *J. Nanoplankton Res.*, 16:59–69.
- Berggren, W.A., Kent, D.V., Swisher, C.C., III, and Aubry, M.-P., 1995. A revised Cenozoic geochronology and chronostratigraphy. In Berggren, W.A., Kent, D.V., Aubry, M.-P., and Hardenbol, J. (Eds.), *Geochronology, Time Scales and Global Stratigraphic Correlation*. Spec. Publ.—Soc. Econ. Paleontol. Mineral., 54:129–212.
- Beslier, M.-O., 1996. Data report: Seismic line LG12 in the Iberia Abyssal Plain. In Whitmarsh, R.B., Sawyer, D.S., Klaus, A., and Masson, D.G. (Eds.), *Proc. ODP, Sci. Results*, 149: College Station, TX (Ocean Drilling Program), 737–739.
- Beslier, M.O., Bitri, A., and Boillot, G., 1995. Structure de la transition continent-ocean d'une marge passive: sismique réflexion multitrace dans la Plaine Abyssale Ibérique (Portugal). *C. R. Acad. Sci. Ser. 2*, 320:969–976.
- Beslier, M.O., and Brun, J.-P., 1991. Boudinage de la lithosphère et formation des marges passives. *C. R. Acad. Sci. Ser. 2*, 313:951–958.
- Beslier, M.-O., Cornen, G., and Girardeau, J., 1996. Tectono-metamorphic evolution of peridotites from the ocean/continent transition of the Iberia Abyssal Plain margin. In Whitmarsh, R.B., Sawyer, D.S., Klaus, A., and Masson, D.G. (Eds.), *Proc. ODP, Sci. Results*, 149: College Station, TX (Ocean Drilling Program), 397–412.
- Boillot, G., Comas, M.C., Girardeau, J., Kornprobst, J., Loreau, J.-P., Malod, J., Mougouet, D., and Moullade, M., 1988b. Preliminary results of the Galinaute cruise: dives of the submersible *Nautile* on the Western Galicia Margin, Spain. In Boillot, G., Winterer, E.L., et al., *Proc. ODP, Sci. Results*, 103: College Station, TX (Ocean Drilling Program), 37–51.
- Boillot, G., Girardeau, J., and Kornprobst, J., 1988a. Rifting of the Galicia Margin: crustal thinning and emplacement of mantle rocks on the seafloor. In Boillot, G., Winterer, E.L., et al., *Proc. ODP, Sci. Results*, 103: College Station, TX (Ocean Drilling Program), 741–756.
- Bouma, A.H., 1962. *Sedimentology of Some Flysch Deposits: A Graphic Approach to Facies Interpretation*. Amsterdam (Elsevier).
- Brun, J.P., and Beslier, M.-O., 1996. Mantle exhumation at passive margins. *Earth Planet. Sci. Lett.*, 142:161–173.
- Cannat, M., 1993. Emplacement of mantle rocks in the seafloor at mid-ocean ridges. *J. Geophys. Res.*, 98:4163–4172.

- Davey, R.J., 1982. Dinocyst stratigraphy of the latest Jurassic to Early Cretaceous of the Haldager No.1 borehole. *Geol. Surv. Denmark Ser. B*, 6:1–57.
- Davies, E.H., 1985. The miospore and dinoflagellate cyst Opperl-zonation of the Lias of Portugal. *Palynology*, 9:105–132.
- de Kaenel, E., and Bergen, J.A., 1996. Mesozoic calcareous nannofossil biostratigraphy from Sites 897, 899, and 901, Iberia Abyssal Plain: new biostratigraphic evidence. In Whitmarsh, R.B., Sawyer, D.S., Klaus, A., and Masson, D.G. (Eds.), *Proc. ODP, Sci. Results*, 149: College Station, TX (Ocean Drilling Program), 27–59.
- Dorhofer, G., and Norris, G., 1975. Discrimination and correlation of highest Jurassic and lowest Cretaceous terrestrial palynofloras in Northwest Europe. *Palynology*, 1:79–93.
- Francis, J.E., 1983. The dominant conifer of the Jurassic Purbeck Formation, England. *Palaeontology*, 26:277–94.
- , 1984. The seasonal environment of the Purbeck (Upper Jurassic) fossil forests. *Palaeogeogr., Palaeoclimatol., Palaeoecol.*, 48:285–307.
- Hill, G., 1989. Distal alluvial fan sediments from the Upper Jurassic of Portugal: controls on their cyclicity and channel formation. *J. Geol. Soc. London*, 146:539–555.
- Hiscott, R.N., Wilson, R.C.L., Harding, S.C., Pujalte, V., and Kitson, D., 1990. Contrasts in Early Cretaceous depositional environments of marine sandbodies, Grand Banks-Iberian corridor. *Bull. Can. Pet. Geol.*, 38:203–214.
- Jansa, L.F., Comas, M.C., Sarti, M., and Haggerty, J.A., 1988. Late Jurassic carbonate platform of the Galicia Margin. In Boillot, G., Winterer, E.L., et al., *Proc. ODP, Sci. Results*, 103: College Station, TX (Ocean Drilling Program), 171–192.
- Karson, J.A., 1990. Seafloor spreading on the Mid-Atlantic Ridge: implications for the structure of ophiolites and oceanic lithosphere produced in slow-spreading environments. In Malpas, J., Moores, E.M., Panayiotou, A., and Xenophontos, C. (Eds.), *Ophiolites: Oceanic Crustal Analogues: Proc. Symp. "Troodos 1987"*: Nicosia, Cyprus (Minist. Agric. Nat. Resour.), 547–555.
- Krawczyk, C.M., Reston, T.J., Beslier, M.-O., and Boillot, G., 1996. Evidence for detachment tectonics on the Iberia Abyssal Plain rifted margin. In Whitmarsh, R.B., Sawyer, D.S., Klaus, A., and Masson, D.G. (Eds.), *Proc. ODP, Sci. Results*, 149: College Station, TX (Ocean Drilling Program), 603–615.
- Leinfelder, R.R., and Wilson, R.C.L., 1989. Seismic and sedimentologic features of Oxfordian-Kimmeridgian syn-rift sediments on the eastern margin of the Lusitanian Basin. *Geol. Rundsch.*, 78:81–104.
- , in press. Third order sequences in an Upper Jurassic rift-related second order sequence, central Lusitanian basin, Portugal. In Graciansky, P.-C., Hardenbol, J., Jaquin, T., Vail, P.R., and Farley, M.B. (Eds.), *Mesozoic and Cenozoic Sequence Stratigraphy of European Basins*. Spec. Publ.—Soc. Econ. Paleontol. Mineral.
- Mamet, B., Comas, M.C., and Boillot, G., 1991. Late Paleozoic basin on the West Galicia Atlantic margin. *Geology*, 19:738–741.
- Martini, E., 1971. Standard Tertiary and Quaternary calcareous nannoplankton zonation. In Farinacci, A. (Ed.), *Proc. 2nd Int. Conf. Planktonic Microfossils Roma*: Rome (Ed. Tecnosci.), 2:739–785.
- Minshull, T.A., 1995. *A Geophysical Study of the Ocean-continent Transition in the Iberia Abyssal Plain, R.R.S. Discovery Cruise 215*. Bullard Labs., Dep. Earth Sci., Cambridge Univ.
- Mohre, A.R., and Schmidt, D., 1988. The Oxfordian/Kimmeridgian boundary in the region of Porto de Mos (Central Portugal): stratigraphy, facies and palynology. *Neues Jahrb. Geol. Palaeontol. Abh.*, 176:245–267.
- Okada, H., and Bukry, D., 1980. Supplementary modification and introduction of code numbers to the low-latitude coccolith biostratigraphic zonation (Bukry, 1973; 1975). *Mar. Micropaleontol.*, 5:321–325.
- Pettijohn, F.J., Potter, P.E., and Siever, R., 1972. *Sand and Sandstone*: New York (Springer-Verlag).
- Pickering, K.T., Hiscott, R., and Hein, F.J., 1989. *Deep-marine Environments: Clastic Sedimentation and Tectonics*: London (Unwin Hyman).
- Pickup, S.L.B., Whitmarsh, R.B., Fowler, C.M.R., and Reston, T.J., 1996. Insight into the nature of the ocean-continent transition off West Iberia from a deep multichannel seismic reflection profile. *Geology*, 24:1079–1082.
- Powell, R., and Holland, T.J.B., 1989. An internally consistent thermodynamic data set with uncertainties and correlations: 3: applications to geobarometry, with worked examples and a computer program. *J. Met. Geol.*, 6:173–204.
- Ravnäs, R., Windelstad, J., Mellere, D., Nøttvedt, A., Stühr Sjøblom, T., Steel, R.J., and Wilson, R.C.L., 1997. A marine Late Jurassic syn-rift succession in the Lusitanian Basin, Western Portugal—tectonic significance of stratigraphic signature. *Sediment. Geol.*, 114:37–266.
- Reston, T.J., Krawczyk, C.M., and Klaeschen, D., 1996. The S reflector west of Galicia (Spain). Evidence for detachment faulting during continental breakup from prestack depth migration. *J. Geophys. Res.*, 101:8075–8091.
- Riding, J.B., and Thomas, J.E., 1988. Dinoflagellate cyst stratigraphy of the Kimmeridge Clay (Upper Jurassic) from the Dorset coast, southern England. *Palynology*, 12:65–88.
- , 1992. In Powell A.J. (Ed.), *A stratigraphic index of dinoflagellate cysts*. London (Chapman and Hall), 7–101.
- Sawyer, D.S., 1994. The case for slow-spreading oceanic crust landward of the peridotite ridge in the Iberia Abyssal Plain. *Eos*, 75:616.
- Sawyer, D.S., Whitmarsh, R.B., Klaus, A., et al., 1994. *Proc. ODP, Init. Repts.*, 149: College Station, TX (Ocean Drilling Program).
- Shipboard Scientific Party, 1988. Site 639. In Boillot, G., Winterer, E.L., Meyer, A.W., et al., *Proc. ODP, Init. Repts.*, 103: College Station, TX (Ocean Drilling Program), 409–532.
- , 1994a. Site 897. In Sawyer, D.S., Whitmarsh, R.B., Klaus, A., et al., *Proc. ODP, Init. Repts.*, 149: College Station, TX (Ocean Drilling Program), 41–113.
- , 1994b. Site 898. In Sawyer, D.S., Whitmarsh, R.B., Klaus, A., et al., *Proc. ODP, Init. Repts.*, 149: College Station, TX (Ocean Drilling Program), 115–146.
- , 1994c. Site 899. In Sawyer, D.S., Whitmarsh, R.B., Klaus, A., et al., *Proc. ODP, Init. Repts.*, 149: College Station, TX (Ocean Drilling Program), 147–209.
- , 1994d. Site 900. In Sawyer, D.S., Whitmarsh, R.B., Klaus, A., et al., *Proc. ODP, Init. Repts.*, 149: College Station, TX (Ocean Drilling Program), 211–262.
- , 1994e. Site 901. In Sawyer, D.S., Whitmarsh, R.B., Klaus, A., et al., *Proc. ODP, Init. Repts.*, 149: College Station, TX (Ocean Drilling Program), 263–268.
- Srivastova, S.K., 1976. The fossil pollen genus *Classopollis*. *Lethaia*, 9:437–457.
- Thusu, B., and Vigran, J.O., 1985. Middle-Late Jurassic (Late Bathonian-Tithonian) palynomorphs. *J. Micropalaeontol.*, 4:113–130.
- Traverse, A., 1988. *Paleopalynology*: Boston (Unwyn Hyman).
- Van Erve, A.W., Besems, R.E., and Love, C.F., 1988. A palynological investigation of some Lower Kimmeridgian deposits from Spain. *J. Micropalaeontol.*, 17: 217–232.
- Van Erve, A.W., and Mohr, B., 1988. Palynological investigations of the Late Jurassic microflora from the vertebrate locality Guimarães coal mine (Leira, Central Portugal). *Neues Jahrb. Geol. Palaeontol. Abh.*, 176:217–232.
- Wernicke, B., 1981. Low-angle normal faults in the Basin and Range Province: nappe tectonics in an extending orogen. *Nature*, 291:645–647.
- Whitmarsh, R.B., and Miles, P.R., 1994. Propagating rift model for the West Iberia rifted margin based on magnetic anomalies and ODP drilling. *Eos*, 75:616.
- , 1995. Models of the development of the West Iberia rifted continental margin at 40°30'N deduced from surface and deep-tow magnetic anomalies. *J. Geophys. Res.*, 100:3789–3806.
- Whitmarsh, R.B., and Sawyer, D.S., 1996. The ocean/continent transition beneath the Iberia Abyssal Plain and continental-rifting to seafloor-spreading processes. In Whitmarsh, R.B., Sawyer, D.S., Klaus, A., and Masson, D.G. (Eds.), *Proc. ODP, Sci. Results*, 149: College Station, TX (Ocean Drilling Program), 713–733.
- Wilson, R.C.L., Sawyer, D.S., Whitmarsh, R.B., Zerong, J., and Carbonell, J., 1996. Seismic stratigraphy and tectonic history of the Iberia Abyssal Plain. In Whitmarsh, R.B., Sawyer, D.S., Klaus, A., and Masson, D.G. (Eds.), *Proc. ODP, Sci. Results*, 149: College Station, TX (Ocean Drilling Program), 617–633.

Ms 173IR-107

NOTE: For all sites drilled, core-description forms ("barrel sheets") and core photographs can be found in Section 3, beginning on page 295. Forms containing smear-slide data, sedimentary thin-section descriptions, and igneous/metamorphic thin-section descriptions can be found on CD-ROM. See Table of Contents for material contained on CD-ROM.

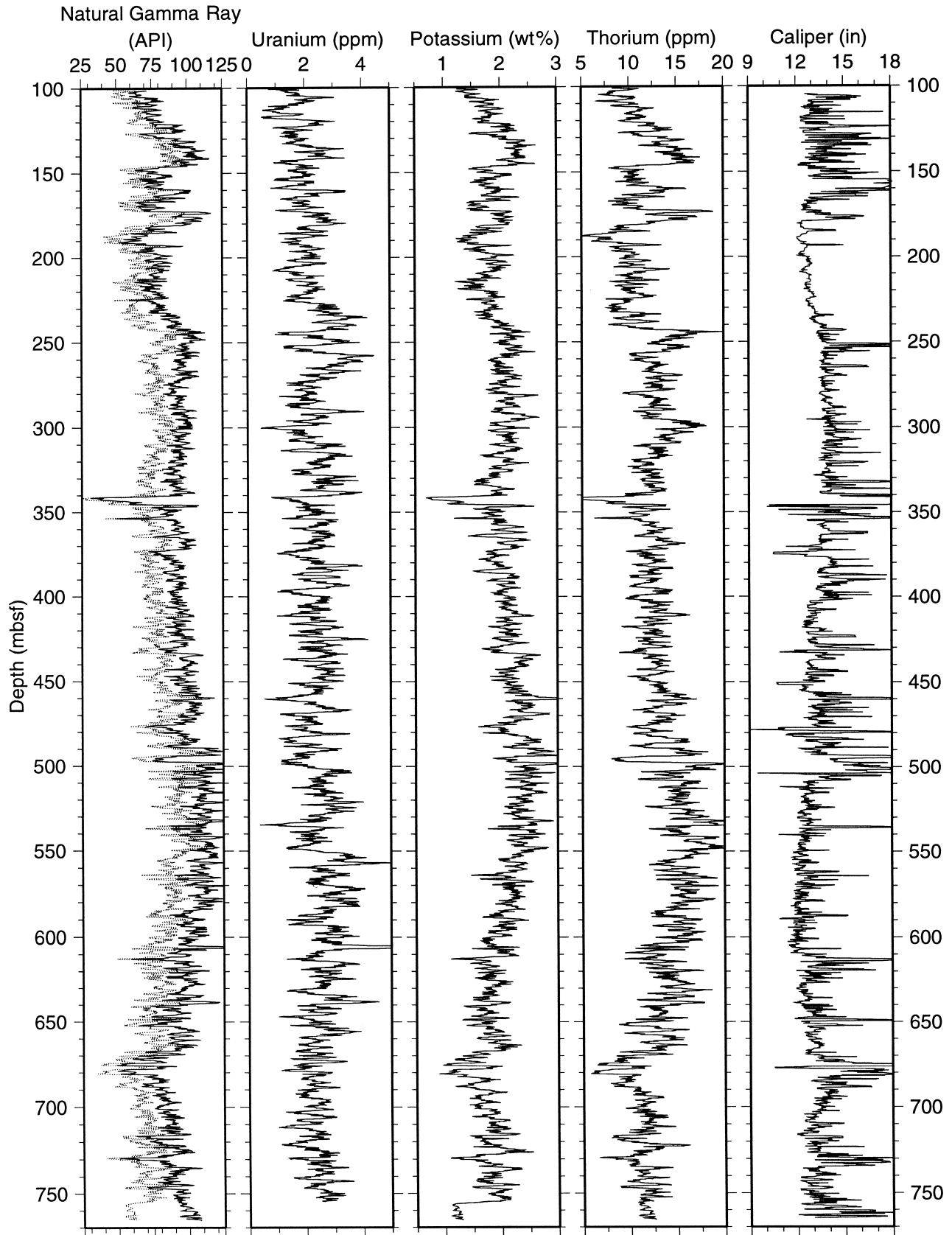


Figure 35. Downhole logs from the HNGS natural gamma-ray tool and caliper from the HLDS, recorded during the run of the triple combination tool string. Depths are in mbsf. Natural gamma-ray (continuous line = total gamma ray; dotted line = computed gamma-ray [total gamma-ray minus uranium], uranium, potassium, and thorium.

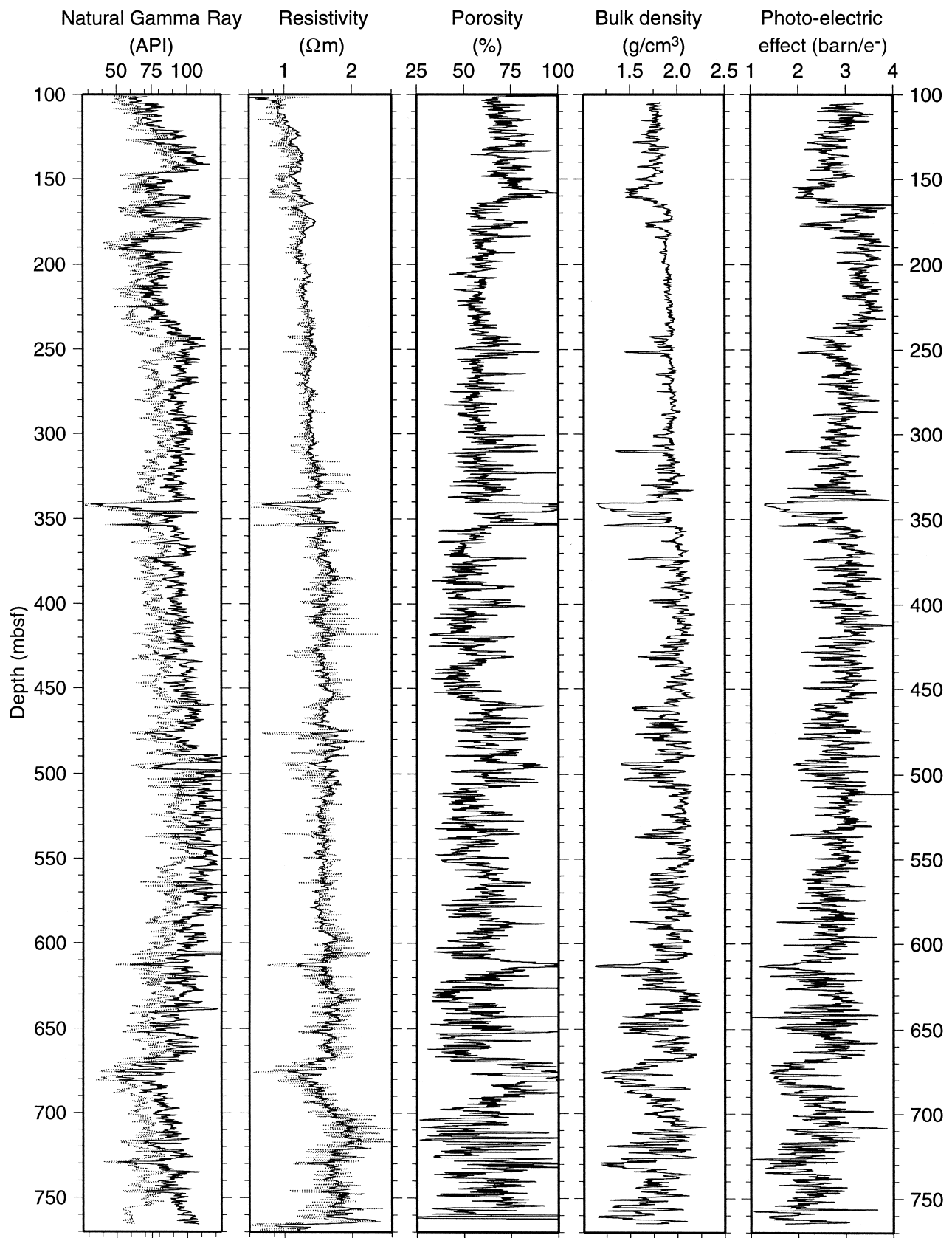


Figure 36. Downhole logs of natural gamma ray (continuous line = total gamma ray; dotted line = computed gamma-ray [total gamma-ray minus uranium], resistivity (ILD = continuous line and SFLU = dotted line), porosity, bulk density, and photo-electric effect factor.

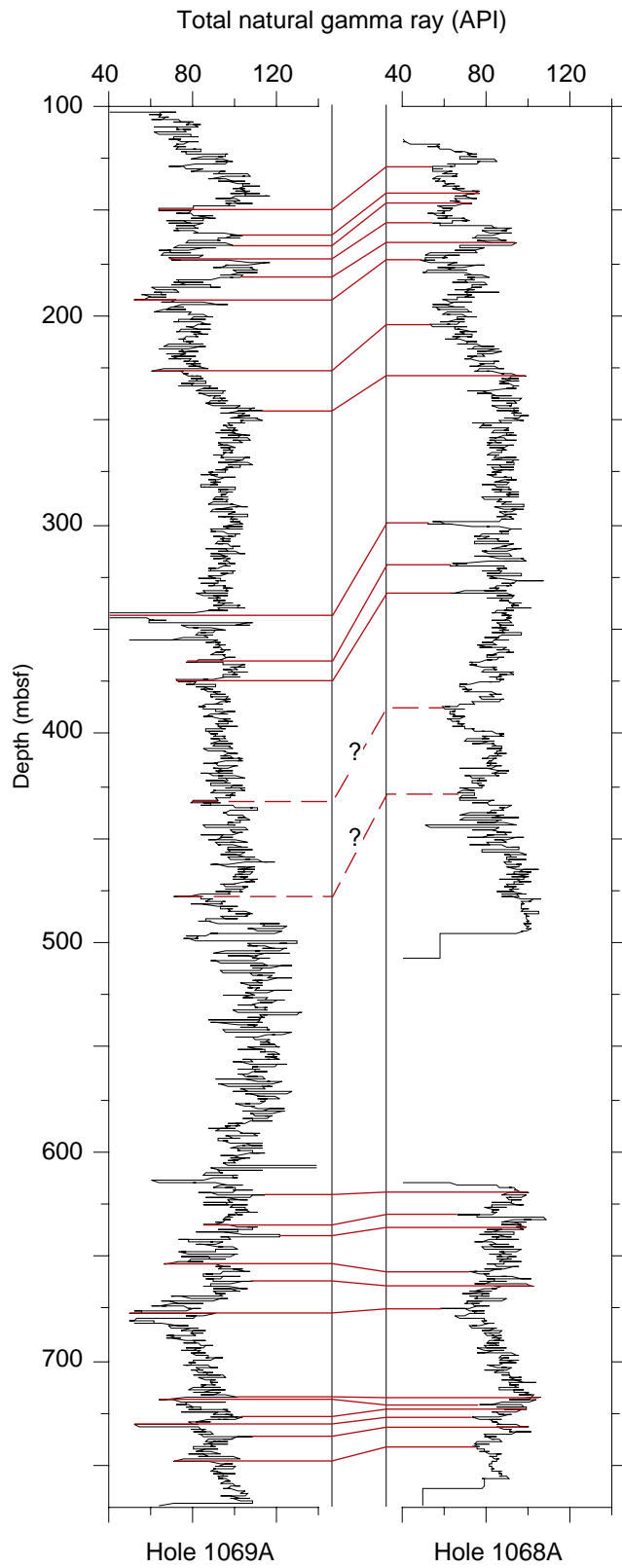


Figure 37. Comparison between total natural gamma-ray logs from Holes 1069A and 1068A at the same vertical scale.

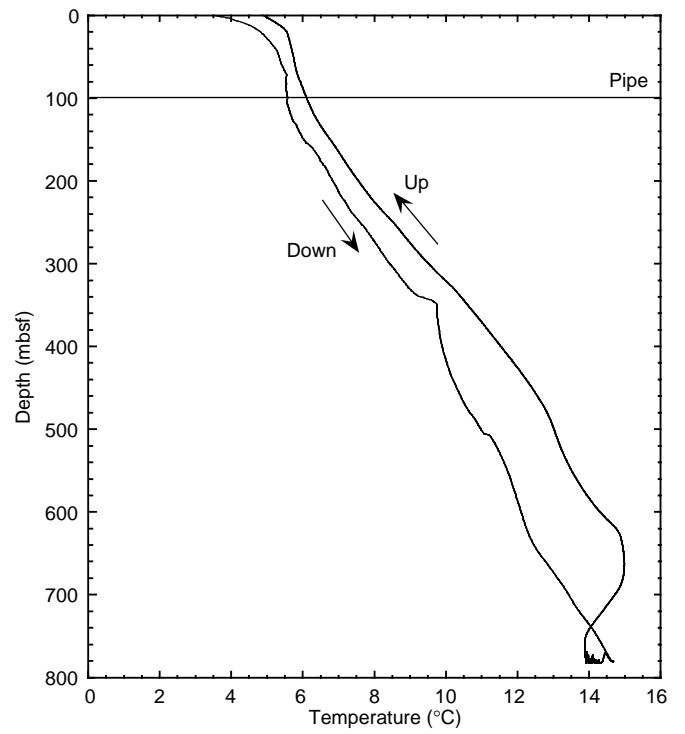


Figure 38. Temperature log from the TLT, recorded during the triple combination tool string run. The horizontal line represents the pipe depth.

APPENDIX 1. PALYNOLOGY¹

Five samples from Site 1069 were analyzed for palynology. In Sample 173-1069-16R-3, 127-131 cm, the presence of the dinocyst *Dichadogonyaulax* (?)*pannea* indicates a Kimmeridgian–upper Portlandian age. This is supported by the remainder of the assemblage.

A marine environment with strong terrestrial influence is suggested by the presence of a restricted dinocyst assemblage in an otherwise strongly miospore dominated palynoflora.

Samples 173-1069-16R-1, 145-149 cm, 16R-2, 87-91 cm, 16R-3, 26-29 cm, and 17R-CC were all barren of in situ palynomorphs.

Results

Sample 173-1069-16R-3, 127-131 cm, contains a moderately abundant assemblage of miospores dominated by the gymnosperms *Classopollis torosus* and *Classopollis echinatus* with common bisaccate pollen, *Vitreisporites pallidus*, and *Alisporites* spp. Also present are *Cerebropollenites macroverrucosus* and (?)*Striatella scanica*. Other miospores recorded are minor constituents and comprise mainly long-ranging Jurassic–Cretaceous forms (e.g., *Araucariacites australis*, *Concavisporites* sp., *Deltoidospora* sp., *Exesipollenites tumulus*, *Ischyosporites variegatus*, and *Spheripollenites psilatus*).

Dinocysts are present in very restricted numbers and are generally poorly preserved. Species recorded include *Apteodinium* sp., *Cribroperidinium globatum*, *Dichadogonyaulax* (?)*pannea*, (?)*Senoniasphaera* sp., and *Sentusidinium brevispinosum*.

Chitinous microforaminiferal test linings and the freshwater algae *Pediastrum* are also present.

See Table 18 (Appendix) for full assemblage details.

Age Significance

The presence of the dinocyst *Dichadogonyaulax* (?)*pannea* indicates a Kimmeridgian–upper Portlandian age, the occurrence of *Cribroperidinium globatum* also suggests an age no younger than upper Portlandian.

The occurrence of *Classopollis echinatus* indicates that this sample is no older than mid-Kimmeridgian.

The presence of *Cicatricosisporites* sp. provides further evidence of a post-Oxfordian age. This spore genus does not occur until the lowermost Kimmeridgian in Spain (Van Erve et al., 1988) and Portugal (Van Erve and Mohr, 1988; Mohr and Schmidt, 1988).

The fern spore (?)*Striatella scanica* ranges from Anisian–lower Callovian, to (?)Portlandian (Batten and Koppelhaus, 1996).

Overall, therefore, a mid-Kimmeridgian–upper Portlandian age is indicated.

Paleoenvironment

The presence of rare marine dinocysts that compose approximately 5% of the total assemblage indicates deposition in a marine environment. Strong terrestrial influences are suggested by the overwhelming dominance of miospores.

The overall nature of the miospore assemblage is typical of that found in the Tethyan Realm with a strongly *Classopollis*-dominated palynoflora and subordinate bisaccate pollen (Thusu and Vigran, 1985). *Classopollis* is a coniferous pollen characteristic of Lower Jurassic to mid-Cretaceous palynofloras. Its occurrence is widespread, particularly in lower latitudes, where it can occur in abundance, often comprising over 90% of the assemblage. It is considered to have been produced mainly by a variety of warmth-loving shrubs, particularly by *Hirmeriella* and other cheirolepidiaceae conifers that grew in masses on low-lying mudflats close to water, although some were able to withstand semi-arid conditions (Francis, 1983, 1984) and others grew on higher ground (Srivastova, 1976). Fern spores such as *Deltoidospora* sp., *Cicatricosisporites* sp., *Concavisporites* sp., *Ischyosporites variegatus*, and (?)*Striatella scanica* were also probably derived from low-lying, possibly swampy areas whereas the source of conifer taxa, *Araucariacites australis*, and bisaccate pollen was most likely a higher, more continental environment.

All samples analyzed were processed in the palynological laboratory at University College London using standard palynological processing techniques.

¹Susan L. Mathews, Dept. of Geological Sciences, University College, London, U.K.

Table 18. Palynology abundance chart for Hole 1069A.

Age range	Core, section, interval (cm)	Depth (mbsf)	Abundance	Miospores										Dinocysts					Others			
				<i>Classopollis torosus</i>	<i>Vitreisporites pallidus</i>	<i>Alisporites</i> sp.	<i>Classopollis echinatus</i>	<i>Cerebropollenites macroverrucosus</i>	<i>Exesipollenites tumulus</i>	<i>Araucariacites australis</i>	<i>Deltoidospora</i> sp.	<i>Cicatricosisporites</i> sp.	<i>Spheripollenites psilatus</i>	<i>Concavisporites</i> sp.	<i>Ischyosporites</i> sp.	? <i>Striatella scanica</i>	<i>Dichadogonyaulax</i> ? <i>pannea</i>	<i>Cribroperidinium globatum</i>	? <i>Senoniasphaera</i> sp.	<i>Apteodinium</i> sp.	<i>Sentusidinium brevispinosum</i>	Microforaminiferal test linings
173-1069A- 16R-1, 145-149 16R-2, 87-91 16R-3, 26-29 mid-Kimmeridgian–Portlandian 16R-3, 127-131 17R-CC		865.1	B																			
		866.0	B																			
		866.9	B																			
		867.9	A	A	C	C	O	R	O	R	R	R	R	R	R	R	R	R	R	R	R	R
		874.4	B																			

Note: R = rare (<4 specimens), O = occasional (5–9 specimens), C = common (10–19 specimens), A = abundant (>20 specimens).